UNIVERSITEIT VAN PRETORIA
UNIVERSITY OF PRETORIA
YUNIBESITHI YA PRETORIA

Experimental Investigation on Natural Convection of Al_2O_3-water Nanofluids in Cavity Flow

by

Hadi Ghodsinezhad

Submitted in partial fulfilment of the requirements for the degree

Master of Engineering (Mechanical Engineering)

in the Department of Mechanical and Aeronautical Engineering,
Faculty of Engineering, Built Environment and Information Technology

University of Pretoria

April 2016

Abstract

Experimental Investigation on Natural Convection of Al_2O_3-water Nanofluids in Cavity Flow

Supervisor: Dr M Sharifpur and Prof JP Meyer

Department: Mechanical and Aeronautical Engineering

University: University of Pretoria

Degree: Master of Engineering (Mechanical Engineering)

Keywords: Nanofluids, natural convection, volume fraction, cavity flow

The thermophysical properties of nanofluids have attracted the attention of researchers to a far greater extent than the heat transfer characteristics of nanofluids have. Contradictory results on the thermal-fluid behaviour of nanofluids have been numerically and experimentally reported on in the open literature. Natural convection has not been investigated experimentally as much as the other properties of nanofluids. In this study, the characteristics and stability of Al_2O_3-water nanofluids (d = 20–30 nm) were analysed using a Malvern zetasizer, zeta potential and UV-visible spectroscopy. The natural convection of Al_2O_3- water nanofluids (formulated with a single-step method) was experimentally studied in detail for the volume fractions 0, 0.05, 0.1, 0.2, 0.4 and 0.6% in a rectangular cavity with an aspect ratio of 1, heated differentially on two opposite vertical walls for the Rayleigh number (Ra) range 3.49×10^8 to 1.05×10^9. The viscosity of Al_2O_3-water nanofluids measured between 15 and 50 ℃. The effect of temperature and volume fraction on viscosity was also investigated. A detailed study of the nanoparticle concentration effect on the natural convection heat transfer coefficient was performed. It was found that increasing the

concentration of nanoparticles improves the heat transfer coefficient by up to 15% at a 0.1% volume fraction. Further increasing the concentration of nanoparticles causes the natural convection heat transfer coefficient to deteriorate. This research also supports the idea that "for nanofluids with thermal conductivity – more than the base fluids – an optimum concentration may exist that maximises heat transfer in an exact condition as natural convection, laminar force convection or turbulence force convection".

Keywords: *Nanofluids, Al_2O_3, natural convection, cavity flow, volume fraction, viscosity, stability.*

Dedication

To my family

Acknowledgments

I would like to acknowledge the following people for their help and support:

- Dr M Sharifpur, for his technical guidance and moral support throughout the study.
- Prof JP Meyer, for his financial support.
- Mr C Govender, Mr Keetse and Dr Rolfes for their technical advice and support with the experimental setup and testing.
- Mr Tshimanga, Mr Mahdavi, Mr Lee, Mr Garbadeen and Mrs Kombo.

I would also like thank the following institutions for their financial support:

- The National Research Foundation (NRF) of South Africa
- The Council for Scientific and Industrial Research (CSIR)
- The University of Pretoria

Table of contents

Abstract……...…I

Dedication……III

Acknowledgment……....IV

List of figures……IX

List of tables……XI

1. Introduction……1

1.1 Background……1

1.2 Natural convection in cavity flow……3

1.3 Motivation of the study……4

1.4 Objective of this study……4

1.5 Scope of work……5

1.6 Overview of the dissertation……5

2. Literature review……6

2.1 Introduction……6

2.2 Preparation of nanofluids……6

2.2.1 The single-step method……6

2.2.1.1 Vacuum evaporation running oil substrate……7

2.2.1.2 Chemical reduction of metal salts and chemical precipitation……7

2.2.1.3 Grinding with bead mills……8

2.2.2 The two-step method……9

2.2.2.1 Adjusting the pH value……9

2.2.2.2 Ultrasonic energy 11
2.2.2.3 Adding surfactants 13
2.3 Indication of nanofluids' stability 17
2.3.1 Zeta potential 17
2.3.2 Characteristics with microscopy 20
2.3.3 Zetasizer 21
2.3.4 UV-visible spectrophotometer 23
2.4 The thermophysical properties of nanofluids 24
2.4.1 Thermal conductivity 25
2.4.2 Viscosity 28
2.4.3 Other thermophysical properties 29
2.5 Heat transfer of nanofluids 31
2.5.1 Natural convection 33
2.6 Conclusion 40
3. Experimental procedure 42
3.1 Introduction 42
3.2 Materials 42
3.3 Equipment 43
3.4 Experimental setup 44
3.5 Experimental method 47
3.6 Experimental data reduction 47

3.7 Experimental validation 50

3.8 Conclusion 53

4. Results: Nanofluid formulation and natural convection 54

4.1 Introduction 54

4.2 Nanofluid characterisation 55

4.2.1 TEM and SEM 55

4.2.2 Zetasizer 58

4.2.3 Zeta potential 62

4.2.4 UV-visible spectrophotometry 64

4.3 The viscosity of nanofluids 66

4.4 The effect of nanofluid volume fraction on *h* 68

4.5 The effect of volume fraction on *Ra* and *Nu* 69

4.6 Temperature distribution 71

4.7 Uncertainty analysis 73

4.8 Conclusion 74

5 Summary, conclusion and recommendation 76

References 79

Appendix A: Thermocouples calibration 89

A.1 Introduction 89

A.2 Thermocouples calibration 89

A.3 Conclusion 101

Appendix B: Uncertainty analysis 102

B.1 Introduction 102

B.2 Theory of uncertainty analysis 102

B.3 Conclusion 109

List of figures

FIGURE 2.1: THE EFFECT OF MILLING TIME ON THE SIZE OF PARTICLES, ADOPTED FROM [14] 8

FIGURE 2.2: SCHEMATIC STERIC MECHANISM FOR THE PREPARATION OF A STABLE COLLOIDAL DISPERSION 14

FIGURE 2.3: A SCHEMATIC STRUCTURE OF THE TYPICAL HYDROPHILIC MOLECULE 15

FIGURE 2.4: OBTAINING THE CMC CONCENTRATION VIA DIFFERENT MEASUREMENTS ADOPTED FROM [38] 16

FIGURE 2.5: A SCHEMATIC OF AN ELECTROSTATIC STABILISATION MECHANISM 17

FIGURE 2.6: THE EFFECT OF PH VALUE ON ZETA POTENTIAL [47] 18

FIGURE 2.7: THE SEM AND TEM IMAGES OF ZNO-WATER NANOFLUIDS (D = 20 NM) 21

FIGURE 2.8: THE SIZE DISTRIBUTION OF ZNO-WATER NANOFLUIDS 23

FIGURE 3.1: HEAT EXCHANGERS WITH A SIMILAR HYDRAULIC DIAMETER IN THE SHELL AND TUBE SIDE 44

FIGURE 3.2: THE EXPERIMENTAL SETUP OF NATURAL CONVECTION 45

FIGURE 3.3: A SCHEMATIC OF THE THERMOCOUPLES IN THE EXPERIMENTAL SETUP 46

FIGURE 3.4: VALIDATION OF THE EXPERIMENTAL SETUP USING NU AS FUNCTION OF RA IN COMPARISON TO THE EXISTENCE OF CORRELATIONS 51

FIGURE 3.5: THE AVERAGE NU AS A FUNCTION OF THE RA, COMPARISON BETWEEN THE NUMERICAL SIMULATION AND THE EXPERIMENTAL RESULTS [137] 52

FIGURE 3.6: THE STREAMLINE OF FLOW FIELD IN THE CAVITY MAPPED WITH A NON-DIMENSIONAL TEMPERATURE [137] 53

FIGURE 4.1: AN SEM IMAGE OF AL_2O_3-WATER (20–30 NM SINGLE-STEP) 55

FIGURE 4.2: AN SEM IMAGE OF DRY ZNO POWDER (20 NM) 56

FIGURE 4.3: AN SEM IMAGE OF ZNO-WATER (D = 20 NM) NANOFLUIDS USING THPD AS A SURFACTANT AT PH = 9.5 56

FIGURE 4.4: AN SEM IMAGE OF (A) SIO_x-WATER (D = 20 NM) AND (B) CUO-WATER (D = 20 NM) 57

FIGURE 4.5: A TEM IMAGE OF DISPERSED AL_2O_3-WATER (D = 20–30 NM) NANOFLUIDS 57

FIGURE 4.6: A TEM IMAGE OF (A) SIO_2 (D = 80 NM); (B) CUO (D = 20 NM); (C) ZNO (D = 20 NM) AND (D) AL_2O_3 (D = 20–30 NM) 58

FIGURE 4.7: THE SIZE DISTRIBUTION OF 0.05% VOLUME FRACTION OF AL_2O_3-WATER NANOFLUID (20 NM) AT 25 °C 59

FIGURE 4.8: THE EFFECT OF SONICATION ENERGY ON THE MEAN SIZE OF AL_2O_3-WATER NANOFLUID 60

FIGURE 4.9: THE EFFECT OF SONICATION ENERGY DENSITY ON THE AVERAGE SIZE OF ZNO-WATER NANOFLUID (D = 20 NM) (TWO-STEP)..... 61

FIGURE 4.10: THE EFFECT OF HIGH SONICATION ENERGY DENSITY ON THE SIZE DISTRIBUTION OF THE ZNO-WATER NANOFLUID (D = 20 NM) 61

FIGURE 4.11: THE ZETA POTENTIAL OF 0.01% VOLUME FRACTION OF AL_2O_3-WATER NANOFLUIDS AT 25 °C 62

FIGURE 4.12: THE EFFECT OF VARIOUS SONICATION ENERGY DENSITIES ON THE ZETA POTENTIAL OF ZNO-WATER NANOFLUID 64

FIGURE 4.13: THE EFFECT OF AL_2O_3-WATER NANOFLUID WAVELENGTH ON ABSORBANCE 65

FIGURE 4.14: THE CHANGING CONCENTRATION OF THE AL_2O_3-WATER NANOFLUID AFTER PREPARATION 66

VISCOUS FORCES ARE INVESTIGATED TO DETERMINE THEIR EFFECT ON NATURAL CONVECTION. THE DISPERSION OF NANOPARTICLES ESCALATES THE VISCOSITY OF THE BASE FLUID [9]. THE VISCOSITY OF AL_2O_3-WATER NANOFLUID IS A FUNCTION OF VOLUME FRACTION AND TEMPERATURE, AS SHOWN IN FIGURE 4.15. 66

FIGURE 4.16: THE THEORETICAL VISCOSITY OF 0.6% VOLUME FRACTION AL_2O_3-WATER (D = 20–30 NM) AND EXPERIMENTAL MEASUREMENT 67

FIGURE 4.17: THE EFFECT OF THE VOLUME FRACTION OF AL_2O_3-WATER NANOFLUID ON THE NATURAL CONVECTION HEAT TRANSFER COEFFICIENT 69

FIGURE 4.18: THE EFFECT OF THE RA AND VOLUME FRACTION OF AL_2O_3-WATER NANOFLUID (D = 20–30 NM) ON THE AVERAGE *NU*..... 70

FIGURE A. 1: THE AVERAGE TEMPERATURES AS MEASURED BY THERMOCOUPLES INSIDE THE THERMOSTAT BATH VERSUS THE REFERENCE TEMPERATURES……..97

FIGURE A. 2: THE THERMOCOUPLES STATION IN THE EXPERIMENTAL SETUP (ROTATED 90 DEGREE CCW)…….....98

FIGURE A. 3: CALIBRATED AND UNCALIBRATED TEMPERATURE OF THERMOCOUPLES CHANNELS AT (A) 8.5 °C, (B) 27.6 °C, (C) 36.8 °C AND (D) 51.9 °C……..……100

List of tables

TABLE 2. 1: THE REGRESSION COEFFICIENT FOR THE MEASUREMENT OF NANOFLUIDS' PH VALUE [26] 11

TABLE 2.2: LIST OF SURFACTANTS THAT ARE USED IN THE LITERATURE 16

TABLE 2.3: THE EFFECTIVE THERMAL CONDUCTIVITY OF 0.6% VOLUME CONCENTRATION USING MODELS 28

TABLE 2.4: THE NUMERICAL INVESTIGATION OF NANOFLUIDS IN A SQUARE CAVITY [114] 36

TABLE 2.5: THE EXPERIMENTAL NATURAL CONVECTION OF NANOFLUIDS 40

TABLE 3.1: THE THERMOPHYSICAL PROPERTIES OF AL_2O_3 AND WATER 42

TABLE 4.1: THE EFFECT OF TEMPERATURE ON THE SIZE AND ZETA POTENTIAL OF 0.01% CONCENTRATION AL_2O_3-WATER NANOFLUID (D = 20–30 NM) 63

TABLE 4.2: THE EXPERIMENTAL MEASUREMENT OF 0.1% VOLUME FRACTION OF AL_2O_3-WATER NANOFLUID 72

TABLE 4.3 THE EXPERIMENTAL MEASUREMENT OF WATER IN THE TEST CELL 73

TABLE 4 4: ACCURACY AND RANGE OF INSTRUMENTS THAT WERE USED 74

TABLE A. 1: THE AVERAGE CALIBRATION FACTORS OF THERMOCOUPLES.....100

TABLE B. 1 INDEPENDENT READING ERROR IN APPARATUS.....105

TABLE B. 2: MAXIMUM UNCERTAINTIES OF THE EXPERIMENT DUE TO PROPAGATED ERRORS.....109

Nomenclature

Ar	Aspect ratio
AWG	American wire gauge
C	Total count
CH	Thermocouple channel number
C_p	Specific heat, J/kg.K
D	Nano particle diameter, m
F_n	Thermophysical properties ratio
G	Gravitational acceleration, m^2/s
Ga	Grashof number
H	Height, m
$\overline{h}$	Average heat transfer coefficient, W/m^2K
H	Heat transfer coefficient, W/m^2K
h_D	Hydraulic diameter, m
I	Intensity
K	Thermal conductivity, W/m.K
L	Depth, m
M	Mass flow rate, kg/S
N	Exponent value Eq (3)
Nu	Nusselt number
$\overline{Nu}$	Average Nusselt number
Pr	Prandtl number, $C_p\mu/k$
$\overline{\dot{q}}$	Average heat transfer rate, W
Q	Heat transfer, J
Ra	Rayleigh number
Re	Reynolds number
S	Distance from the hot heat exchanger surface

t	Time, hour
T	Temperature, °C
W	Width, m
wt	Mass fraction
ΔT	Temperature difference, °C
ZP	Zeta Potential, mV

Greek symbols

α	Ultrasonic energy density, KJ/ml
β	Thermal expansion coefficient,1/K
ζ	Milling time, hour
λ	Wave length
ρ	Density, kg/m^3
μ	Dynamic viscosity, Pa.s
θ	Dimensionless temperature
δ	Dimensionless distance
φ	Volume fraction
ω	Volume
κ	Initial concentration percentage

Subscript

P	Nanoparticle
bf	Based fluids
nf	Nanofluids
ref	Reference temperature

PUBLICATIONS IN JOURNALS AND CONFERENCE PROCEEDINGS

Articles in peer-reviewed journals:

1. H. Ghodsinezhad, M. Sharifpur,J.P. Meyer, Experimental investigation on the cavity flow natural convection of Al_2O_3-water nanofluid, International Communications in Heat and Mass Transfer, Volume 76, August 2016, Pages 316–324

2. M. Mahdavi, M. Sharifpur, H. Ghodsinezhad, J.P. Meyer, Experimental and numerical study of the thermal and hydrodynamic characteristics of laminar natural convective flow inside a rectangular cavity with water, ethylene glycol–water and air, Experimental Thermal and Fluid Science, Volume 78, November 2016, Pages 50–64

Conference papers:

1. C. Grobler, M. Sharifpur, H. Ghodsinezhad, R. Capitani, J.P. Meyer, 2015, Experimental study on cavity flow natural convection in porous medium, saturated with an Al_2O_3 60% EG-40% water nanofluid, 11th International Conference on Heat Transfer, Fluid Mechanics and Thermodynamics (HEFAT 2015), Kruger National Park, South Africa, pp. 828–832 (proceeding).

2. H. Ghodsinezhad, M. Sharifpur, J.P. Meyer, H. Rolfes, 2015, Investigation on the ultrasonication energy density effect on the characterisation of zinc oxide (ZnO) nanoparticle size distribution with a Zeta-Sizer, 11th International Conference on Heat Transfer, Fluid Mechanics and Thermodynamics, Kruger National Park, South Africa, pp. 211–216 (proceedings).

3. M. Mahdavi, H. Ghodsinezhad, M. Sharifpur, J.P. Meyer, A. 2015, Engineering, South Africa, Boundary condition investigation for cavity flow natural convection, 11th International Conference on Heat Transfer, Fluid Mechanics and Thermodynamics (HEFAT 2015), Kruger National Park, South Africa, pp. 813–818 (proceedings).

1. Introduction

1.1 Background

Over the last few years, environmental consideration has received much attention as a result of the depletion of global natural energy resources and industrial environmental pollution. The advancement of technology in many professions requires a greater flow of information, which results in a greater motion of electrons in circuits or the rapid flow of photons in optical fibres [1]. This increased flow of electrons or photons causes a scaling up of resistance due to higher speed, which consequently leads to greater heat generation, especially in electronic devices. A trend in miniaturising advanced technologies has brought space constraint challenges in their design. Therefore, a new design method is required to increase the performance of machines by manipulating natural laws to decrease their environmental impact and overcome space constraints. A cooling mechanism design using natural convection rather than forced convection might, therefore, be considered. The flow of cooling fluids in forced convection, facilitated by applying external forces, results in higher energy consumption, increased system noise, augmented design size, an increase in malfunctioning probability, reliability reduction of systems and increased system maintenance cost. In contrast to forced convection, natural convection does not need any external devices to cause fluid flow. However, the heat transfer coefficient of natural convection is very low in comparison to forced convection or boiling. Thus, attempts to increase the natural convection heat transfer coefficient should be investigated with confined volume (cavity) constraints.

Natural convection has been used broadly as a cooling mechanism in industry. It has been used, for example, in the cooling of a nuclear reactor, thermal regulation in electronic devices, the cooling of buildings and solar collectors, as well as in many applications in the

food and agricultural industries. The widespread application of natural convection has drawn many researchers' attention to enhancing its performance.

Convection heat transfer mediums in industry are usually fluids, such as water, or a mixture of water and ethylene glycol (EG) or glycerol. The heat transfer rate of conventional fluids is limited by their low thermal conductivity value. On the other hand, metals and metal oxides in solid forms have a much higher thermal conductivity than fluids at room temperature. For example, copper and copper oxide, respectively, have thermal conductivities that are 700 times and 30 times higher than water [2]. Thermal effort to improve the thermal conductivity of a base fluid by suspending solid particles has been investigated considerably. Maxwell [3] was the pioneer who proposed the enhancement of base fluid heat transfer by suspending millimeter- or micrometer-sized solid particles in the base fluid. The challenge of suspending solid particles of this size includes rapid sedimentation, clogging and erosion, especially in microchannels. In the 1990s, advancement in technology facilitated the opportunity to manufacture nanometre-sized solid particles. The heat transfer enhancement of fluids by suspending a diluted concentration of very tiny solid particles (less than 100 nm) resulted in the overcoming of one heat transfer performance limitation (low thermal conductivity). Choi [4] called fluids of this kind nanofluids. Nanofluids are promising advanced colloidal coolant fluids for different application, such as solar collectors, nuclear reactors, air conditioning, drug delivery, cancer treatment, lubrication and the cooling of electronic devices [5].

Feynman's talk [6] in 1959, entitled "There is plenty room at the bottom", proposed an inspirational framework for the future. He proposed the possibility of storing all books in a tiny piece, making micromachines that could go into the human body and arrange atoms in favourable ways. Subsequently, his hypothesis has been put to practice in the form of nanofluids. Technology advancement since the last decade has resulted in the growth of nanotechnologies that are at their early stage of development [1]. From a microscopic point of

view, classical laws are not able to give a full description of phenomena on a nano scale. Therefore, researchers have been examining different mechanisms that could explain abnormal energy transportation in nanofluids, such as Brownian motion, photons, electrons, the clustering of nanoparticles and nanolayering at the interface of liquid and solids [7].

Anomalous alteration in base fluid properties by suspending diluted concentrations of nanomaterials, such as nanoparticles, nanofibers, nanotubes, nanosheets and nanowires, have been subjected to scientific studies. The thermophysical properties of nanofluids have been experimentally investigated in many studies [8–10]. In comparison to the characteristic properties of nanofluids, their heat transfer characteristics have not been investigated in much detail. In particular, very limited literature is available on the experimental investigation of the natural convection of nanofluids.

1.2 Natural convection in cavity flow

Heat transfer in fluids due to the buoyancy force and lack of external driving forces is known as natural convection. The density difference as a driving force causes a spontaneous flow in the presence of the temperature gradient. The application of natural convection in a confined volume is widespread in heat transfer engineering practice. The engineering application of natural convection was reviewed by Barr et al. [11]. Many researchers have investigated the geometrical effect and inclination angles of a cavity on heat transfer. Natural convection in a cube, the simplest geometrical shape, with two opposite vertical walls heated at different temperatures, was studied experimentally. A literature survey revealed that many studies have examined air-filled cavities. However, limited studies have been reported on water-filled cavities.

1.3 Motivation of the study

The low natural convection heat transfer coefficient of water could be improved by suspending nanoparticles in it. This results in improving the performance of engineering devices, as well as the inspiration behind the innovative design of equipment that operates by the natural convection heat transfer mechanism.

A heat transfer literature review of nanofluids has revealed few investigations of natural convection in nanofluids. In addition, contrasting results of the numerical and experimental investigation of natural convection in nanofluids proposed more details for the experimental study of natural convection in nanofluids.

The slow current of convection is a challenge for the investigation of natural convection using nanofluids, which resulted in the quick sedimentation of particles due to the semi-stationary state of nanofluids in comparison to forced convection. Therefore, diluted concentrations of nanofluids at a very high Raleigh number (Ra) should be investigated.

1.4 Objective of this study

This study aimed to design and build an experimental setup, which could investigate the natural convection of diluted nanofluid concentrations in cavity flow. Due to the slow current of the flow, nanofluids were characterised using transmission electron microscopy (TEM), scanning electron microscopy (SEM), a zetasizer and a viscometer to accommodate a study of natural convection in nanofluids. The nanofluids' stability was also ensured using UV-visible spectroscopy, zeta potential and visual observation. The effect of the nanofluid volume fraction on the performance of the nanofluid heat transfer coefficient at various *Ra* values was investigated experimentally. The correlation for the average Nusselt number (*Nu*) as a function of *Ra* and the volume fraction of Al_2O_3-water nanofluid was developed. Finally, the temperature distribution of nanofluids at different volume fractions was observed in the test cell.

1.5 Scope of work

In this study, the morphology of Al_2O_3-water (d = 20–30 nm) was investigated using TEM and SEM. The effect of sonication energy density ranges from 0 to 5 kJ/ml on mean average size distribution was examined to find the optimum energy density that resulted in minimum mean size. A UV-visible spectrophotometer measured the volume fractions of 0.01, 0.02 and 0.04% volume fractions (vol.%) to find the coefficient of absorption as a function of nanofluid concentration. Checking the concentration of nanofluids during the experiment gave an indication of the stability of the nanofluid. Moreover, this stability was studied by measuring the zeta potential of different volume fractions. The effect of the temperature variation from 5 to 55 °C for zeta potential and the mean average size of the nanofluids were investigated. The viscosity of the nanofluid as a function of the temperature range 15 to 50 °C and nanofluid concentrations of 0 to 0.6% volume fractions were studied. After the characterisation of the nanofluid, the natural convection of the nanofluid was investigated in terms of the effect of Al_2O_3-water (d = 20–30 nm) for different concentrations (0, 0.05, 0.1, 0.2, 0.4 and 0.6% volume fractions) on the natural convection heat transfer coefficient at a *Ra* range of 3.49×10^8 to 1.05×10^9 by using a square cavity. Finally, the temperature distribution in the test cell was monitored for all volume fractions.

1.6 Overview of the dissertation

Chapter 2 contains a detailed literature review of nanofluid characterisation and the formulation of a stable nanofluid, as well as experimental and numerical investigations on natural convection in nanofluids. In Chapter 3, nanofluid formulation details are provided, the experimental setup is described, and the experimental setup is validated. Chapter 4 contains the results of the nanofluid formulation, such as TEM, SEM, zetasizer, zeta potential and the viscosity measurement of the nanofluid, as well as the result of the experimental measurement of the nanofluid heat transfer coefficient for different volume fractions. Chapter 5 presents the conclusion of the study and recommendations for future work.

2. Literature review

2.1 Introduction

In this chapter, a literature review of the different stable nanofluid preparation methods is presented and various techniques of nanofluid stability are verified. The thermophysical properties of nanofluids, which play an important role in the heat transfer of nanofluids, are reviewed in detail. Finally, a numerical and experimental investigation of nanofluids' natural convection heat transfer is discussed.

2.2 Preparation of nanofluids

Nanofluids are not just a simple colloidal suspension of liquids and solids due to the large surface area of particles in comparison to their volume, which results in strong attraction forces between particles. Therefore, some techniques should be applied to make a stable suspension. The following two major methods of nanofluid preparation are used:

a. Single-step method
b. Two-step method

2.2.1 The single-step method

The single-step method is a physical or chemical process in which colloidal particles have been made directly and suspended simultaneously into their host fluids. Methods such as physical vapour condensation [12], chemical vapour deposition [13], wet grinding with ball mills [14], chemical reduction and chemical precipitation [15] were applied to produce nanofluids. It has the advantages of reducing the aggregation of nanoparticles and improving the stability of prepared nanofluids. However, bulk production using the single-step method is not cost-efficient and this approach is limited to host fluids with a low vapour pressure.

2.2.1.1 Vacuum evaporation running oil substrate

Nanofluid production using a vacuum evaporation running oil substrate (VEROS) is described in this section. Metal is evaporated in a vacuum. Heating elements in a crucible are then deposited on the surface of a running oil substrate, which simultaneously operates on the surface of the rotating disc, after which nano-sized particles are collected in suspension. A very low vapour pressure is needed for the substrate oil, which is the limitation of this technique [13].

2.2.1.2 Chemical reduction of metal salts and chemical precipitation

Metallic nanoparticles could be prepared using the chemical reduction of metal salts. Brust et al. [16] prepared a colloidal gold suspension in dodecanethiol ($C_{12}H_{25}SH$). Different techniques were used to separate the desired nanofluids from primary chemicals. For example, after an organic phase was added to the solution, it was stirred to separate the organic phase, which was accompanied by some other chemicals. This was followed by washing, for example, with ethanol. Precipitation was then used to prepare the desired concentration of nanofluids in the desired base fluid. Chandrasekar et al. [17] prepared Al_2O_3 powder with the microwave-assisted chemical precipitation technique. A solution of aluminium chloride was hydrolysed in a water reflux condenser for 20 minutes, after which it was neutralised by an ammonia solution.

Lastly, distilled water was used to wash away the precipitate, which was then was dried [17]. Zinc oxide (ZnO) nanoparticles were formed with chemical precipitation. First, aqueous $ZnOSiO_4.7H_2O$ was diluted until a 0.1 M concentration was obtained, after which NaOH was added to adjust the pH value to 13. After this process, the solution was stirred at 80 °C for 30 minutes. The milky solution was washed several times with deionised water and anhydrous alcohol to separate the by-product sulphate ($NaSO_4$). Finally, the solution was filtered, and the final product was dried at 200 or 600 °C for four hours [18].

2.2.1.3 Grinding with bead mills

In ancient times (1 000 BC), the aerodynamic drag force of the wind was harnessed using light wings. This drag force was used to turn a grinding stone to make flour. The same principle could be used to prepare nanopowders using small balls. Chopkar et al. [14] used milling as a method to prepare $Al_{70}Cu_{30}$. Determining the optimum milling time is important to produce nanopowders of the smallest possible size. They should be milled for 10 hours to reduce the size from 300 to 40 nm. Figure 2.1 illustrates how a significant size reduction was achieved during ten hours of milling. However, further milling resulted in an insignificant reduction in particle size. The effect of preparation time on nanoparticle size when using the ball-milling method should be studied to determine the optimum milling time to achieve the minimum particle size. Nevertheless, this method of preparation is expensive due to the high cost of milling balls and not being able to use the same balls to prepare different nanoparticles due to contamination. The cost of the ball-milling nanofluid preparation method limits the widespread application of this method.

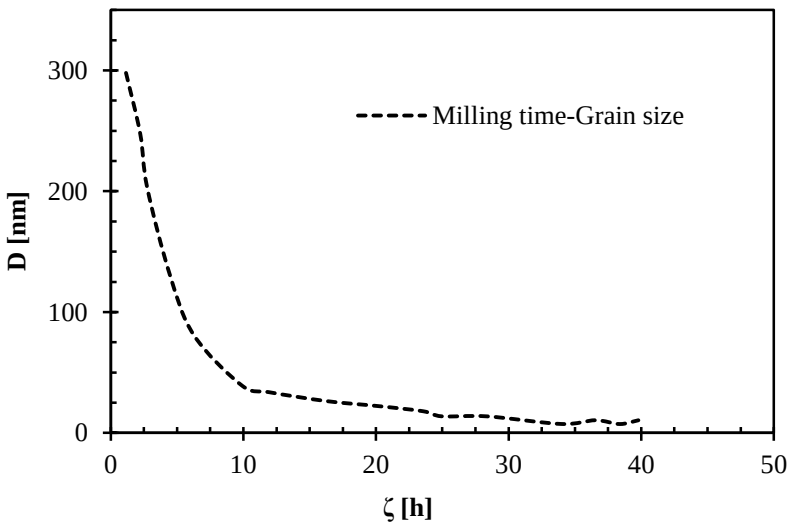

Figure 2.1: The effect of milling time on the size of particles, adopted from [14]

2.2.2 The two-step method

Many researchers use the two-step preparation method to formulate nanofluids. Nanoparticles in powder form have been purchased from a company that uses one of the abovementioned methods to produce nanoparticles in bulk. A suspension of the desired concentration in the desired base fluids could then be made by applying a high-shear homogeniser ultrasonication and magnetic stirrer [19]. This method is a more economical way of preparing large quantities of nanofluids. Nanoparticles have an enormous specific surface area. The tendency of particles towards aggregation is very high due to Van der Waals forces. It is therefore not easy to produce stable nanofluids using the two-step method. However, researchers use different techniques, such as adjusting the pH value of a suspension or adding an adequate surfactant and ultrasonic energy to formulate stable nanofluids.

2.2.2.1 Adjusting the pH value

Surface repulsive forces are changed by the adsorption of ions in a colloidal suspension. A fluctuation in the pH value changes the charge that is acquired between the surface of the particles and its surrounding liquid medium. Adjusting the electrostatic forces due to the increasing repulsive forces between the colloidal particles as a result of adjusting the pH, which fluctuates in ionic concentrations, might lead to a stable nanofluid. However, high acidity (low pH value) and high alkalinity (high pH value) are limited in industrial applications due to the high rate of corrosion. Wang et al. [20] investigated the effect of pH on the stability of Al_2O_3-water nanofluids. They reported the optimum absolute zeta potential value to be 40 mV for 0.05 weight percentage (wt.%) Al_2O_3-water nanofluids at pH = 8.0. Wang et al. [20] adjusted the pH value from 2 to 12, which resulted in increasing the absolute zeta potential value with increasing pH until the maximum zeta potential value of pH = 8 was reached.

A further increase in the pH level resulted in a reduced zeta potential value. Many researchers pointed out the effect of adjusting the pH level on the thermal conductivity and viscosity of nanofluids. Zhu et al. [21] reported the effect of a changing pH value on the thermal conductivity enhancement of alumina nanofluids. They stated the existence of an optimum pH level, which resulted in the highest enhancement of nanofluid thermal conductivity. Lee et al. [22] showed the effect of different pH values on the size of Al_2O_3-water nanofluid. They reported an average alumina particle size of approximately 145 nm at a pH range of between 3.16 and 8.2, while changing the pH to 10.9 increased the average nanoparticle size to 230 nm. Subsequently, at a pH of 12.1, a particle with an average size of 1 100 nm was reported. The effects of nanofluids' pH value on average particle size consequently resulted in improved nanofluid heat transfer performance, due to the influence of nanoparticle size on nanofluid thermal conductivity and viscosity. Warrier and Teja [23] presented the effect of metallic particle size on nanofluids' thermal conductivity. They reported that the thermal conductivity of metal nanofluids increased as the nanoparticle size increased. To the contrary, Chon et al. [24] proposed an enhancement of the thermal conductivity of Al_2O_3-water nanofluid by decreasing the nanoparticle size. They found that the dominant factor of thermal conductivity enhancement was a result of Brownian motion, in which smaller particles have a higher mobility capacity.

Goudarzi et al. [25] investigated the pH-adjusting effect on the thermal efficiency of a solar collector. They reported that the maximum enhancement in the performance of the solar collector was 64.5% when Al_2O_3-water nanofluid is applied at a pH level of 10.5. They reported the effect of changing the pH on the performance of the solar collector, but did not state any reason for this enhancement.

Konakanchi et al. [26] presented a correlation for calculating the pH values of Al_2O_3, SiO_2 and ZnO nanofluids as a function of temperature, volume fraction and nanoparticle size, as shown in Equation 2.1.

$$\frac{pH_{nf}}{pH_{bf}} = [a_1(\frac{T}{T_0})^2 + a_2(\frac{T}{T_0}) + a_3][b_1\varphi^2 + b_2\varphi + b_3][c_1(\frac{d}{d_0})^2 + c_2], \quad \text{Equation 2. 1}$$

where, a_1, a_2, a_3, b_1, b_2, b_3, c_1 and c_2 are regression coefficients, as presented in Table 2. 1.

Table 2. 1: The regression coefficient for the measurement of nanofluids' pH value [26]

Regression coefficients	Al_2O_3	SiO_2	ZnO
a_1	−0.1714584	−0.1404768	−0.1404768
a_2	0.376192	0.1858231	0.1858231
a_3	−0.13514079	0.40701076	0.40701076
b_1	−7.088066	29.769588	29.769588
b_2	1.463864	0.95514341	0.95514341
b_3	0.5181933	1.486459	1.486459
c_1	33.8946855	0.746912628	0.44459085
c_2	12.0607088	2.296413168	1.3669126

There is no report of the effect of pH value on the natural convection of nanofluids. It has been stated that the influence of a variation in the pH value on nanoparticle size and stability could improve nanofluids' heat transfer performance.

2.2.2.2 Ultrasonic energy

In the two-step method, the preparation of nanofluids' weak aggregation of particles should be broken down. Electrical power in the ultrasonic generator was converted to signals that drove a piezoelectric transducer. The electrical signals were converted to a mechanical vibration using a transducer.

During the process of sonication, sound waves with different amplitudes propagated into the sample through an ultrasonication probe. The propagation of sound waves produces high- and low-pressure cycles in which high-intensity sonic waves produce bubbles. These bubbles collapse through a cavitation process. The erosion and collapse of thousands of micro bubbles in cavitation create shock effects. Ultrasonication is accompanied by a rise in local heating temperature. Ultrasonication also makes an annoying high-pitched noise [27]. The time of sonication could be controlled by the number of energy waves that have been transferred into the colloidal suspensions.

Some researchers have pointed out the necessary sonication time without providing any reason why the sonication effect on the nanoparticle size distribution was reported in the open literature. Chung et al. [28] studied the effect of different methods of sonication on the preparation of ZnO nanofluids. They concluded that using an ultrasonic horn is more effective than using an ultrasonic bath. Their results showed the effect of sonication time on the average particles size, which changes from 140 to 100 nm if sonication time is increased from 10 to 60 minutes. The average primary size given by the manufacturer was 20 nm.

Sonication time also affects the thermal conductivity and viscosity of nanofluids due to a change in the average size of the nanoparticles as a result of sonication. Suganthi and Rajan [29] showed the effect of sonication time on the viscosity measurement of ZnO. The viscosity of a 4% volume fraction of ZnO dispersed in propylene glycol was changed from 41 mPa.s to 34 mPa.s if the sonication time was increased from four to 16 hours. Another study showed that the average particle size of CuO nanoparticles (d = 10–30 nm according to the manufacturers' claim) dispersed in EG was changed from 90 to 56 nm if sonication time was increased from one hour to nine hours [30].

Hong et al. [31] investigated the effect of sonication time on thermal conductivity enhancement using Fe nanoparticles. They reported an 18% increase in the thermal conductivity of EG at 0.55% volume fraction of Fe when the sonication time was increased from 0 to 55 minutes. The effect of sonication time on the preparation of Al_2O_3-water nanofluids by measuring the zeta potential value was studied by Lee et al. [32]. They reported that five hours' sonication time provided the highest value of zeta potential (34 mV at 0.1 vol.% and 25 °C). A further increment in the sonication time reduced the zeta potential value. Pastoriza-Gallego et al. [33] prepared Al_2O_3-water nanofluid, of which the nanoparticles were supplied by different manufacturers and the stability study of a single-step dispersed nanofluid was compared with a two-step prepared nanofluid. The stability of various preparation techniques has been investigated using UV-visible spectroscopy of 0.004 wt% of Al_2O_3-water nanofluid at 25 °C. It was found that applying an ultrasonic homogeniser provided better stability than using ultrasonic baths. The dispersed single-step Al_2O_3-water nanofluid has better stability in comparison to two-step prepared Al_2O_3-water nanofluid.

2.2.2.3 Adding surfactants

The preparation of stable nanofluids is crucial to investigating the thermal characteristics of nanofluids. Adding surfactants might improve the stability of nanofluids. The interaction between a base fluid and solid particles at the interface is manipulated to formulate stable nanofluids. If the interface possesses positive energy, it could overcome the weak attraction energy between particles [34].

Moreover, the magnitude of surface tension plays a role in the interfacial region, which is related to the interfacial energy. Liquid molecules pull each other in all directions. However, in the presence of solid particles, this will change the spatial intermolecular force balances. On the one hand, liquid molecules attract one another with intermolecular forces if this

attraction force is stronger than the forces between the liquid and the solid particles. Therefore, liquid molecules at the interface move away from the particle-liquid interaction region. On the other hand, fluid compression resistance will reduce the size of the interfacial layer until the force balance can be established. Nevertheless, the surface tension of solid particles would be changed by the adsorbtion of a surfactant. Interfacial energy would be released by the adsorption of a surfactant, which results in increasing the attraction forces between solid particles and liquid molecules. Using a surfactant to prepare a stable sample is known as a steric mechanism in colloidal dispersion, as shown in Figure 2.2.

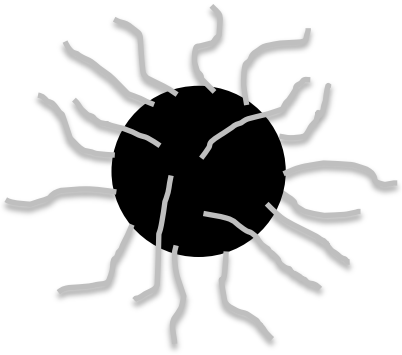

Figure 2.2: Schematic steric mechanism for the preparation of a stable colloidal dispersion

Generally, surfactant molecules can be divided into the following categories [34]:

a. Surfactants with hydrophobic (oil-loving, water-fearing) tails and hydrophilic (water-loving) heads, as shown in
b. Figure 2.3.
c. Surfactants with hydrophilic (water-loving) tails and hydrophobic (water-fearing) heads.

In water, as a polar solvent, the hydrophobic tail usually contains hydrocarbons, fluorocarbons or siloxane chains, while in a less polar solvent, for example, polypropylene glycol, a fluorocarbon or siloxane chain might be suitable.

Hydrophilic head group Hydrophobic tail

Figure 2.3: A schematic structure of the typical hydrophilic molecule

An excess amount of a surfactant agent could mean the instability of a nanofluid, as well as the heat transfer rate, due to the production of micelles. An optimum value for surfactant concentration to formulate a stable nanofluid should be studied as a function of the base fluids and nanoparticles. The optimum concentration of surfactant agent is known as the critical micelle concentration (CMC).

The best way of finding the CMC is by systematically measuring the surface tension of a nanofluid. The surface tension rapidly decreases as the concentration of a surfactant increases until it reaches the CMC value. Further adding the surfactant does not change the surface tension any more. The equivalent conductivity measurement of a suspension could also indicate the CMC of the surfactant. Figure 2.4 illustrates how the equivalent conductivity gradient changes with surfactant concentration, so that, at that specific concentration, the slope of equivalent conductivity shifts; this is known as the CMC. Jiang et al. [35] studied the suspension of carbon nanotubes (CNT) in water using sodium dodecyl sulfate (SDS). By using a phase diagram, they reported that a 0.5 wt% CNT concentration needed a 2.5 wt% as the CMC of the surfactant. They showed that homogenous dispersions were formulated by varying the concentration of CNT and keeping the ratio of the concentration of the surfactant to the nanotubes the same (the surfactant's mass fraction is five times that of the nanotube concentration). An Al_2O_3-water nanofluid was prepared using Triton X-100 of a CMC at 0.021 wt%, as presented by Yousefi et al. [36]. This value was close to CMC = 0.2 mM, which was reported by Dennis [37].

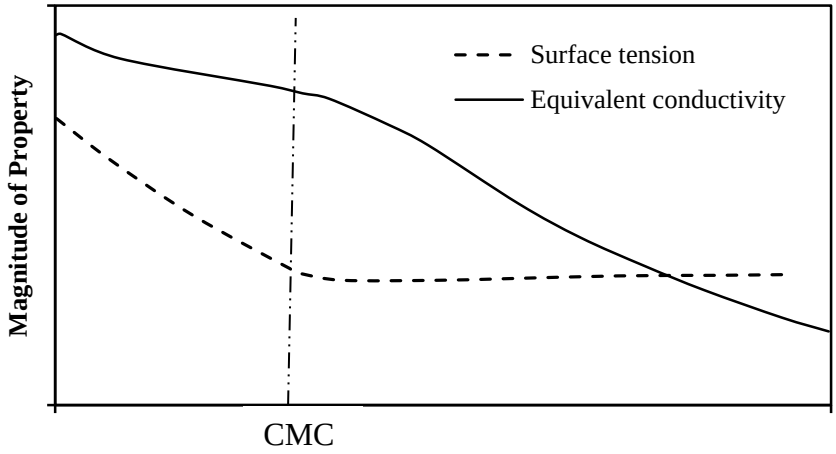

Figure 2.4: Obtaining the CMC concentration via different measurements adopted from [38]

Sakamoto et al. [39] showed the effect of the tail length of cetyltrimethylammonium bromide (CTAB) on the CMC. They showed that when the tail length increases, the CMC decreases. For example, stearyl trimethyl ammonium chloride had a 0.34 mM CMC. A list of common surfactants that have been used by researchers is given in Table 2.2.

Table 2.2: List of surfactants that are used in the literature

Surfactant name	Base fluid	Nanofluid	Concentration
Benzalkoniumchloride, benzethoniumchloride [40]	TH66	SiO_2	5 wt% (0.12 M)
Oleic acid and cetyltrimethyl ammonium bromide [41]	Water	TiO_2	0.01 to 0.02%
Sodium hexametaphosphate [42]	Water	ZnO	20% mass of ZnO
Sodium dodecyl sulfate [43]	Water	TiO_2	0.1 wt%
Triton [44]	Water	CuO	40% mass of CuO
Gum arabic [45]	Water	(MWCNT)	0.25 wt%
Sodium dodecylbenzene sulfonate [20]	Water	Al_2O_3, Cu	0.1 wt%
Polyvinylpyrrolidone [46]	Water	Graphite	0.5 wt%

2.3 Indication of nanofluids' stability

2.3.1 Zeta potential

Colloidal suspensions have an electrical charge. The base fluid and solid particles contribute to the dispersion surface charge that could change by adjusting the pH value. Particles have two distinct electrical imaginary layers. The first layer, which is a very confined volume around the particles, contains congested opposite charge ions known as the Stern layer. In the second layer, ions can move more freely within the layer. An imaginary layer of base fluid, within which the ions have bonded, will move when a particle moves. The ions that are far from the boundary in the bulk fluid will not move with the particle [47]. The zeta potential is an electrical potential difference between the second boundary (double layer) and a bulk fluid [47]. As shown in Figure 2.5, the zeta potential gives an indication of the stability of a suspension.

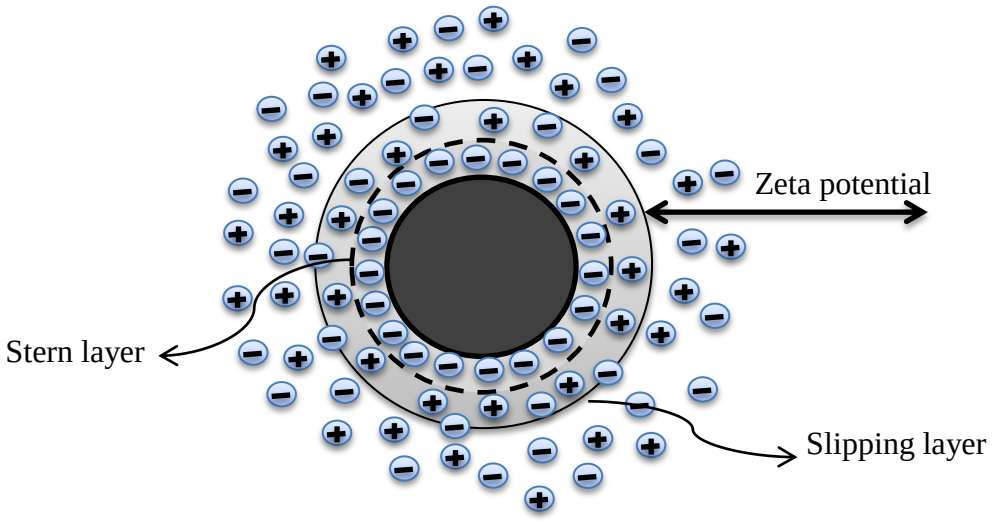

Figure 2.5: A schematic of an electrostatic stabilisation mechanism

Stable nanofluids can be prepared by adjusting the pH value. The zeta potential value changes by changing the pH. The iso-electric point (IEP), where there are no electrical forces between the suspended particles and the base fluid, can be indicated by measuring the zeta potential value as a function of pH, in which the specific pH value's zeta potential equals zero.

Deviation of zeta potential from the IEP gives an indication of a nanofluid's stability. An absolute zeta potential value greater than 30 mV indicates good stability of the sample [47]. Figure 2.6 shows the effect of a changing pH value on the zeta potential.

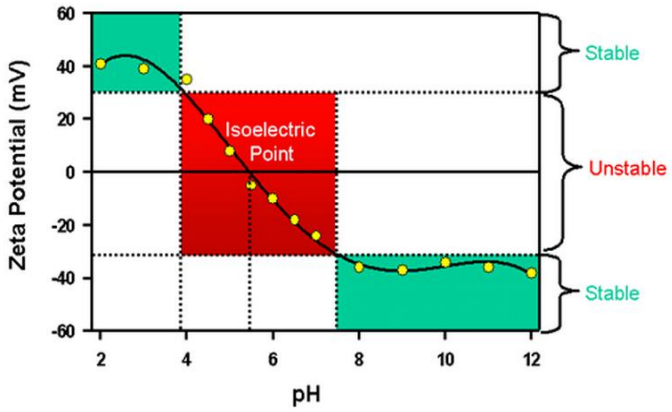

Figure 2.6: The effect of pH value on zeta potential [47]

Adjusting the pH value helps the formulation of stable nanofluids, but it should be considered that a high or a low pH value puts constraints on nanofluids' industrial applications due to the high corrosion rate.

Zhu et al.[21] studied the effect of a pH ranging from 2 to 12 on the zeta potential of Al_2O_3-water nanofluid. They showed that the nanofluid had the highest absolute zeta potential value at a pH of around 8. In order to change the pH value, HCl and NaOH were used. Lee et al. [48] showed that CuO-water nanofluids with a pH of 3 had a higher thermal conductivity than nanofluids with a pH of 8. They also illustrated that CuO-water had a higher zeta potential at pH = 3 than pH = 8. Therefore, they pointed out the effect of pH value on the particle's aggregation size, and subsequently, its effects on the thermal conductivity of the nanofluid.

Konakanchi et al. [26] have investigated the effect of temperature on nanofluids' pH value. They showed that the pH value of ZnO, Al_2O_3 and SiO_2 nanofluids decreased (1 to 3 units) when the temperature increased. Subsequently, nanofluids' zeta potential should be considered a function of temperature.

The pH value of nanofluids has an influence on the mean aggregation size of nanoparticles due to changing electrostatic forces. Subsequently, the thermophysical properties of a nanofluid are a function of the pH. Hence, nanofluids' zeta potential was influenced by nanoparticle volume fractions, as stated by Suganthi and Rajan [42], who pointed out that 0.25 vol.% and 2 vol.% concentrations had zeta potential values of -38 mV and -50.4 mV, respectively.

When nanofluids are prepared by changing the pH value, the IEP of the nanofluid should be avoided in order to formulate a stable nanofluid. Berg et al. [49] studied the IEP of some metal-oxide nanofluids, such as Al_2O_3, ZnO, CeO_2, TiO_2 and Fe_2O_3. The manufacturer claimed the nanoparticle size to be roughly 30 nm. The results of the study by Berg et al. [49] showed the nanofluids' IEPs at the pH value for Al_2O_3 = 7.06, ZnO = 7.13, CeO_2 = 6.71, TiO_2 = 5.19 and Fe_2O_3 = 4.24. They showed that a zeta potential of Al_2O_3 changed from 45 mV to 30 mV as the pH value changed from 3 to 9. However, Wang et al. [20] reported 0.05 wt% of Al_2O_3-water (d = 15–50 nm) with surfactant sodium dodecylbenzene sulfonate (SDBS) (0.1 wt%) at pH = 8 and pH = 7 had zeta potentials of -40 mV and -38 mV respectively. Zhu et al. [21] prepared an Al_2O_3-water nanofluid by using surfactant SDBS. They reported similar results to those of Wang et al. [20]. Witharana et al. [50] investigated Al_2O_3 (a mixture of 50% water and 50% EG) (d = 13 nm) and reported a zeta potential of 0 (IEP) at a pH of 9.5. An IEP of 0.005% v/v Al_2O_3-water in 0.01 molar (M) KCl was observed at pH = 10.3, as stated by Pastoriza-Gallego et al. [33]. Colla et al.[51] measured 1 wt% of ZnO-water nanofluid with pH = 7.5 to have a zeta potential of +48 mV. Chang and Tsai [52] reported an IEP of 0.05 wt% of ZnO-water at a pH of 9.

It can be concluded that the inconsistency of nanofluids' IEPs is evident in literature. The zeta potential value measurement of nanofluid gives an indication of its stability, which should be investigated by researchers to ensure the stability of nanofluids.

2.3.2 Characteristics with microscopy

Developments in technology provided an opportunity to use very accurate microscopy with a powerful magnification. Researchers use TEM and SEM to characterise nanofluids.

The study of nanofluids with normal TEM and SEM is accompanied by the drying of samples. Therefore, the aggregation effect due to the preparation of the samples is not clear. However, researchers have been using TEM and SEM to study the morphology of nanopowders. Chang and Tsai [52] showed the size of the synthesised ZnO with a novel model. They do not clarify whether the aggregations resulted from the drying out of the sample or whether they had been produced during a malfunction of the nanopowder manufacturing process. Chang and Tsai [52] reported that the average size, measured by a zetasizer, was 150 nm when suspended in water as a base fluid.

The characterisation of nanofluids with the two-step method should be accompanied by TEM and SEM images to ensure the manufacturer's claim concerning the size and morphology of the nanoparticles. Usually, there is a size distribution of nanoparticles and the reported average size of nanoparticles was bigger than that claimed by the manufacturer. Chung et al. [53] reported a mean size of 92 nm for ZnO nanoparticles, which the manufacturer claimed was d = 20 nm. Sharifpur et al. [54] examined the particle size distribution of Al_2O_3-glycerol (19 nm, 139 nm and 160 nm) nanoparticles with TEM and reported a size distribution. However, they did not measure the mean size of their samples with a zetasizer.

Figure 2.7 demonstrates TEM and SEM images of ZnO-water nanofluid. The manufacturer claimed that the diameter of the nanoparticles was 20 nm. However, the SEM image, which was taken from dried powders before applying sonication energy, showed the aggregation of the ZnO nanoparticles. The TEM image illustrates the size distribution of the ZnO-nanofluids

after applying sonication energy density (α = 2 kJ/ml). One can see particles as big as 20 and 60 nm in the TEM image.

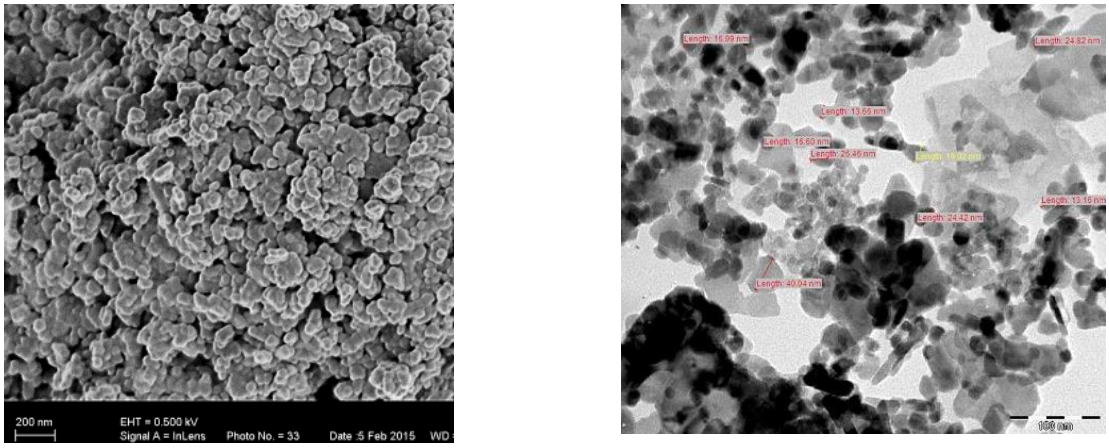

Figure 2.7: The SEM and TEM images of ZnO-water nanofluids (d = 20 nm)

The TEM and SEM images could help establish the morphology of nanoparticles. Some parts of the TEM images are darker than others due to particles sitting on top of each other during the drying out of the sample, which results from using a much diluted nanofluid as a test sample. Garg et al. [55] pointed out the uncertainty of the reported image with the conventional method of TEM. They used novel techniques, such as wet TEM, to observe multi-walled carbon nanotubes (MWCNTs). They reported the effect of specific energy – the division of sonication energy to the sample mass – on the viscosity and heat transfer performance of the MWCNTs. This new technique could make it possible to observe the sample in liquid form. Therefore, there is no need to dry the sample. Hence, whatever is shown in the microscopy image has the same characteristics as the original sample.

2.3.3 Zetasizer

The characteristics of the nanofluid samples in liquid form are essential for researchers due to the similarity of the sample characteristic to the original nanofluid. A zetasizer is capable of measuring the average size, as well as the size distribution of nanoparticles in base fluids in liquid form. Haghighi et al. [56] reported the average size of Al_2O_3-water (the manufacturer's claim was d = 10 nm) both with and without a surfactant (polyacrylic acid copolymer sodium

salt (0.5 wt.%) based on the nanoparticle amount) as 60 and 180 nm respectively. Berg et al. [49] measured the average size of Al_2O_3-water (the manufacturer's claim was d < 50 nm) as being approximately 250 nm. The average size of 182 nm for Al_2O_3-water (the manufacturer's claim was d = 40–50 nm) was reported by Lee et al. [57]. They also reported 326 nm as the average size of CuO-water (the manufacturer claimed d = 23–37 nm). Taylor et al. [58] reported 256 nm as the average size of alumina nanoparticles suspended in water. They pointed out that the higher value for the average size was due to a small agglomeration of nanoparticles and a measurement technique that was used by the Malvern zetasizer to estimate the average size of nanoparticles. The Malvern zetasizer uses the Stoke-Einstein [59] as correlated in Equation 2.2:

$$d = \frac{\kappa_B T}{3\pi D\mu} \qquad \text{Equation 2.2}$$

where d is the hydraulic diameter, κ_B is the Boltzmann constant ($1.3806488 \times 10^{-23}$ m^2 kg s^{-2} K^{-1}), T is the absolute temperature, D is the diffusive coefficient and μ is the dynamic viscosity of the medium.

The average size reported when using a zetasizer was usually greater than the manufacturer's claim or the reported size when using TEM and SEM. Mahbubul et al. [60] prepared Al_2O_3-water (the manufacturer's claim was d = 13 nm). They investigated the sonication time effect on the size distribution of the nanofluids. They reported that the average size of the nanoparticles, measured by the model Malvern 3000HS zetasizer, changed from 210 to 115 nm, respectively, when the sonication time was increased from 0 to 120 minutes. Yu et al. [61] reported that the average size of ZnO (primary size 10 to 20 nm) in EG varied from 500 nm (after five minutes of sonication) to 227 and 209 nm after two hours and four hours of sonication, respectively. Chang and Tsai [52] studied ZnO-water (d = 20 nm) in which 150 nm was reported as the mean average size.

Nanoparticle size distribution, which was measured with a zetasizer, is usually in the form of normal distribution function and intensity percentage. It illustrates the existence of size distribution rather than uniform size, as shown in Figure 2.8, which is in agreement with the TEM images.

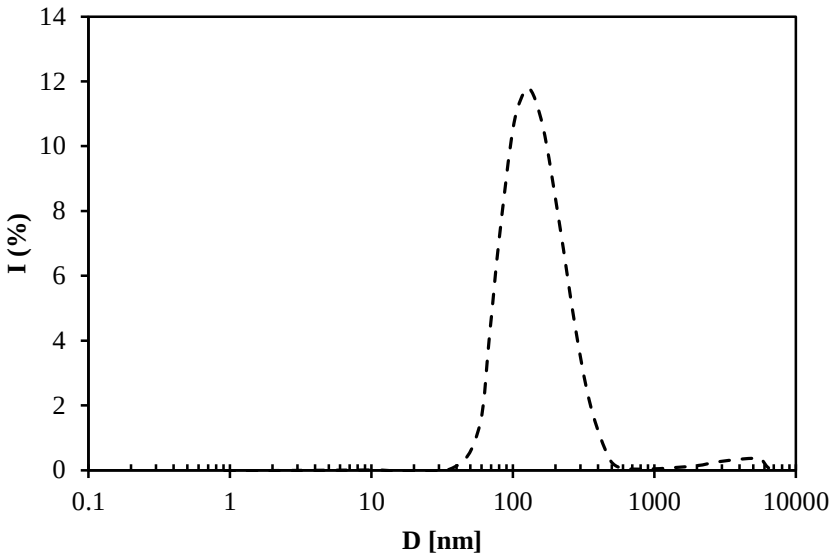

Figure 2.8: The size distribution of ZnO-water nanofluids

2.3.4 UV-visible spectrophotometer

The investigation of colloidal particles should include a stability analysis of samples. Many researchers have just visually examined the stability of nanofluids. The different stages of aggregation in a colloidal system is illustrated in[47]. Visual techniques could just confirm sedimentation in the phase separation stage.

Putra et al. [62] confirmed the stability of Al_2O_3-water and CuO-water nanofluids only by the visual observation method. Chen et al. [63] investigated the treatment of MWCNTs. They examined the stability of their samples visually and, owing to that, a phase separation was obviously an indication of instability. Visual observation is an indication of stability in terms of phase separation. However, for nanofluids in which some particles are coagulated or flocculated and phase separation has not completely happened yet during an experiment, there

is no benefit to using a visual method to ensure the accuracy of the results of an experiment. In fact, the visual observation method as an indication that stability should be confirmed using other scientific methods.

A UV-visible spectrophotometer is able to examine the stability of nanofluids. In this method, the first absorbance of a sample has been measured at different wavelengths. The maximum absorbance would be checked over time to ensure the stability of the sample if there is no change in the absorbance over time. Cabaleiro et al. [64] examined the changing absorptivity at the highest wavelength (310 nm) of ZnO nanoparticles suspended in a mixture of ethane-1,2-diol + water. They reported a 13% decrease in absorptivity during 70 hours of the test for a nanofluid of 0.01 wt% concentration. The volume fraction of a nanofluid affects its stability, such that, at a very low volume fraction, the sedimentation of nanofluids occurs more rapidly than at a high volume fraction. Mo et al. [65] studied the effect of volume fraction on the stability of TiO_2-water nanofluid. Concentrations of 0.05, 0.3 and 0.7wt% were investigated. They showed a 20 and 2.7% reduction in the absorbency of samples at the 0.05 and 0.3wt% concentrations respectively. Malvern [66] stated that nanofluids' zeta potential decreases with an increase in nanofluid concentration. To the contrary, Suganthi and Rajan [42] confirmed the scaling up of zeta potential with an increasing volume fraction of ZnO-water nanofluid. Therefore, examining the stability of nanofluids with UV-visible spectroscopy is in line with increasing the zeta potential with increasing volume fractions of nanofluids.

2.4 The thermophysical properties of nanofluids

Ho et al. [67] showed the effect of thermophysical properties on natural convection. They showed that the feasibility of enhancing natural convection depends on the property ratio factor of the thermophysical properties, which play a role in natural convection, as shown in Equation 2.2.

$$F_n = \left(\frac{\beta_{nf}}{\beta_{bf}}\right)^n \left(\frac{\rho_{nf}}{\rho_{bf}}\right)^n \left(\frac{c_{p.nf}}{c_{p.bf}}\right)^n \left(\frac{k_{nf}}{k_{bf}}\right)^{1-n} \left(\frac{\mu_{nf}}{\mu_{bf}}\right)^{-n} \quad \text{Equation 2.2}$$

In this way, if F_n has a value of more than 1, the nanofluid enhances natural convection. The exponent in the equation should have a value between 0 and 1. A typical exponent (n) is chosen as n = 1/3.

2.4.1 Thermal conductivity

Conventional heat transfer fluids have a very low thermal conductivity, which is a barrier to a higher heat transfer rate in comparison to solid metal particles. Scientists proposed a theory that the suspension of solid particles with a higher thermal conductivity could improve the heat transfer rate. This could be traced back to Maxwell's work in the late 19th century [3]. Advancements in technology give scientists the opportunity to produce solid particles with a size range of nanometres to overcome challenges like sedimentation and corrosion, which accompany solid particles in the micrometre range and greater size.

Choi [4] investigated enhancing the performance of heat exchangers with a suspension of metallic nanoparticles in conventional coolant fluids. He pointed out the theoretical possibility of reducing pumping power with a factor of 10 by using nanofluids due to an increase in the thermal conductivity of their base fluids with a factor of 3. However, the thermal conductivity of nanofluids was improved with a dispersion of nanoparticles. On the other hand, the viscosity of nanofluids also increases with escalating nanoparticle concentrations [9], [42] and [68].

When the enhancement in the thermal conductivity of 1 and 4% volume fractions was measured experimentally, Al_2O_3-water nanofluid (d = 33 nm) was 2 and 15% [69]. Colangelo et al. [70] experimentally measured the thermal conductivity of Al_2O_3 (d = 45 nm), CuO (d = 30 nm) and ZnO (d = 60 nm) in deionised water. At 1% volume fraction, a 2.5, 3.2 and 3.6%

enhancement was reported respectively. At 3% volume fraction, the effective thermal conductivity of the base fluid was 6.7, 8.3 and 11.4% respectively. Increasing the volume fraction improves the thermal conductivity of nanofluids. For example, the thermal conductivity enhancement jumped from 2.5 to 6.7% for 1 and 3% volume fraction of Al_2O_3-water nanofluid, respectively.

The escalation of nanofluids' viscosity with increasing volume fraction, as well as the stability of nanofluids at higher volume fractions, needs to be considered. Das et al. [71] pointed out a 2.5% improvement in the thermal conductivity of water with a dispersion of 1% volume fraction Al_2O_3 nanoparticles (d = 38 nm). The improvement climbed to 10% at a 4% volume fraction. Said et al. [72] measured the thermal conductivity of 1 and 5% volume fraction Al_2O_3-water (d = 13 nm). They reported 3 and 8% enhancements in the thermal conductivity of water. Nevertheless, the nanofluid viscosity at 5% volume fraction improved by 300%. Therefore, the beneficial thermal conductivity enhancement of nanofluids is offset by increasing pumping power because of the increasing viscosity of the base fluids due to suspending nanoparticles.

In addition to volume fraction, other factors such as temperature, particle size, the thermal conductivity of the nanoparticle and the thermal conductivity of the base fluid play a role in enhancing thermal conductivity [8], [73], [74] and [75]. Das et al. [71] showed the thermal conductivity of Al_2O_3-water (d = 38 nm) and CuO-water (d = 28 nm) nanofluids to be enhanced with increasing temperature.

Changing the temperature from 20 to 50 °C resulted in a 15% enhancement for 4% volume fraction Al_2O_3-water and a 25% enhancement for 4% volume fraction CuO-water nanofluids. Vajjha and Das [2] reported that the thermal conductivity of ZnO-nanofluid (60 wt% EG and 40 wt% water) decreased slightly (5%) by increasing the size of the nanoparticles from 29 to

77 nm. Syam Sundar et al. [76] showed a 6% enhancement in the effective thermal conductivity of 1.5% volume fraction of Al_2O_3-water nanofluid by changing the base fluid mixture from 60% EG and 40% water to 20% EG and 80% water. The base fluid's thermal conductivity changed from 0.334 to 0.492 W/m.K when the base fluid changed from 60% EG and 40% water to 20% EG and 80% water. The thermal conductivity measurement of nanofluids reveals the influence of many factors on effective thermal conductivity.

To predict the effective thermal conductivity of nanofluids, researchers suggested mathematical models. In addition to the abovementioned factors to determine the effective thermal conductivity, other factors, such as Brownian motion, the clustering of nanofluids, nanolayering in the interface of the solid particle and the liquid, ballistic transport and thermophoretic effect, should also be considered by researchers [77]. Maxwell expressed a simple model for a solid-liquid mixture [78] as shown in Equation 2.4.

$$k_{nf} = k_{bf}\left(1+\frac{3\left(\frac{k_p}{k_{bf}}-1\right)\varphi}{\left(\frac{k_p}{k_{bf}}+2\right)-\left(\frac{k_p}{k_{bf}}-1\right)\varphi}\right) \qquad \text{Equation 2. 3}$$

In Equation 2.4, effective thermal conductivity depends on the thermal conductivity of the base fluid, the thermal conductivity of the nanoparticle and the volume fraction. It does not show the effect of other factors, for example, size, temperature and shape. The Wasp model has also been used to predict the thermal conductivity of spherical nanoparticles [79], as given in Equation 2.5.

$$k_{nf} = k_{bf}\frac{k_p + 2k_{bf} - 2\varphi(k_{bf}-k_p)}{k_p + 2k_{bf} + \varphi(k_{bf}-k_p)} \qquad \text{Equation 2. 4}$$

The Wasp model has simplified the Hamilton-Crosser model by assuming that the shape factor equals 3 for spherical particles [79]. Many other thermal conductivity models were

presented by Aybar et al. [77] and Kleinstreuer and Feng [80]. The predicted effective thermal conductivity, using the available models and experimental thermal conductivity measurement of nanofluids, showed different values, in particular at higher volume fractions [79]. However, for a low volume fraction (less than 1% volume concentration), the predicted value of nanofluids' thermal conductivity was the same when using various models, as stated by Sharifpur et al. [81]. Therefore, the theoretical thermal conductivity of Al_2O_3-water nanofluids with a 0.6% volume concentration as the maximum volume fraction, which was used in the study, is presented in Table 2.3.

Table 2.3: The effective thermal conductivity of 0.6% volume concentration using models

Model	**Formulation**	**K_{nf} (0.6 vol%) [w/m.K]**	**Enhancement**
Maxwell [8]	$k_{nf} = k_{bf}\left(1+\frac{3\left(\frac{k_p}{k_{bf}}-1\right)\varphi}{\left(\frac{k_p}{k_{bf}}+2\right)-\left(\frac{k_p}{k_{bf}}-1\right)\varphi}\right)$	0.635	2%
Wasp [8]	$k_{nf} = k_{bf}\frac{k_p+2k_{bf}-2\varphi(k_{bf}-k_p)}{k_p+2k_{bf}+\varphi(k_{bf}-k_p)}$	0.635	2%
Maïga and Nguye [69]	$k_{nf} = k_{bf}(1+2.72\varphi+4.97\varphi^2)$	0.634	2%

The calculated thermal conductivity of nanofluid has an enhancement of 2%, while the experimental measurement of Al_2O_3-water nanofluid confirmed a similar enhancement as presented by Colangelo et al. [70], Das et al. [71] and Said et al. [72]. It can be concluded that the thermal conductivity models at low volume fractions (less than 1% volume concentration) can be used to determine the effective thermal conductivity of nanofluids.

2.4.2 Viscosity

Viscosity is the internal resistance of fluids against the current of convection. Viscous forces have a significant effect on nanofluids' natural convection. Suspending nanoparticles in a

base fluid changes the effective viscosity of the base fluid. Many factors, such as volume fraction, temperature and particle size, play a role in the viscosity of colloidal suspensions [9]. Many researchers reported an increase in nanofluids' viscosity as particles' volume fraction increases [9]. However, an increase in temperature causes the viscosity of nanofluids to decline exponentially, as presented by Namburu et al. [82], Namburu et al. [83], Nguyen et al. [10] and Syam Sundar et al. [76]. Nevertheless, the viscosity of nanofluids increases as the size of the nanoparticles decreases [82] and [84]. This enhancement is more pronounced at a smaller size.

Many researchers have used classical theoretical models, such as those of Einstein [85] and Brinkman [86], to calculate the effective viscosity of nanofluids, as stated in Equation 2.6 and Equation 2.7:

$$\mu_{nf} = \mu_{bf}(1+2.5\ \ ) \qquad \text{Equation 2. 5}$$

$$\mu_{nf} = \frac{\mu_{bf}}{(1-\varphi)^{2.5}} \qquad \text{Equation 2. 6}$$

Experimental measurements showed a deviation between the calculated value using theoretical models and experimental measurements, especially at high volume fractions [10] .

The effect of adopting various viscosity models on the simulation of nanofluids' natural convection, which was more dominant than the effect of various thermal conductivity models, has led to contradictory results [67]. Therefore, an experimental measurement of the viscosity of nanofluids may ensure a more accurate conclusion in the experimental study of nanofluids' natural convection heat transfer.

2.4.3 Other thermophysical properties

Effective nanofluid thermophysical properties, such as density, specific heat and thermal expansion coefficient, are less important than the thermal conductivity and viscosity of

nanofluids in the natural convection of nanfluids. The theoretical model of density for the two-phase mixture was presented by Cheremisinoff [87] and Pak and Cho [88], as shown in Equation 2. 7.

$$\rho_{nf} = \varphi\rho_p + (1-\varphi)\rho_{bf} \quad \text{Equation 2. 7}$$

where ρ_{nf} is the nanofluid density, ρ_p is the nanoparticle density, ρ_{bf} is the nanofluid density and φ is the volume fraction. This shows the effective density of nanofluids as a function of volume fraction, the density of the base fluid and the density of the nanoparticles. Pak and Cho [88] experimentally measured the density of Al_2O_3-water (d = 13 nm) and TiO_2-water (d = 27 nm). They reported a 0.6% deviation between the measured density of nanofluids (volume fraction less than 4%) and the calculated value of density using Equation 2. 7.

Pastoriza-Gallego et al. [33] reported that the influence of particle size on the changing density was negligible and in the range of uncertainty error. Vajjha et al. [89] experimentally measured the density of Al_2O_3 and ZnO in a mixture of 60 wt% EG and 40 wt% water. They showed a negligible deviation between the experimental measurement and the calculated density using Equation 2. 7. Therefore, Equation 2. 7 is capable of accurately calculating nanofluid density.

Pak and Cho [88] used Equation 2.8 to calculate the specific heat of nanofluids.

$$c_{p_{nf}} = \varphi c_{p_p} + (1-\varphi)c_{p_{bf}} \quad \text{Equation 2.8}$$

However, Buongiorno [90] calculated the specific heat of nanofluids using Equation 2.9.

$$c_{p_{nf}} = \frac{\rho_p \varphi c_{p_p} + (1-\varphi)\rho_{bf} c_{p_{bf}}}{\rho_{nf}} \quad \text{Equation 2.9}$$

The specific heat of nanofluids with an increasing nanofluid concentration decreased according to Pak and Cho [88]. A comparison of the experimental measurements of Al_2O_3-water nanofluid and Equation 2.8 and Equation 2.9, illustrated in Equation 2.9 has better agreement with experimental measurements [91]. Vajjha and Das [92] experimentally measured the specific heat of nanofluids and confirmed that Equation 2.9 showed a better agreement with the experimental data. Thus, this equation was used in this study.

Nanofluids' volumetric thermal expansion coefficient may be calculated using the mixing solid-liquid theory [93] and [67], as shown in Equation 2.10.

$$\beta_{nf} = \varphi\beta_p + (1-\varphi)\beta_{bf} \qquad \text{Equation 2.10}$$

The volumetric thermal expansion coefficient of liquids is usually larger than the thermal expansion coefficient of solid nanoparticles. For example, the thermal expansion coefficient of water and Al_2O_3 is 4×10^{-4} [1/°C] and 8×10^{-6} [1/°C] respectively [93]. Usually, researchers have used a diluted nanofluid volume fraction. Therefore, the value of 1-φ is greater than φ, which resulted in the approximation of nanofluids' thermal expansion coefficient with their base fluids' thermal expansion coefficient. Nayak et al. [94] showed that the volume metric expansion coefficient increased with increasing temperature. Ho et al. [69] experimentally measured the volumetric expansion coefficient of Al_2O_3-water nanofluid. The experimental results were in better agreement with the formula stated in Equation 2.11.

$$\beta_{nf} = \frac{\varphi\rho_p\beta_p + (1-\varphi)\rho_{bf}\beta_{bf}}{\rho_{nf}} \qquad \text{Equation 2.11}$$

2.5 Heat transfer of nanofluids

Nanofluid is a modern engineered colloidal suspension and promises better thermal management. An abnormal increase in effective thermal conductivity is not the only factor to play a role in the improvement of nanofluids' heat transfer rate, as pointed out by Buongiorno

[90]. Factors of intensifying turbulence and thermal dispersion, such as inertia, Brownian diffusion, thermophoresis, diffusiophoresis, Magnus effect, fluid drainage and gravity, which play a role in the slip velocity of nanoparticles relative to the base fluids, might explain the heat transfer enhancement or deterioration of nanofluids according to Buongiorno [90].

Many experimental investigations of forced convection have reported an increase in the concentration of nanofluids [95], [96], [97] and [98], which resulted in the enhancement of nanofluids' heat transfer coefficient. However, Tanaka and Easton [99] reported that turbulent kinetic energy could either be augmented by adding nanoparticles or decline. Haghighi et al. [100] showed that the equal pumping power using nanofluids (Al_2O_3, TiO_2, and ZrO_2 suspended in water) reduced the heat transfer performance of the base fluid (water).

However, for the same Re, higher heat transfer coefficients were reported by suspending nanoparticles in the base fluid. The heat transfer enhancement of nanofluids with increasing nanoparticle concentration has a penalty of increasing shear stresses and pressure losses in forced convection. Thus, care should be taken when choosing an optimum value for the concentration in order to improve the system's heat transfer performance. Wu et al. [101] investigated the heat transfer coefficient of Al_2O_3-water in the laminar regime and proposed Equation 2.12.

$$\frac{h_{nf}}{h_{bf}} = \left(\frac{\rho_{nf}}{\rho_{bf}}\right)^{0.85}\left(\frac{k_{nf}}{k_{bf}}\right)^{0.6}\left(\frac{\mu_{bf}}{\mu_{nf}}\right)^{0.45}\left(\frac{c_{p_{nf}}}{c_{p_{bf}}}\right)^{0.4} \quad \text{Equation 2.12}$$

The increase in volume fraction improved the heat transfer coefficient at a similar Re. However, for the same velocity improvement in natural convection, heat transfer coefficient was not reported due to suspending the nanofluid.

2.5.1 Natural convection

Natural convection occurs in fluids due to a density gradient as a result of temperature differences. One way to study natural convection is using a confined volume due to its widespread applications in engineering. The cooling of electronic equipment, solar collectors, the ventilation and cooling of buildings, aeronautics, transportation, the cooling of nuclear reactors, pharmaceutics and the food industry are some applications of natural convection in a confined volume [11]. Natural convection inherently has a low heat transfer coefficient. Investigations of how to increase the heat transfer coefficient of natural convection should be considered. Two methods are used to enhance the heat transfer performance of a system. The first method is a new design, for example, geometry optimisation, which is not applicable to a miniaturised system, such as micro-electromechanical systems (MEMS). An alternative way of enhancing heat transfer capacity is by using advanced heat transfer fluids.

Many researchers focus on nanofluids as a promising heat transfer medium. Many numerical investigations of the natural convection of nanofluids have been reported in the open literature [102]. Nanofluid numerical simulation studies are categorised into two groups: single-phase and two-phase approaches. In the single-phase approach, colloidal suspensions are treated as a single phase. Therefore, the effective thermophysical properties are used in the simulation. Consequently, the numerical results are highly sensitive to effective thermophysical properties. Khanafer et al. [103] numerically investigated the natural convection of ultrafine copper particles and water. The models of Brinkman [86] and Wasp et al. [104] are used to predict viscosity and thermal conductivity, respectively.

For any given Grashof number (*Ga*), an increase in the volume fraction improves the heat transfer rate. Büyük Öğüt [105] numerically scrutinised the heat transfer of nanofluids (Cu, CuO, Al_2O_3 and TiO_2 in water) using a constant heat flux in an inclined cavity. The nanofluids' heat transfer escalated with increasing nanoparticle concentrations. To the

contrary, Abu-Neda [106] numerically examined the influence of applying the different thermal conductivity and viscosity models of Chon et al. [24] and Nguyen et al. [107] on the nanofluid heat transfer coefficient. They observed the effect of the *Ra* and concentration of Al_2O_3-water nanofluid on the natural convection heat transfer. The enhancement of the *Nu* with increasing volume fractions was reported at $Ra = 10^3$. However, for $Ra \geq 10^4$, the average *Nu* deteriorated with the scaling up of the concentration of ultrafine particles.

Lin and Violi [108] numerically examined the effect of alumina nanoparticles' diameter distribution on the augmentation or mitigation of heat transfer in a cavity. On the one hand, their results showed that there was an increase in the heat transfer coefficient of smaller nanoparticles when nanoparticles were added (8% enhancement at $\varphi = 1\%$ where d = 5 nm). On the other hand, there was mitigation in the heat transfer coefficient of big nanoparticles when nanoparticles were added (26% mitigation at $\varphi = 1\%$ with d = 250 nm). The effect of using different viscosity and thermal conductivity models in the two-dimensional numerical simulation of a square enclosure filled with Al_2O_3-water nanofluid was analysed by Ho et al. [67]. They found that the prediction of nanofluids' heat transfer was more sensitive to the selected viscosity model than the thermal conductivity model.

Buongiorno [7] pointed out that thermophoresis and Brownian diffusion were the most important slip mechanisms in the two-phase mixture of nanofluids, which was used for a two-phase nanofluid simulation. Haddad et al. [109] examined the effect of thermophoresis and Brownian motion on CuO-water nanofluid in natural convection when using the finite element method. They concluded that both thermophoresis and Brownian diffusion enhanced the heat transfer rate at any volume fraction. Nevertheless, by neglecting the effect of thermophoresis and Brownian motion, the natural convection heat transfer declined with an increase in particles' concentration.

Segni and Bennacer [110] numerically examined the effect of a heterogenous mixture model on the prediction of nanofluids' natural convection. The *Nu* improves when the nanoparticle concentration is increased up to 5% (for alumina particles). It deteriorates when the nanoparticle concentration is boosted further. The same trend was reported for TiO_2 and Cu nanoparticles. However, they showed that using a homogeneous mixture model predicts a systematic decline in the *Nu* with increasing nanoparticle concentration.

He et al. [111] conducted a numerical investigation on alumina nanofluids in a square cavity. The *Nu* constantly decreased when alumina nanoparticles were added. Sheikhzadeh et al. [112] compared the new transport and homogeneous models to predict the effect of nanoparticle concentration on the natural convection heat transfer of Al_2O_3-water nanofluid. A drop in natural convection heat transfer when adding nanoparticles was reported when using both models. However, their results showed that the transport model predicts a greater reduction with the application of nanofluid and it had better agreement with the experimental results reported by Ho et al. [69]. Meng and Li [113] numerically investigated alumina water nanofluid (φ =1–4% and *Ra* between 7×10^6 and 7×10^7) in a horizontal cylinder. The natural convection heat transfer coefficient decreased when the alumina concentration was increased. A summary of the numerical simulation of natural convection is given in Table 2.4.

Table 2.4: The numerical investigation of nanofluids in a square cavity [114]

Authors	Model	Properties	Nanofluid	Volume fraction (%)	K_n	μ_n	Heat transfer versus φ
Kanafer et al. [115]	Single-phase	Constant	Cu (d = 10 nm) + H_2O	0–25%	Maxwell [78] and Amiri and Vafai [116]	Brinkman [86]	Increase
Ho et al.[67]	Single-phase	Constant	Al_2O_3 + H_2O	0–4%	Maxwell [78] and Charuyakorn et al. [117]	Brinkman [86] and Maïga et al. [118]	Increase or decrease
Eiyad Abu-Nada et al. [119]	Single-phase	F(T)	Al_2O_3 + H_2O (d = 47 nm)	0–6%	Chan [120]	Nguyen et al. [107]	Decrease
Lin and Violi [108]	Single-phase	Constant	Al_2O_3 + H_2O (d = 5–250 nm)	0–5%	Xu et al. [121]	Jang et al. [122]	Increase or decrease
Oueslati and Bennacer [110]	Two-phase	Constant	Cu, Al_2O_3 and TiO_2 + H_2O	0–10%	Maxwell [78]	Maïga et al. [118]	Show a peak
Corcione et al. [123]	Two-phase	F(T)	Al_2O_3 (d = 25–100 nm) + H_2O	0–6%	Corcione [124]	Corcione [124]	Show a peak
Aminifar and Haghgoo [125]	Two-phase	F(T)	Al_2O_3 (d = 33 nm) + H_2O	0–3%	Maxwell [78]	Ho et al. [69]	Decrease
Shekhizadeh et al.[112]	Two-phase	F(T)	Al_2O_3 (d = 33 nm) + H_2O	0–4%	Corcione [124]	Corcione [124]	Decrease
Alipanah et al. [126]	Single-phase	F(T)	Cu or Al_2O_3 or TiO_2 + H_2O	0% –5%	Maxwell [78]	Brinkman [86]	Increase

Contradictory results on the numerical investigation of natural convection in an enclosure and lack of enough experimental works lead to more experimental investigations. Relatively few experimental investigations are available in the literature due to the difficulty of measuring effective parameters. Putra et al. [127] examined the effect of nanoparticle concentration on the natural convection heat transfer coefficient. Natural convection in a horizontal cylinder heated from one side and cooled from the other was investigated. Al_2O_3 (d = 131.3 nm) and CuO (d = 87.3 nm) were suspended in distilled water. Four hours of sonication was used to break down the aggregation of particles (50 ml volume). Putra et al. [127] assumed that sonication time was enough to prevent sedimentation from occurring during the experiment,

and the visual observation method was used to ensure the stability of nanofluids. The systematic deterioration of heat transfer with an increasing concentration of nanoparticles (φ = 1–4%) was reported. However, to ensure the stability of nanofluids, which needs to be accurately examined, a scientific method, such as the UV-visible spectroscopy method and/or the measurement of zeta potential, should be applied.

Wen and Ding [128] experimentally investigated the natural convection of TiO_2-water nanofluid (the nominal diameter size claimed by the manufacturer was 30–40 nm) in a disc-shaped enclosure for 0.19, 0.36 and 0.57% volume fraction. A stable nanofluid was formulated at pH = 3 with a measured zeta potential of +45 mV at 0.024% volume fraction. However, such a level of acidity in the solution increased the corrosion rate, which restricted its industrial application. A high-shear homogeniser was used to reduce the average aggregation size of the ultrafine particles. It was observed that the mean size of aggregation was reduced from 193 to 170 nm for 0 to 50 minutes of applying a high-shear homogeniser. However, a small amount of sedimentation was reported in the study. The experimental average *Nu* for only water was found to be between two correlated equations that were proposed by Leong et al. [129] (Equation 2.13) and Cioni et al. [130] (Equation 2.14).

$$\overline{Nu} = 0.08461Ra^{0.3125} \qquad \text{Equation 2.13}$$
$$10^4 < Ra < 10^8$$

$$\overline{Nu} = 0.145Ra^{0.292} \qquad \text{Equation 2.14}$$
$$3.7\times10^8 \le Ra \le 7\times10^9$$

The systematic deterioration of the natural convection heat transfer coefficient with an increasing volume fraction of nanoparticles (φ = 0-0.57 %) was reported.

Nnanna [131] experimentally investigated Al_2O_3 (d = 27 nm) deionised water in a rectangular cavity with an aspect ratio of approximately 6 within the *Ra* range of between 1×10^7 and 3×10^7. The thermal conductivity and viscosity of the nanofluid were employed from the experimental measurement of different authors [131]. The performance of the cavity, considering *Nu* versus Ra, was 35 and 41% lower than the reported results for water only at $Ra = 2 \times 10^7$ by Putra et al. [127] and Wen and Ding [128] respectively. Different volume fractions (0.2, 1.5, 2.7, 4.5 and 7.9%) were prepared, and the results showed that the presence of the nanoparticle enhanced the heat transfer coefficient by up to 1.2% volume fraction. Then, a further increase in concentration decreased the heat transfer coefficient. It is not clear how an optimum value of 1.2% was obtained using volume fractions 0.2, 1.5, 2.7, 4.5 and 7.9%. It is also not clear why there is such a large gap between 0.2 and 1.5 vol.%

Li and Peterson [132] conducted an experiment with Al_2O_3 (d = 47 nm) deionised water in a cylindrical cavity. A 90-minute ultrasonic bath was used to break down the aggregation of nanoparticles. The nanofluid concentration was φ = 0.5, 2, 4 and 6%. A continuous decline in the heat transfer coefficient with an increasing volume fraction was reported. They pointed out that the possible causes for the deterioration of natural convection in the presence of the nanoparticle could be the influence of Brownian motion and thermophoresis, which perhaps delayed the onset of natural convection, as well as their damped effect on natural convection. To the contrary, the results of Haddad et al. [109] illustrated the beneficial effect of natural convection when the effect of Brownian motion and thermophoresis is taken into account in simulations.

Ho et al. [69] experimentally scrutinised a natural convection heat transfer alumina nanoparticle (33 nm) suspended in an ultra-pure Milli-Q water. Volume fractions were chosen (0.1, 0.3, 1, 2, 3 and 4%) and the *Ra* range was between 6.21×10^5 and 2.56×10^8. A stable

Al_2O_3-water nanofluid was formulated by magnetically stirring the suspension for two hours and keeping the pH level at 3. However, just using a magnetic stirrer was less effective than using an ultra-sonication probe to break down the aggregation of nanoparticles [31]. In addition, the low pH value increased the rate of corrosion, which puts a constraint on the industrial application.

The cavity's performance was examined in comparison to the available correlations, and it was found that, at approximately $Ra = 10^8$, the corresponding *Nu* of only the water-filled cavity equals 26, which was 16.1% less than both the calculated *Nu* using Equation 2.13 and this study's reported results. The results of Ho et al. [69] indicated a maximum 18% heat transfer coefficient enhancement at 0.1% volume fraction. A further increase in the nanoparticle concentration decreased the heat transfer coefficient in the cavity. The uncertainty of the reported results was 7 to 26.9%. The optimum volume fraction was reported at 0.1% volume fraction. However, volume fractions between 0 and 0.1 % and between 0.1 and 0.3% were not examined. Therefore, a detailed study of volume fractions higher and lower than the optimal volume fraction is needed to examine the optimum volume fraction of an alumina nanoparticle.

The experimental and numerical study of Hu et al. [133] that uses the two-phase lattice Boltzmann model proposed an increase in the heat transfer coefficient for a diluted suspension of Al_2O_3-water nanofluid (φ = 0.25 %). However, a further increase in the concentration of the nanoparticles deteriorated the heat transfer coefficient. They used the same cavity size as Ho et al. [69], but, according to their uncertainty analysis, the error for the measured temperature was 0.001 °C, the thermal conductivity was 2%, the calculated *Nu* was 8.275% and the repeatability error was 4.6%. They reported approximately a 2% enhancement in the thermal conductivity of nanofluids, as well as a 2% augmentation of the nanofluid's *Nu* at 0.25% volume fraction, which was in the range of the uncertainty error. A

high concentration of nanoparticles was observed at the hot wall and a low concentration was observed at the cold wall, which confirms the major role of temperature difference as a driving force. There was no indication of stability or nanoparticle characterisation.

Zeinali et al. [134] conducted an experimental study on the effect of inclination angle on natural convection in a cubic cavity. The cavity was filled with a suspension of Al_2O_3, TiO_2 and CuO in turbine oil at three concentrations (0.2, 0.5 and 0.8 wt%). They showed that, at zero inclination angles, when heating from the bottom and cooling from the top, the average *Nu* of Al_2O_3-turbine oil systematically deteriorated with increasing nanoparticle concentrations. However, at a 90 ° inclination angle, the 0.8 wt% had the highest *Nu*.

A summary of the available literature with regard to the experimental natural convection of nanofluids is given in Table 2.5.

Table 2.5: The experimental natural convection of nanofluids

Authors	**Nano-particles**	**Base fluid**	**Concentration/vol %**	***Nu* versus concentration**	***Ra***
Putra et al. [127]	Al_2O_3, CuO	Distilled water	1–4%	Systematic deterioration	$(1.38 – 8.88) \times 10^8$
Wen and Ding [128]	TiO_2	Water	0.19, 0.36, 0.57%	Systematic deterioration	$(0.01 – 1) \times 10^6$
Nnanna [131]	Al_2O_3	Deionised water	0.2, 1.5, 2.7, 4.5, 7.9%	Optimum *Nu* at 1.2 vol.%; further increase deteriorates *Nu*	$(0.9 – 3) \times 10^7$
Li and Peterson [132]	Al_2O_3	Deionised water	0.5, 2, 4 and 6%	Continuous deterioration	8 000 – 28 000
Ho et al. [69]	Al_2O_3	Utra-pure Milli-Q water	0.1, 0.3, 1, 2, 3 and 4%	Optimum *Nu* at 0.1 vol.%; further increase deteriorates *Nu*	$(0.06 – 25.6) \times 10^7$
Hu et al. [28]	Al_2O_3	Water	0.25,0.5 and 0.75%	Optimum *Nu* at 0.25 vol.%; further increase deteriorates *Nu*	$(3.0 – 3.6) \times 10^7$
Zeinali et al. [134]	Al_2O_3, TiO_2 CuO	Turbine oil	0.2,0.5 and 0.8 wt%	Continuous increase of *Nu*	$(0.45 – 1.9) \times 10^8$

2.6 Conclusion

In summary, the characterisation of nanofluids should be included in the heat transfer study of nanofluids. For the characterisation of nanofluids, techniques such as TEM and SEM,

zetasizer and zeta potential should be used. The visual observation of the stability of nanofluids should be confirmed with a scientific method, for example, UV-visible spectroscopy and zeta potential measurement. Because there is no universal formula for the thermal conductivity and viscosity of nanofluids, the selection of any theoretical models should be considered carefully due to contradictory results of natural convection in nanofluids when using different models. It is preferable for researchers to experimentally measure the viscosity and thermal conductivity of nanofluids as the experimental results would be utilised in their heat transfer investigations.

Contradictory results of numerical investigations of natural convection in nanofluids, as well as the inconsistency of the experimental study of natural convection in nanofluids, lead to a more experimental investigation of natural convection in nanofluids. A few researchers have studied the effect of nanofluid concentration on the enhancement of natural convection in nanofluids at various *Ra* in a cavity flow. However, no experimental study on a very high *Ra* $> 4 \times 10^8$ in cavity flow using water as the base fluid has been reported. Moreover, a detailed study of the effect of the nanofluid's volume fraction on the natural convection heat transfer coefficient has not yet been conducted. Therefore, this study aims to address these challenges.

3. Experimental procedure

3.1 Introduction

The purpose of this chapter is to provide a brief introduction to the nanofluid materials and equipment that are used to characterise Al_2O_3-water nanofluids, such as sonicators, TEM and SEM, zetasizers, UV-visible spectrophotometers and viscometers. The experimental setup that was used to experimentally conduct studies on the natural convection of Al_2O_3-water nanofluid consisted of a confined volume with two isothermal walls. The rest of walls were insulated. Components of the experimental setup and materials of the test section, as well as the instrumentation used, are discussed briefly. The validation of the experimental setup is discussed using the existing correlations and numerical simulation. Finally, the uncertainty analysis of the experimental measurements is demonstrated.

3.2 Materials

The formulation of a stable nanofluid is a critical step in nanofluid investigation. A dispersed α-Al_2O_3 20 wt% in water was acquired from Nanostructure and Amorphous Material Inc. in the USA. For Al_2O_3 nanoparticles, the measurements stated by the manufacturer were used: d = 30 nm, purity = 99.9% and true density = 3 950 kg/m^3. The nanofluid and base fluid properties are listed in Table 3.1.

Table 3.1: The thermophysical properties of Al_2O_3 and water

Property	Base fluid (water)	Nanoparticle Al_2O_3
c_p (J/kg. K)	4 180	765
ρ (kg/m^3)	997.1 at 25 ℃	3 950
k (W/m. K)	0.607	36
μ(kg/m. s)	8.91×10^{-4}	-
β(k^{-1})	2.1×10^{-4}	8.4610^{-6}
$\propto$ (m^2/s)	1.46×10^{-7}	1.29×10^{-5}

The desired volume fraction (φ) of the nanofluids was diluted by adding deionised water, which was supplied by Merck (Pty) Ltd.

3.3 Equipment

The aggregation of the nanofluid is broken down using an ultrasonic horn. Alternating current line power is transformed to ultrasonic signals (20 kHz) and the signals are converted to mechanical vibrations using a transducer. The vibrations at the tip of the horn, which has been dipped in the liquid sample, can be amplified by the user, which results in a cavitation field. The formation and collapse of bubbles release an enormous amount of energy in the sample and the shock effect of the rapid bubbles collapse, as well as their erosion effect, resulting in the dispersion of nanoparticles. The volume of the sample is constrained by the diameter of the tip. A small tip has a higher energy intensity with a small effective area of sonication. However, using a large tip decreases the intensity of the sonication energy, but increases the volume of the samples that could successfully be sonicated. An ultrasonic agitation probe (Qsonica Q-700 20 kHz and 700 W with five seconds pulse on and two seconds pulse off with an intensity of 98%) was used to break down the aggregation of the nanoparticles.

Ultrasonic energy density was defined as the ratio of sonication energy divided by the volume of the sample. It illustrates a sufficient amount of sonication to break down the aggregation of nanoparticles for the various volumes of the sample. During the sonication process, the temperature of the sample increases. Therefore, the temperature of the samples was controlled using a programmable constant temperature bath (LAUDA ECO RE1225 Silver).

The weight of the nanofluid was measured with a RADWAG AS 220.R2 precision balance, to formulate the desired nanofluid volume fractions. Then, to dilute the dispersed nanofluid, a predetermined mass of water was added to prepare the various nanofluid concentrations.

The stability of the nanofluid was characterised by a UV-visible spectrophotometer (Model 7315 from Jenway in the UK). The zeta potential measurement was obtained using a zetasizer Nano ZS (Malvern Instruments in the UK). Moreover, the morphology of the particles was investigated using TEM and SEM.

The viscosity of the nanofluid was measured using a SV-10 sine wave vibro-viscometer (A&D in Japan). A Jenway 3 510 pH meter was used to measure the pH level.

3.4 Experimental setup

A square cavity of 96 × 120 × 102 mm [height (H) x width (W) x depth (D)] was used with differential temperatures at the two opposite vertical walls. The rest of the walls were insulated. Two heat exchangers (contour flow shell and tube) were designed and manufactured from copper to serve as walls with a constant temperature. Furthermore, the similar hydraulic diameter (h_D) was used for both the shell and the tube side to facilitate uniform mass and temperature distribution in the heat exchanger, as shown in Figure 3.1.

Figure 3.1: Heat exchangers with a similar hydraulic diameter in the shell and tube side

The efficiency of the constant temperature wall was validated by using an air-filled cavity. The result showed a maximum difference between readings of 0.4 °C at different points on the heated/cooled wall. Two constant PR20R-30 Polyscience thermal baths with a temperature range of -30 to 200 °C and an accuracy of 0.005 °C were used. The constant thermal baths were maintained at the desired volume flow rate (range from 0.0141 to 0.0324 L/s) with a constant temperature range from 5 to 70 °C for the experiments. The experimental setup is shown in Figure 3.2.

Figure 3.2: The experimental setup of natural convection

The temperature was monitored at different locations by applying T-type thermocouples, purchased from Omega Engineering Inc. in the USA, with part number (TT-T-30 SLE(ROHS)) of 30 AWG. The accuracy of the thermocouple was 0.02 °C after calibration. Thermocouples were calibrated at the experiment range between 5 and 70 °C inside the bath. At the surface of both the heated and the cooled wall, three thermocouples were mounted to monitor temperature. Thermocouples were buried 2 mm deep inside the walls, and thermal glue and silicon were applied to ensure accurate readings of the surface temperature. Seven thermocouples were mounted between the hot and the cold walls at the horizontal centre line,

and five thermocouples were placed in the vertical position at the mid-point between the hot and the cold walls. The schematic position of the thermocouples is shown in Figure 3.3.

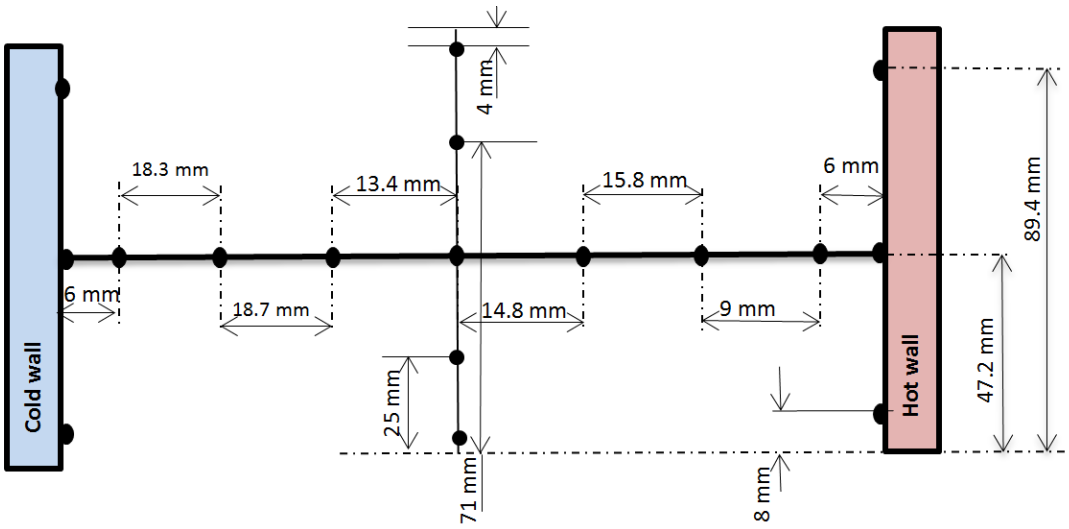

Figure 3.3: A schematic of the thermocouples in the experimental setup

To evaluate the heat transferred to the cavity at the hot wall, as well as the removed heat from the cavity at the cold wall, Equation 3.1 was used.

$$\dot{\bar{q}} = \dot{m} c_p \Delta T = \dot{m} c_p (T_{in} - T_{out}), \qquad \text{Equation 3.1}$$

where ΔT is the temperature difference between the inlet and the outlet of the heat exchangers.

A mixer was used at the outlet of the heat exchanger's tube to assure the cup-mixing temperature. There was enough distance from the constant bath to the heat exchangers to ensure a fully developed flow. The volume flow rate was measured by two ultrasound flow meters (Burkert type 8081) with a range of 0.0666 to 0.3333 L/s and an accuracy of ± 0.01% full scale + 2% of measured value and a repeatability of 1% measured value. All data was recorded with a National Instrument (NI) Data Logger SCXI-1303 with a 32 channel input. All sides of the cavity were insulated from the ambient temperature by applying 20 cm insulation (k = 0.033 W/m.K) to prevent heat loss from the cavity. The

temperature gradient between the thermocouples inside the insulated material showed approximately 3% heat loss.

3.5 Experimental method

The desired volume fraction of Al_2O_3-water nanofluid (d = 20–30 nm, 20 wt% dispersed in water) was calculated. The volume fraction for values higher than the target concentration was taken due to the limitation of the sonication probe. A 12.7 mm probe tip capable of handling a volume less than 250 ml was used, while 1 500 ml of the nanofluid was needed. Therefore, the higher volume fraction of the nanofluid was sonicated and diluted to the desired volume fraction, which is going to be examined in the test cell. After dilution, sonication was carried out to ensure the proper distribution of the nanoparticles. A small volume of the sample was taken to experimentally measure its viscosity immediately after the preparation.

Approximately 60 minutes after starting the experiments, the steady-state condition was confirmed by examining the thermocouple station readings, which showed less than 0.1% change inside the test cell.

A thousand points of data were acquired with a frequency of 2 Hz. Then, different temperature ranges were set to obtain the desired Ra. The amount of heat transfer from the hot wall to the cold wall could be regulated with a flow rate of water inside the heat exchangers. Nevertheless, the flow rate should be adjusted to provide a temperature difference of 1.5 °C or less between the inlet and the outlet of the heat exchanger so as not to violate the assumption of constant wall temperature.

3.6 Experimental data reduction

The natural convection in an enclosure can be characterised by defining non-dimensional variables, such as *Nu* (Equation 3.2) and *Ra* (Equation 3.3).

$$Nu = \frac{Rate\ of\ convection\ heat\ transfer}{Rate\ of\ conduction\ heat\ transfer} = \frac{hL_c}{k}$$ Equation 3.2

where L_c is the characteristic length, h is the heat transfer coefficient and k is the thermal conductivity.

If *Nu* is bigger than 1, advection becomes larger than conduction. In natural convection, the typical value of the *Nu* is small compared to another kind of heat transfer, for example, forced convection. Therefore, scientists have been trying to improve the natural convection *Nu* using nanofluids.

$$Ra = \frac{Buoyancy\ forces}{Viscous\ forces} Pr = GrPr$$ Equation 3.3

Critical *Ra* values like the critical Reynolds number (*Re*) show the initiation of turbulent flow.

$$Ra = \frac{g\beta(T_h - T_c)L_c^3 Pr}{\upsilon^2},$$ Equation 3.4

where υ is the kinematic viscosity, β is the thermal expansion coefficient, *Pr* is the Prandtl number, L_c is the characteristic length, and for an enclosure, equals the distance between the hot and the cold walls. All the properties of the fluids are evaluated at the average temperature of the hot and the cold walls ($\frac{T_h+T_c}{2}$).

If $Ra_L > 3 \times 10^5$, the fluid motion becomes turbulent if the hot plate is at the bottom and the cold plate is at the top (Rayleigh Bernard cells).

The heat transfer in the hot and the cold walls was evaluated using Equation 3.5.

$$\dot{\bar{q}} = \dot{m}c_p\Delta T = \dot{m}c_p(T_{in} - T_{out})$$ Equation 3.5

A mixer was used at the outlet of the heat exchanger's tube to ensure the cup-mixing temperature. There was enough distance between the constant bath and the heat exchangers, which assured that the flow was fully developed. The volume flow rate was measured using

two ultrasound flow meters (Burkert type 8081) with a range between 0.0666 and 0.3333 L/s, and an accuracy of ± 0.01% full scale + 2% of measured value, and repeatability of 1% measured value.

The heat transfer from the hot wall to the cold wall occurs through conduction, advection and radiation. A portion of the heat transfer due to radiation and conduction is negligible as a result of the small temperature difference between the hot and the cold walls, and the small thermal conductivity in compression to the distance between the walls. Thus, natural advection is the major heat transfer mechanism in the insulated cavity, as shown in Equation 3.6.

$$\bar{\dot{q}} = \bar{h} A(\bar{T}_H - \bar{T}_C)$$

$$\bar{h} = \frac{\bar{\dot{q}}}{A(\bar{T}_H - \bar{T}_C)}$$

Equation 3.6

where A is the face of the heat exchanger inside the test cell. The non-dimensional heat transfer coefficient, according to Equation 3.2, was defined if the natural convection heat transfer coefficient is multiplied by the characteristic length and divided by the thermal conductivity of the fluid.

The thermophysical properties of the base fluid were substituted with the nanofluid's thermophysical properties using following equations.

$$\rho_{nf} = \varphi\rho_p + (1-\varphi)\rho_{bf}$$

Equation 3.7

$$\beta_{nf} = \beta_p + (1-\varphi)\beta_{bf}$$

Equation 3.8

$$c_{p_{nf}} = c_{p_p} + (1-\varphi)c_{p_{bf}}$$

Equation 3.9

The viscosity of the nanofluid was experimentally measured and, due to a small volume fraction (less than 1%), a thermal conductivity model was used to determine the effective thermal conductivity of the nanofluid. Therefore, the following equations were used to calculate the *Ra* and *Nu* of the nanofluid:

$$Ra_{nf} = \frac{g\beta_{nf}(T_H - T_C)\rho_{nf}{}^2 c_{pnf} L_c{}^3}{\mu_{nf}\ k_{nf}} \qquad \text{Equation 3.10}$$

$$\overline{Nu}_{nf} = \frac{\bar{h}_{nf} L_c}{k_{nf}} \qquad \text{Equation 3.11}$$

3.7 Experimental validation

The *Nu* of the water-filled cavity was examined as a function of *Ra* values, which was facilitated by setting different temperatures at the heat exchangers to validate the experimental setup. The flow rate of water coming from the isothermal baths should be regulated so that the temperature difference between the inlet and the outlet of the heat exchangers is less than 1 °C. Leong et al. [129] investigated the natural convection of air in the cubical cavity with an aspect ratio of 1, and proposed a correlation that calculates the average *Nu* in the cavity as a function of Ra, as given in Equation 3.12.

$$\overline{Nu} = 0.08461 Ra^{0.3125} \qquad \text{Equation 3.12}$$
$$10^4 < Ra < 10^8$$

Cioni et al. [130] examined the natural convection of a water-filled cylindrical cavity with an aspect ratio of 1 in the *Ra* range of 3.7×10^8 to 7×10^9. They expressed the correlation for the average *Nu* as a function of Ra, as shown in Equation 3.13.

$$\overline{Nu} = 0.145 Ra^{0.292} \qquad \text{Equation 3.13}$$
$$3.7 \times 10^8 \le Ra \le 7 \times 10^9$$

Berkovesky and Polevikov [136] stated a correlation for *Nu* as a function of the *Ra* and Pr, as given in Equation 3.14.

$$\overline{Nu} = 0.18\left(\frac{Pr}{0.2+Pr}Ra\right)^{0.29} \qquad 1 < H/L < 2 \quad and \quad \frac{Ra \times Pr}{0.2+Pr} > 10^3 \qquad \text{Equation 3.14}$$

To validate the experimental results, the cavity was filled with water at various *Ra* values. Setting different temperatures at the baths gives different wall temperature sets. This follows from the experimental results that were compared with existing correlations of the natural convection of water in an enclosure, as shown in the following graph.

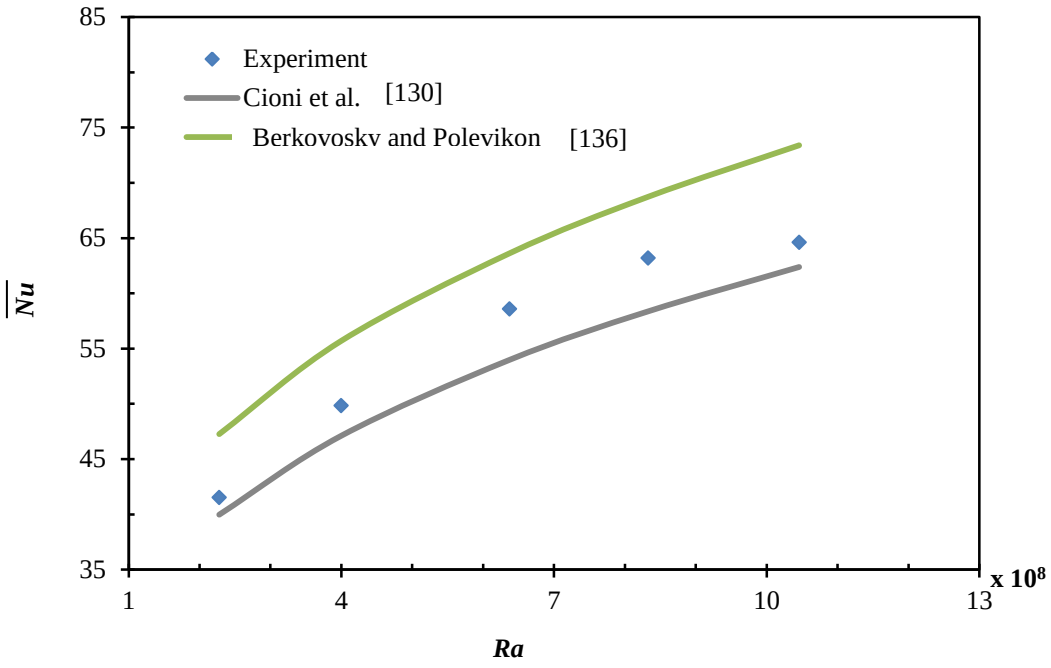

Figure 3.4: Validation of the experimental setup using *Nu* as function of *Ra* in comparison to the existence of correlations

Experimental results for the water-filled cavity showed good agreement with the correlation of Cioni et al. [130], Equation 3.13. In addition to that, the numerical simulation of the cavity predicted the same results as presented by Mahdavi et al. [137]. Navier-Stoke equation were solved for turbulent flow by using a coupled solver in a steady state situation. Momentum-

and pressure-based continuity equations were iteratively solved at the same time in the coupled solver. The Boussinesq assumption was used to solve the equations ($\beta \Delta T$ <<0.1). A second-order upwind interpolation scheme was used to discretise equations, and the body force weighted scheme was chosen to interpolate pressure in the equations.The k-ε model was chosen with an enhanced wall function as the wall treatment in the shell and tubes. Natural convection has very thin boundary layer, therefore, very fine mesh should be used in order to obtain accurate results (y^+>0.5). Consiquently, the closest nodes to the shell and tube walls, and the cavity were chosen as 0.4 and 0.3 mm, respectively. Mesh independency study was done by chosen heat flux at the wall and temperature and velocity at the cavity centre-line. (694279 nodes). The reported two-dimensional and three-dimensional model predicts the similar average *Nu* at a specific Ra, as shown in Figure 3.5 and Figure 3.6.

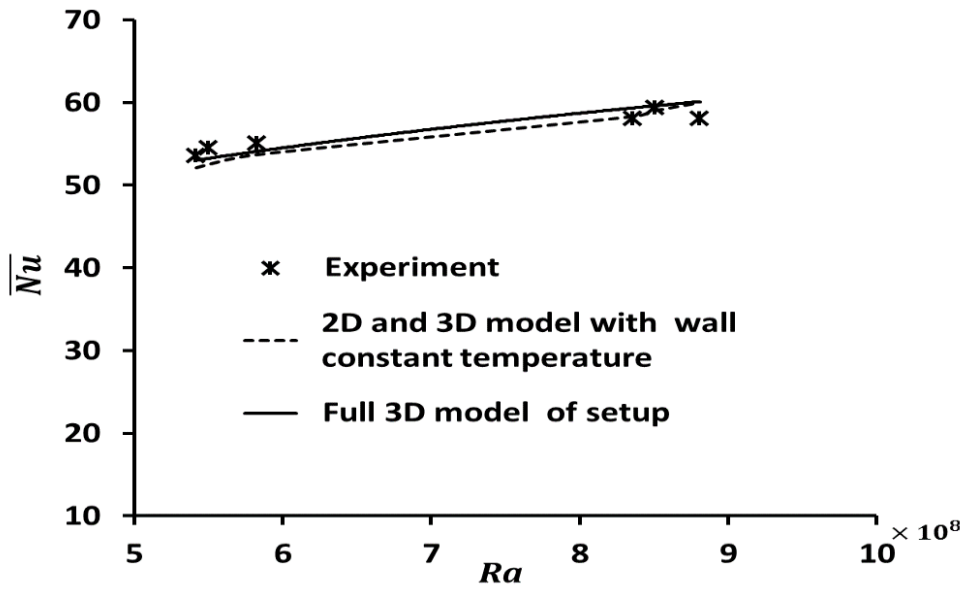

Figure 3.5: The average *Nu* as a function of the Ra, comparison between the numerical simulation and the experimental results [137]

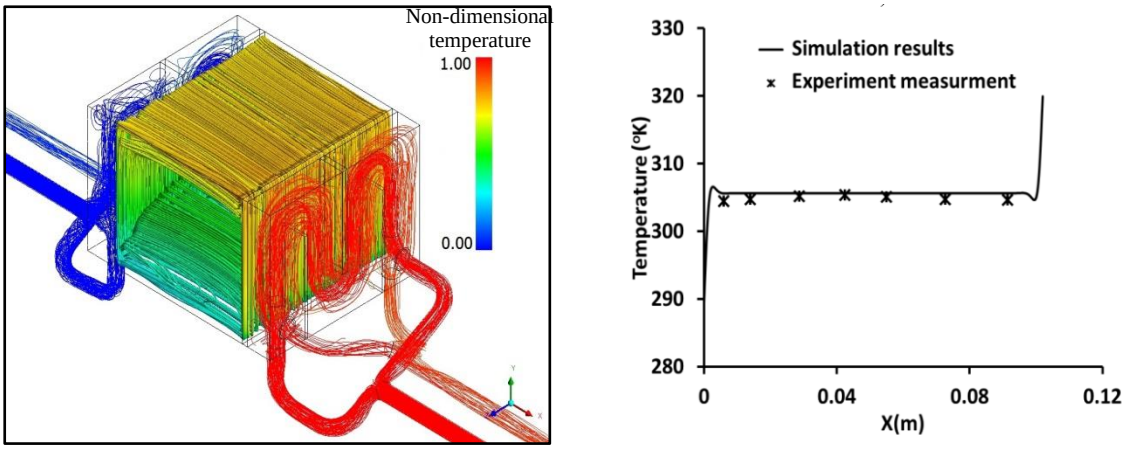

Figure 3.6: The streamline of flow field in the cavity mapped with a non-dimensional temperature [137]

3.8 Conclusion

Al_2O_3-water nanofluid (d = 20–30 nm, dispersed 20 wt% in water) was used to formulate the desired volume fraction as a heat transfer fluid. A brief description of the equipment that was used to characterise the nanofluid was given. The experimental apparatus that was manufactured is a square cavity with an aspect ratio of 1 and two constant walls, which act as shell and tube counterflow heat exchangers. The temperature of the walls (the hot and the cold wall) was regulated by using two constant temperature thermal baths. A *Ra* range of 3.49×10^8 to 1.05×10^9 was provided by setting an appropriate temperature in the baths. The data reduction for the validation of the experimental apparatus was discussed. Finally, validating the experimental apparatus filled only with water against previous experimental investigations ensured the accountability of the experimental apparatus. Therefore, the capability of the test cell to scrutinise the natural convection of nanofluids was confirmed.

4. Results: Nanofluid formulation and natural convection

4.1 Introduction

The thermal management of advanced technologies puts a constraint on their rapid growth, in particular in confined volumes, such as in the case of MEMS and electronic cooling. Natural convection could improve thermal management. However, natural convection has a low heat transfer coefficient. The natural convection heat transfer coefficient of conventional fluid in the presence of a confined volume could be improved by using an advanced colloidal engineering type of fluid, known as nanofluids.

In this chapter, the preparation of Al_2O_3-water nanofluid is first examined in detail. TEM and SEM images provide information about its morphology. The stability of the nanofluid was examined using visual observation, a zetasizer, zeta potential and UV-visible spectroscopy. Secondly, the natural convection of dispersed single-step Al_2O_3-water nanofluid (d = 20–30 nm) was studied experimentally due to it having fewer stability problems.

A significant amount of research has also been done to shed light on the thermophysical properties of alumina nanofluid. A rectangular cavity with an aspect ratio of 1, with two opposite constant walls formed vertically, with the rest of walls insulated, has been used to investigate natural convection in nanofluids. The constant wall temperature is regulated using two constant temperature baths so that the temperature difference provides the desired *Ra* (3.49×10^8 to 1.05×10^9). The diluted volume fractions of Al_2O_3-water nanofluid (φ = 0, 0.05, 0.1, 0.2, 0.4 and 0.6% volume fraction) were prepared to investigate the effect of nanofluid volume fractions on nanofluids' natural convection heat transfer coefficient. Correlations to determine the *Nu* as a function of the *Ra* and φ were developed. The temperature distribution of nanofluids is presented at a different volume fraction and Ra.

4.2 Nanofluid characterisation

4.2.1 TEM and SEM

The morphology of Al_2O_3-water nanofluid was tested using TEM and SEM. Samples for the TEM and SEM characterisation were prepared at 1% volume fraction. The samples first need to be dried out according to the prescribed procedure, which might result in some agglomeration of particles. Therefore, a further characteristic of nanofluid using a zetasizer, for example, is needed. An SEM picture of Al_2O_3 nanopowder is shown in Figure 4.1.

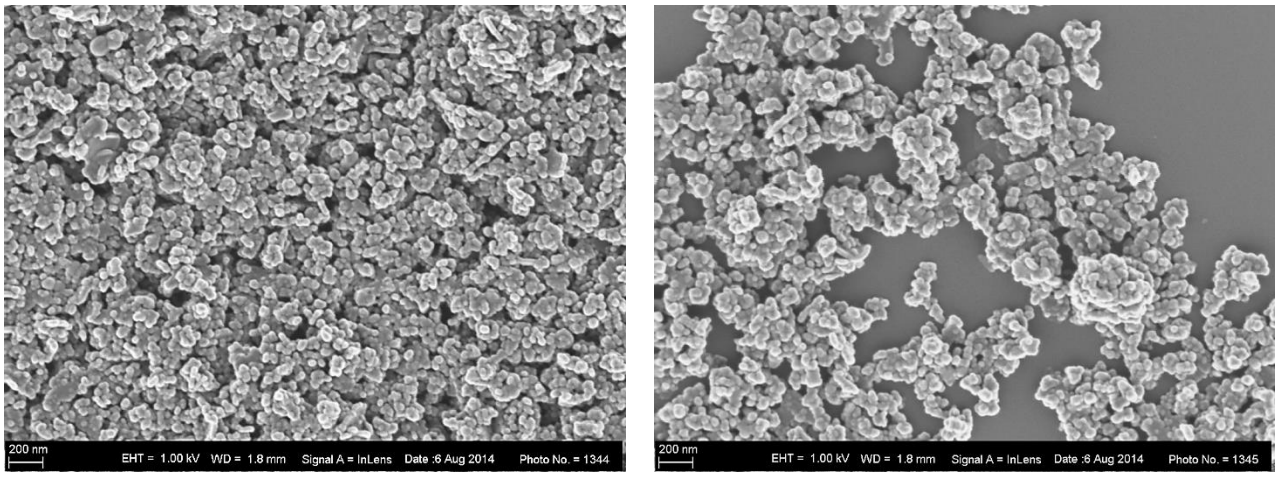

Figure 4.1: An SEM image of Al_2O_3-water (20–30 nm single-step)

The spherical shape of the dispersed Al_2O_3-water nanofluid is recognised, as shown in Figure 4.1. However, some aggregations of the particles are shown in the image, in which it is not clear whether this aggregation is due to the drying out of the sample or whether the aggregations had been in existence since the manufacturing process.

The accuracy of the discussed observation is examined using the SEM image of dry ZnO powder (d = 20 nm) (see Figure 4.2) and a suspension of ZnO (d = 20 nm) in water using the surfactant tetramethylammonium hydroxide pentahydrate (THPD).

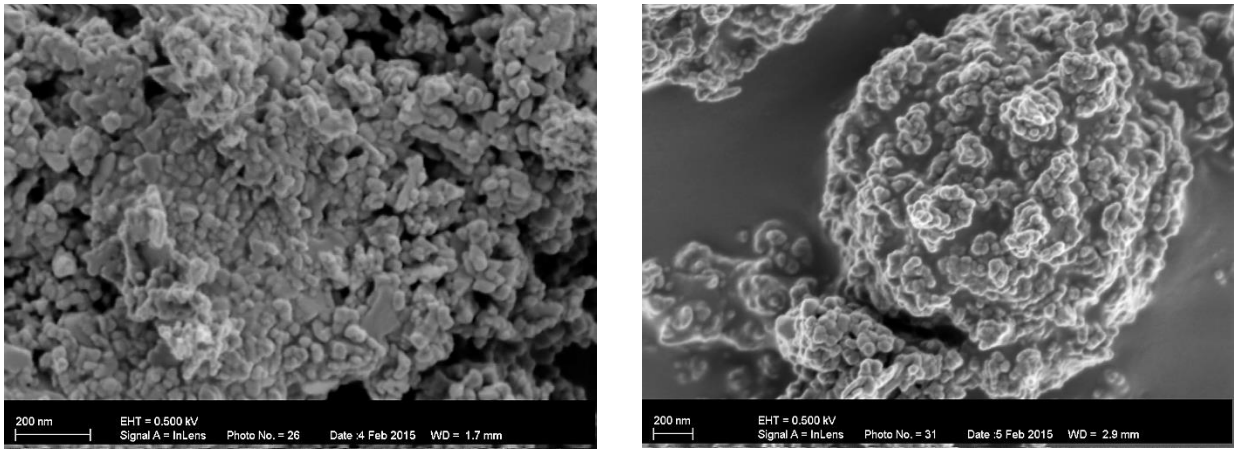

Figure 4.2: An SEM image of dry ZnO powder (20 nm)

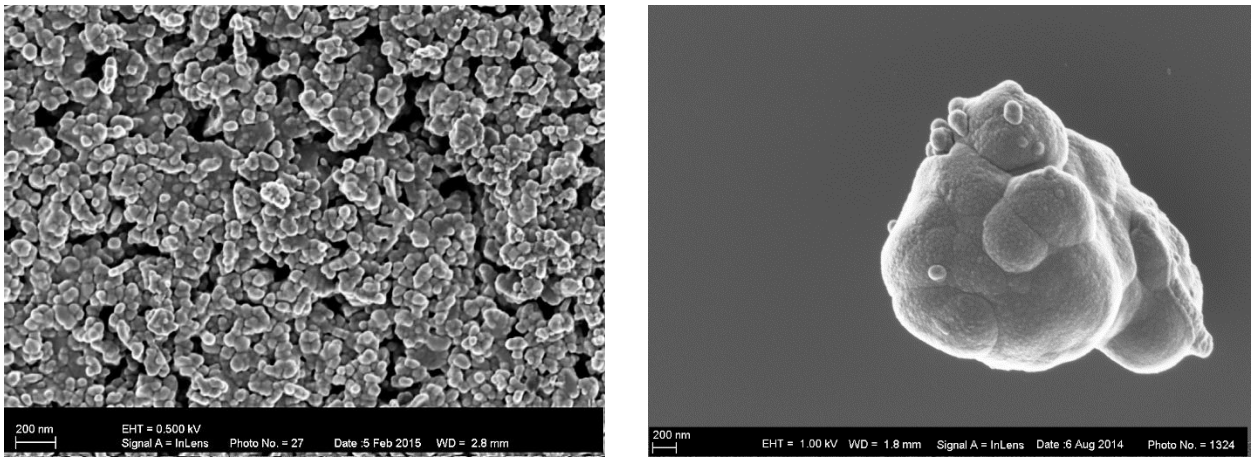

Figure 4.3: An SEM image of ZnO-water (d = 20 nm) nanofluids using THPD as a surfactant at pH = 9.5

Figure 4.2 shows the aggregation of ZnO nanoparticles that will probably break down during the sonication process. However, it is possible that the sonication energy is not strong enough to break down all the aggregations. In fact, the existence of large particles ruins the nanfluid's stability. Figure 4.3 depicts the more homogeneous distribution of ZnO-water (d = 20 nm) nanoparticles than dry ZnO nanopowder. Nevertheless, the existence of nanoparticles larger than 20 nm, which the manufacturer had stated as d = 20–30 nm, was confirmed in Figure 4.3. The SEM picture of SiO_x-water nanofluid (d = 20 nm) and CuO-water nanofluid (d = 20 nm) also confirms the existence of aggregations, as shown in Figure 4.4.

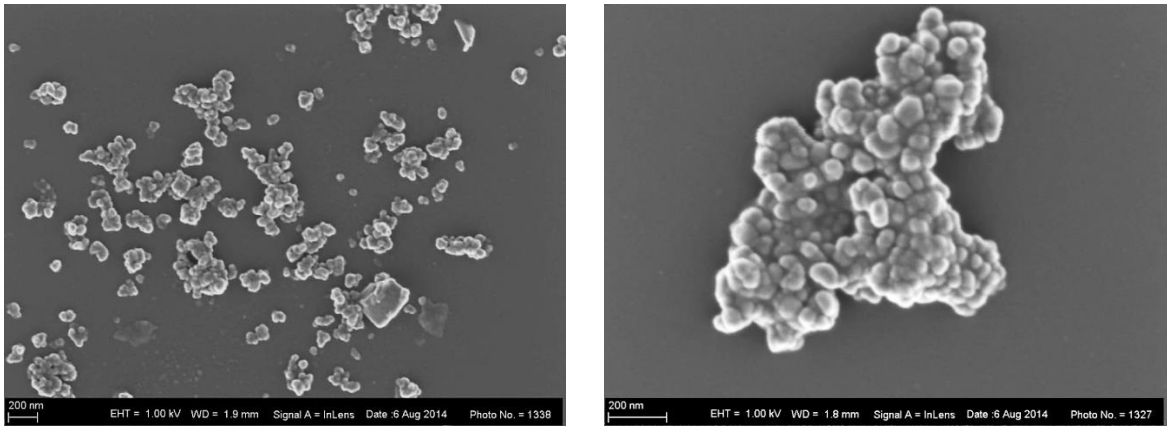

(A) (B)

Figure 4.4: An SEM image of (A) SiO_x-water (d = 20 nm) and (B) CuO-water (d = 20 nm)

The characterisation of nanofluids using TEM is common in literature, even though the preparation method includes the drying out of samples. The TEM images of Al_2O_3-water nanofluid (d = 20–30 nm) is shown in Figure 4.5.

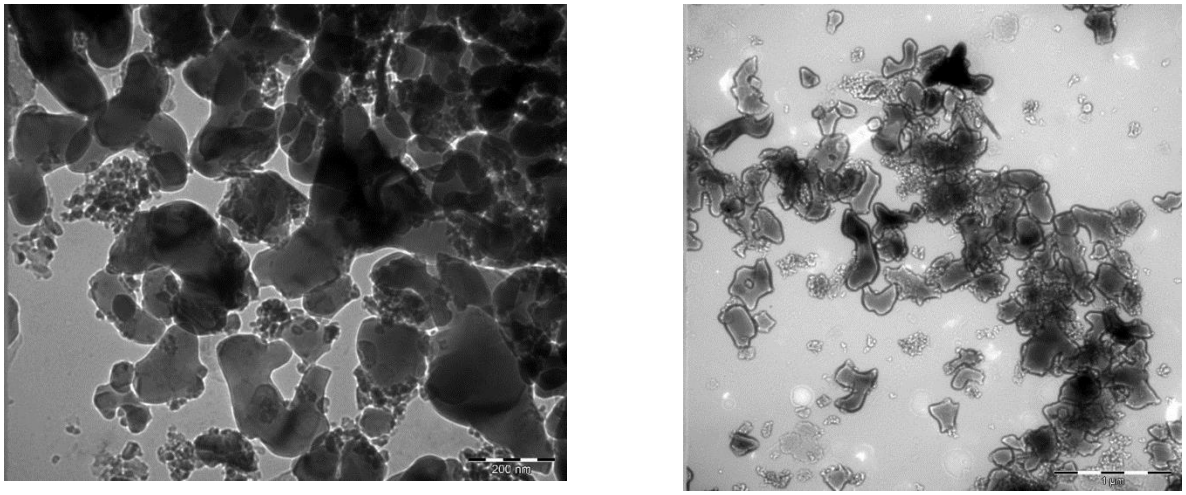

Figure 4.5: A TEM image of dispersed Al_2O_3-water (d = 20–30 nm) nanofluids

The TEM images provide a better understanding of the nanofluids' morphology. Figure 4.5 shows that the nanoparticles' size is bigger than the manufacturer stated. The small particles in the images could be an indication of the breaking down of the particles during the sonication process. The TEM images of other nanoparticles are shown in Figure 4.6, which confirms the spherical shape of particles (SiO_2: d = 80 nm, CuO: d = 20 nm, ZnO: d = 20 nm and Al_2O_3: d = 20–30 nm).

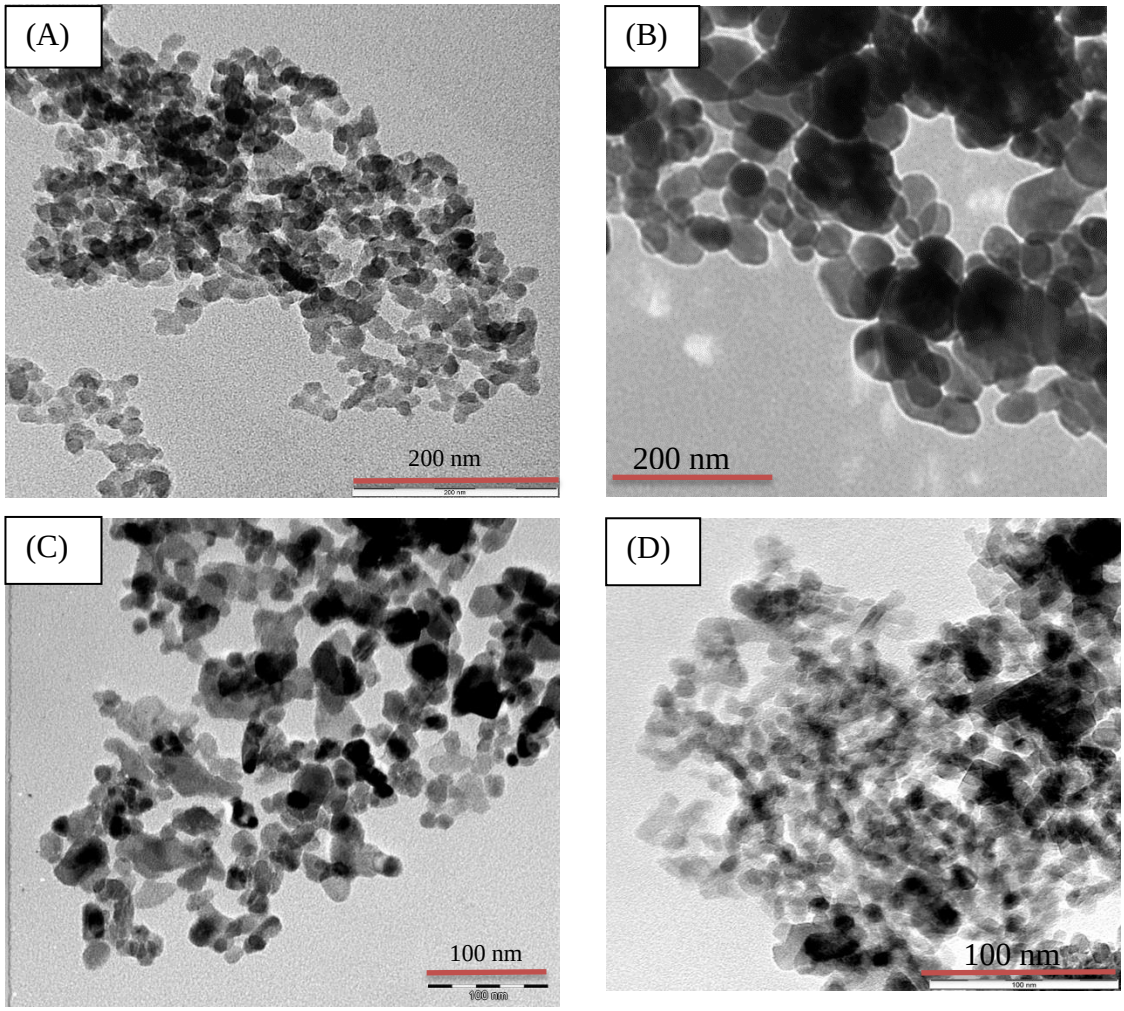

Figure 4.6: A TEM image of (A) SiO_2 (d = 80 nm); (B) CuO (d = 20 nm); (C) ZnO (d = 20 nm) and (D) Al_2O_3 (d = 20–30 nm)

The TEM picture of nanoparticles gives an indication of their size distribution. For SiO_2, d = 80 nm (A). The nanoparticles are smaller than stated by the manufacturer. To the contrary, the size distribution in CuO (d = 20 nm) is bigger than the manufacturer's claim.

4.2.2 Zetasizer

A zetasizer could give an indication of the size distribution of particles in a liquid medium. It is based on the dynamic light scattering (DLS) technique that uses Brownian motion to determine the size of nanoparticles. The Zetasizer ZS (Malvern Instrument Limited in the UK) uses a 4 mW He-Ne 633 nm laser as a source, which measures particle sizes in the range of 0.3 to 10 000 nm. The unit's accuracy is better than ±2% NIST traceable latex standards

and has a repeatability ±1% of measured data for size and ±0.4% of measured data for zeta potential measurement. Measurement continues at 25 °C with an assigning viscosity of water at 25 °C to 0.8872 cP. To measure mean hydrodynamic size, the formula of Stokes and Einstein [138] is used, as shown in Equation 4.1.

$$d = \frac{\kappa_B T}{3\pi D\mu} \qquad \text{Equation 4.1}$$

where d is the hydraulic diameter, κ_B is the Boltzmann constant ($1.3806488 \times 10^{-23}$ m^2 kg s^{-2} K^{-1}), T is the absolute temperature, D is the diffusive coefficient and μ is the dynamic viscosity of the medium. The size distribution of 0.05% volume fraction of Al_2O_3-water nanofluid prepared with the single-step method (claimed by the manufacturer to be d = 20–30 nm) is shown as the intensity of light, which is the intensity of scattered light as a result of particles, as illustrated in Figure 4.7.

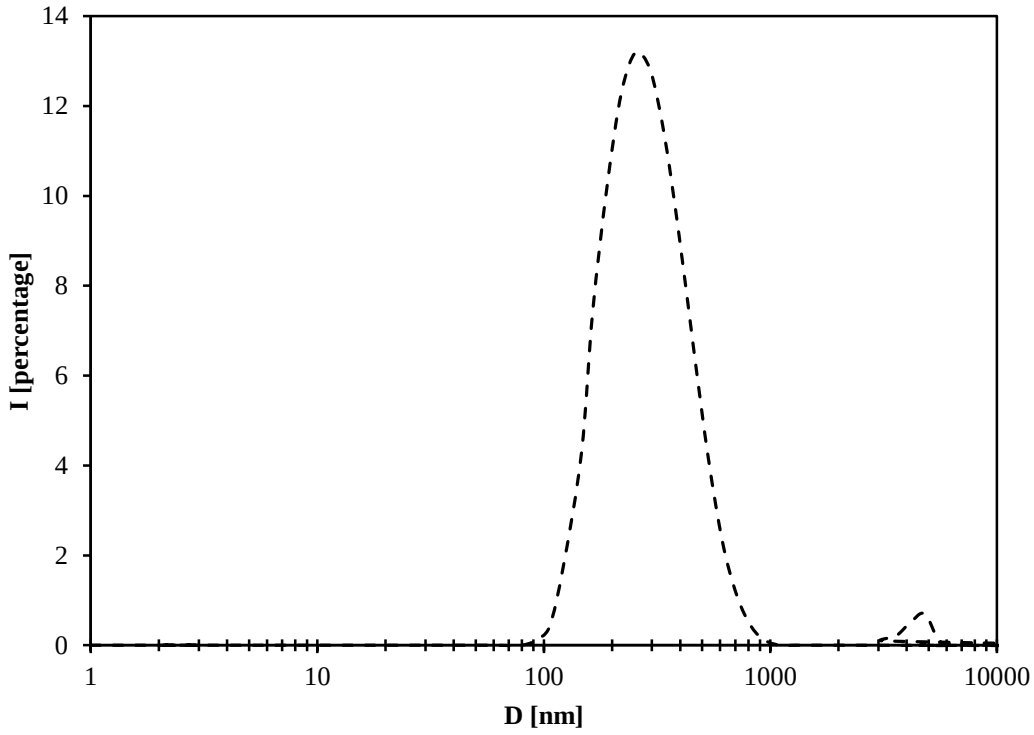

Figure 4.7: The size distribution of 0.05% volume fraction of Al_2O_3-water nanofluid (20 nm) at 25 °C

The average size was reported as 269.1 nm and the standard deviation was 127.2 nm, which is much bigger than the manufacturer's claim (d = 20 nm). A small tail at the right side of the graph indicates the existence of particles of a large diameter. The equipment uses a normal cuvette cell, which is not suitable to measure samples at high concentrations. Therefore, it puts a constraint on characterising the samples that are going to be used in the experiment.

An adequate amount of sonication energy was applied to break down loose aggregations of Al_2O_3-water nanofluid. In this study, 1.4 liter volumes of nanofluid with various volume fractions were needed. Therefore, a variable, energy density (α) was defined, which is the ratio of applied sonicated energy divided by the volume of the sonicated sample's volume, as given in Equation 4.2.

$$\alpha = \frac{Applied\ sonication\ energy}{Volume} = \frac{kJ}{ml} \qquad \text{Equation 4.2}$$

The effect of sonication energy density on the reported average size of Al_2O_3-water nanofluid is shown in Figure 4.8.

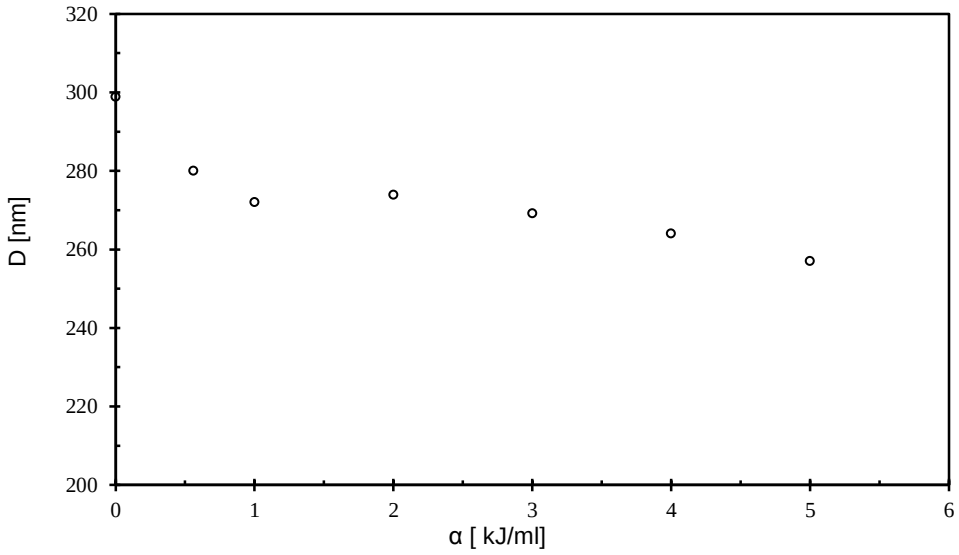

Figure 4.8: The effect of sonication energy on the mean size of Al_2O_3-water nanofluid

It follows from Figure 4.8 that increasing the sonication time does not have a significant effect on the average size of dispersed (single-step) Al_2O_3-water nanofluid. However, the

mean size of nanofluids that have been prepared using the two-step technique, such as ZnO nanofluid (d = 20 nm), is more sensitive to energy density, as shown in Figure 4.9.

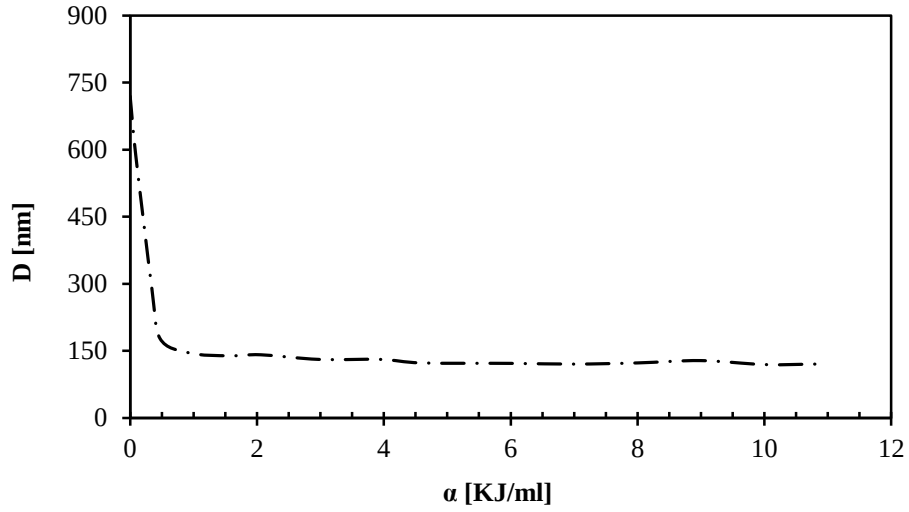

Figure 4.9: The effect of sonication energy density on the average size of ZnO-water nanofluid (d = 20 nm) (two-step)

The graph below shows the plunging of ZnO (20 nm) nanoparticles' average size with increasing sonication energy at the beginning of the sonication process. A further increase in sonication energy density does not reduce the average size of the nanofluid. In fact, applying more sonication energy density will have a negative effect on the stability of the nanofluid. This can be followed in Figure 4.10.

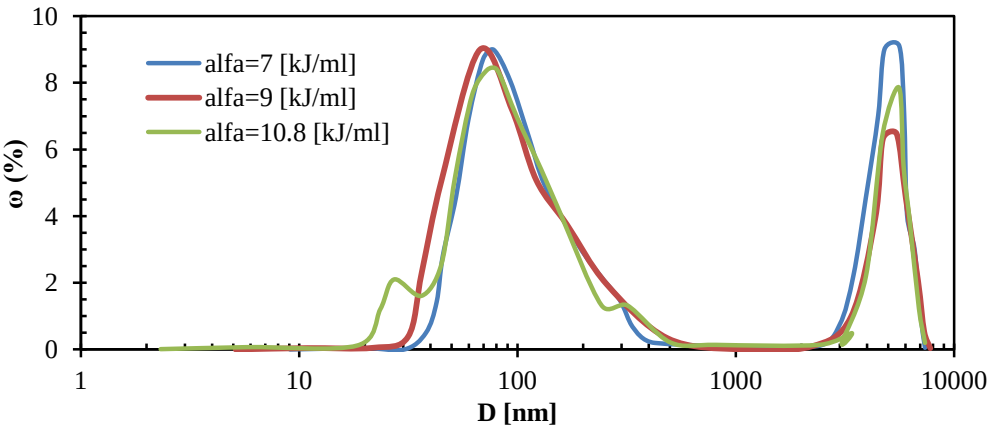

Figure 4.10: The effect of high sonication energy density on the size distribution of the ZnO-water nanofluid (d = 20 nm)

The second peak that appears on the right side of the graph depicts particles with a large diameter, which could ruin the sample's stability. Therefore, to avoid this second peak in the size distribution of nanoparticles, the energy density was chosen as α = 2 kJ/ml.

4.2.3 Zeta potential

The stability of nanofluids could be verified using zeta potential value. A Zetasizer ZS (Malvern Instruments Limited in the UK) was used to measure the zeta potential of the 0.01% volume fraction of Al_2O_3-water nanofluid. The average zeta potential was reported as -32 mV with a standard deviation of 4.67 mv, which is in the range of stable nanofluid [47]. Figure 4.11 shows the zeta potential distribution of the nanofluid.

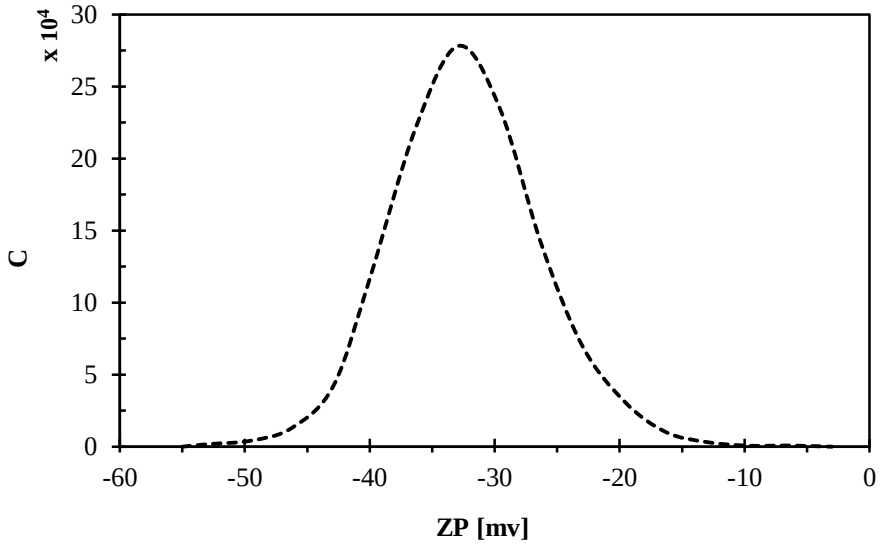

Figure 4.11: The zeta potential of 0.01% volume fraction of Al_2O_3-water nanofluids at 25 °C

The effect of the temperature on the zeta potential value of Al_2O_3-water nanofluid was investigated using a Malvern zetasizer, as listed in Table 4.1.

Table 4.1: The effect of temperature on the size and zeta potential of 0.01% concentration Al_2O_3-water nanofluid (d = 20–30 nm)

Temperature (°C)	Zeta potential (mV)	Mean size (nm)
5	-35.4	221.9
15	-34.5	240
25	-32.6	250
35	-28.9	255.4
45	-28	264.7
55	-26.8	275.7

Al_2O_3-water nanofluid at 5 °C has 8.5 and 32% higher zeta potential value at 25 and 55 °C respectively. An increase in the viscosity of the base fluid (water) might be the reason for an increase in the zeta potential value. The effect of temperature on the mean average size is also unavoidable due to the Stokes-Einstein equation [138] to calculate the mean average size. The mean average size of nanoparticles increases when the temperature increases, as shown in Equation 4.1.

The effect of sonication on the average mean size was discussed before and it was reported that an increase in sonication energy density does not significantly reduce the mean size of Al_2O_3-water nanofluid. The appearance of the second peak in the size distribution could also ruin the nanofluid's stability. Figure 4.12 shows the zeta potential distribution of ZnO-water nanofluid (d = 20 nm) as a function of various energy densities (α = 0.2 and 7 kJ/ml), as shown in Figure 4.12.

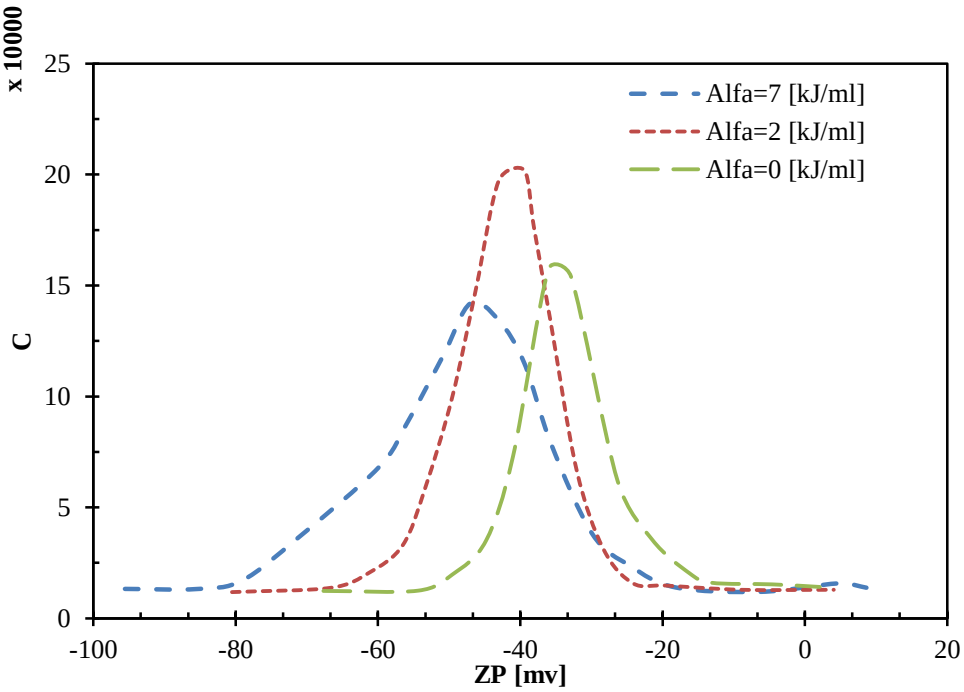

Figure 4.12: The effect of various sonication energy densities on the zeta potential of ZnO-water nanofluid

The graph shows that increasing sonication energy density increases the zeta potential's normal distribution domain of ZnO-water nanofluid. It follows from Figure 4.12 that some percentages of the sample have a very low zeta potential, which might ruin the stability of the sample. This observation agrees with the size distribution of the sample. Therefore, an optimum value for energy density should provide the minimum average size and minimum standard deviation value for zeta potential, which was chosen for ZnO-water nanofluid (d = 20 nm) α = 2 kJ/ml.

4.2.4 UV-visible spectrophotometry

The UV-visible spectrophotometry analysis was used to verify the stability of nanofluids. Using the Beer-Lambert Law (Equation 4.3), the light absorbency ratio index of the nanofluid can be calculated using Equation 4.3.

$$A_b = -\log\frac{I_0}{I} = \varepsilon l \Psi. \qquad \text{Equation 4.3}$$

where A_b is the absorbance of light, I_0 is the intensity of the UV-visible light through the blank cuvette, I is the intensity of the light through the samples, ε is the molar absorptivity, l is the length of the optical path, and Ψ is the molar concentration of the particles in suspension. The 0.01, 0.02 and 0.04% volume fractions of Al_2O_3-water nanofluid were prepared. First, the equipment (spectrophotometer Jenway model 3715 wavelength range 198–1 000 nm and absorbance -0.3–3.5 A) is calibrated using a cuvette filled only with the base fluid, and the desired wavelength is set. This is followed by the scanning wavelength range 200–999 nm to find the maximum absorbance. At the specific wavelength at which the maximum absorbance occurred, as shown in Figure 4.13, three concentrations with different volume fractions (0.01, 0.02 and 0.04%), which are a function of absorbance, were set. The line passing through these three points gives a linear trend that will be used to measure the unknown concentration of samples at a different time. The concentration of the sample was measured after preparation at a 228 nm wavelength. The wavelength at which maximum absorbance occurred is shown in Figure 4.13 during the experiment.

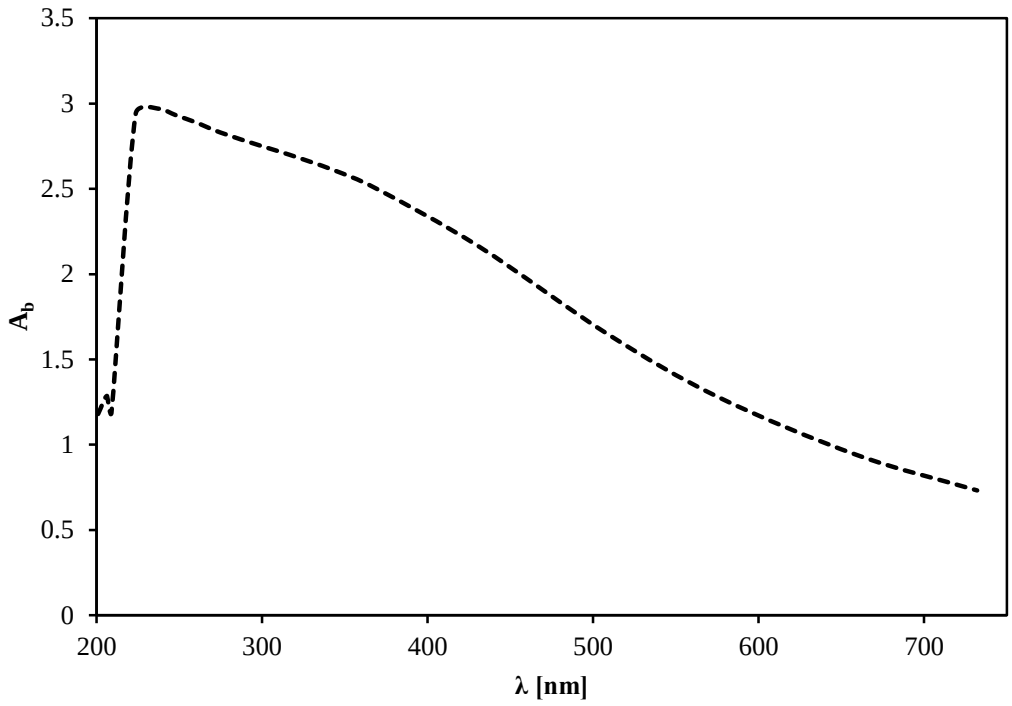

Figure 4.13: The effect of Al_2O_3-water nanofluid wavelength on absorbance

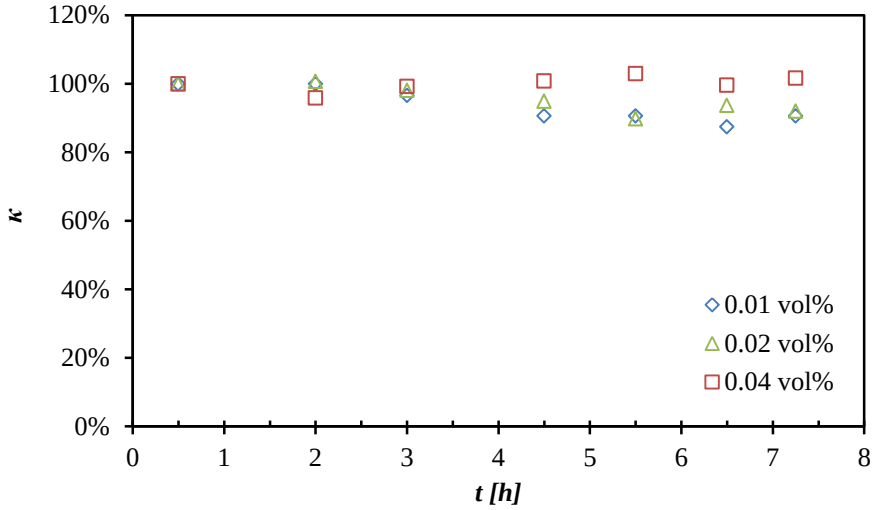

Figure 4.14: The changing concentration of the Al_2O_3-water nanofluid after preparation

Figure 4.14 illustrates that during the six hours after the nanofluid preparation (the time needed for the experimental investigation of nanofluid natural convection), no sedimentation of 0.04% volume fraction of Al_2O_3-water nanoparticles was observed. It was shown that Al_2O_3-water nanofluid is stable for longer with an increasing concentration of nanofluid.

4.3 The viscosity of nanofluids

Viscous forces are investigated to determine their effect on natural convection. The dispersion of nanoparticles escalates the viscosity of the base fluid [9]. The viscosity of Al_2O_3-water nanofluid is a function of volume fraction and temperature, as shown in Figure 4.15.

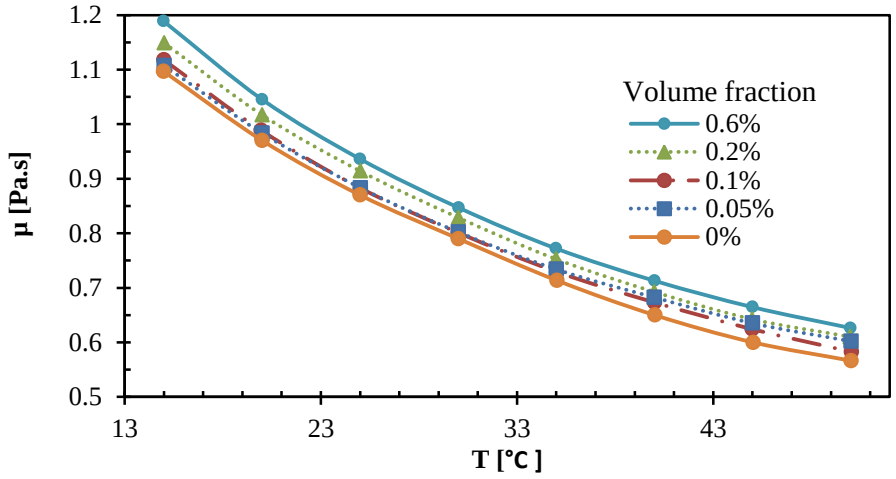

Figure 4.15: The effect of temperature and volume fraction on the viscosity of Al_2O_3-water nanofluid (d = 20–30 nm)

From Figure 4.16, it follows that the viscosity of the Al_2O_3-water nanofluid is enhanced by 7.5% with increasing nanoparticle concentrations from 0.0 to 0.6% volume fraction. The viscosity decreases when the temperature of the nanofluid is increased from 15 to 50 °C.

Many researchers use the theoretical models of Einstein [82] (Equation 4.4) and Brinkman [86] (Equation 4. 5) to predict the viscosity of nanofluids. However, these formulae do not take the effect of temperature or the size and shape of the nanoparticles into account.

$$\frac{\mu_{nf}}{\mu_f} = (1 + 2.5\varphi) \qquad \text{Equation 4.4}$$

$$\frac{\mu_{nf}}{\mu_f} = \frac{1}{(1-\varphi)^{2.5}} \qquad \text{Equation 4. 5}$$

Meyer et al. [9] demonstrate that the theoretical viscosity models of Al_2O_3-water nanofluid, specifically at a high volume fraction, predict different values. In addition, the deviation between the experimental measurement of the viscosity of Al_2O_3-water nanofluid (d = 20–30 nm) and the theoretical models was observed, as shown in Figure 4.16.

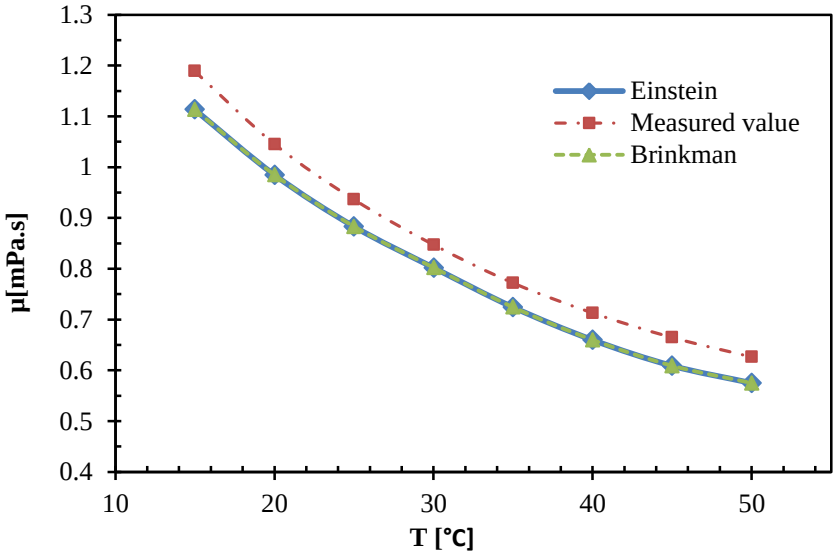

Figure 4.16: The theoretical viscosity of 0.6% volume fraction Al_2O_3-water (d = 20–30 nm) and experimental measurement

Figure 4.16 showed a 7.5% deviation in the viscosity of 0.6% volume fraction Al_2O_3-water (d = 20–30 nm) using theoretical models and experimental measurements. The deviation between the predicted viscosity and measured viscosity increased when the volume fraction of alumina nanoparticles increased. Therefore, the author measured the viscosity of the nanofluid.

4.4 The effect of nanofluid volume fraction on *h*

Nanofluid concentration is a major factor that could affect the heat transfer coefficient of nanofluids. Researchers have reported contradictory results with regard to the effect of nanofluid concentration on nanofluids' natural convection heat transfer coefficient. The study was conducted on much diluted concentrations (0, 0.05, 0.1, 0.2, 0.4 and 0.6% volume fraction) of Al_2O_3-water nanofluid (d = 20–30 nm). From Figure 4.17, it follows that the suspending alumina nanoparticle improved the natural convection heat transfer coefficient by an average of 15% in comparison to its base fluid (water) at 0.1% volume fraction. However, a further increase in the volume fraction of the nanofluid resulted in a decrease in the heat transfer coefficient with an increase in volume fraction. The combination effect of changing thermophysical properties of nanofluids by increasing nanoparticle concentrations, in particular viscosity and thermal conductivity of the nanofluids, leads to a reduction of *Ra* number which consequently result in low heat transfer coefficient using equation 2.13. However, dominant effect of viscosity increment for high volume fractions makes a reduction effect in natural convection heat transfer as well.

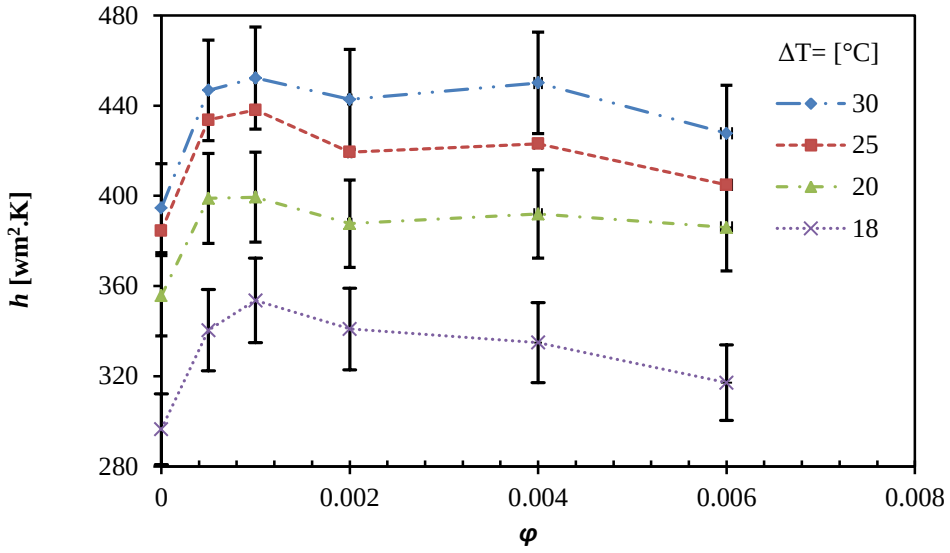

Figure 4.17: The effect of the volume fraction of Al_2O_3-water nanofluid on the natural convection heat transfer coefficient

From Figure 4.17, it follows that the increase in the temperature difference between the hot and the cold walls improves the *Ra* and subsequently enhances the natural convection heat transfer coefficient. For example, changing the walls' temperature difference from 18 to 30 °C brings about an improvement of 25.6% in the heat transfer coefficient at 0.1% volume fraction. In this study, the nanofluid concentrations were less than 0.6% volume fraction in order to find the volume fraction that resulted in the maximum nanofluid heat transfer coefficient.

4.5 The effect of volume fraction on *Ra* and *Nu*

Nanofluids' natural convection heat transfer variables are presented in non-dimensional form (*Nu* and *Ra*) to facilitate the comparison of the results with previous natural convection studies of nanofluids. The effect of the nanofluid concentration (φ = 0% to 0.6% volume fraction) and *Ra* (3.49×10^8 to 1.05×10^9) on the average *Nu* was studied and plotted in Figure 4.18.

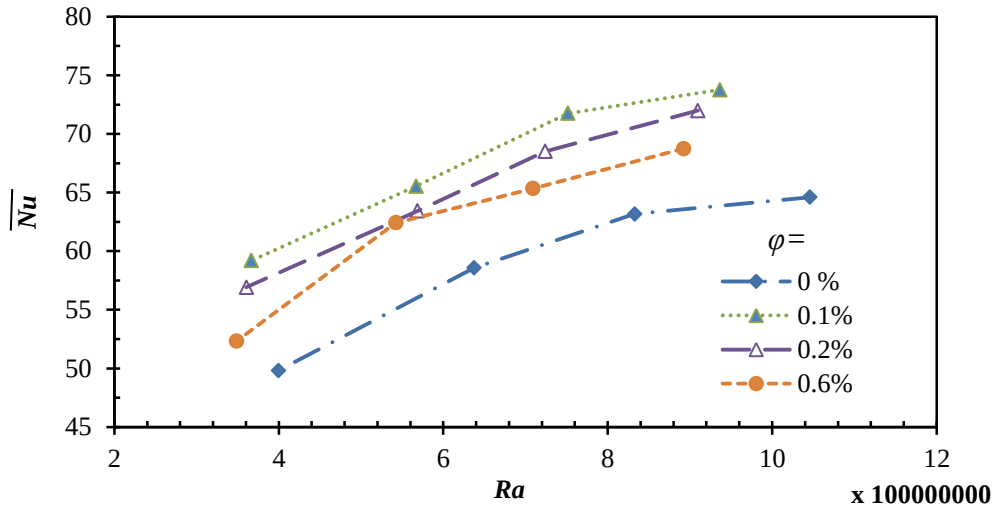

Figure 4.18: The effect of the *Ra* and volume fraction of Al_2O_3-water nanofluid (d = 20–30 nm) on the average *Nu*

Figure 4.18 illustrates that the average *Nu* increased with an increasing *Ra* for both the base fluid and the Al_2O_3-water nanofluid. However, at the same Ra, increasing the nanofluid volume fraction from 0.1 to 0.6% results in a 13% reduction of the average *Nu*. Although an increase in the volume fraction enhanced the thermal conductivity and viscosity of the nanofluid, the *Ra* decreased with an increasing volume fraction of the nanofluid. Therefore, the nanofluid volume fraction also has an influence on the *Ra* in such a way that when the same temperature is set for the heated and cooled walls, the *Ra* value decreases as the concentration of nanofluids increases. For example, when the volume fraction increases from 0 to 0.6%, the *Ra* value decreases by 15.5%. Equation 3.10 depicts that the *Ra* is more sensitive to the enhancement of both viscosity and thermal conductivity in comparison to the other thermophysical properties by increasing the nanofluids concentration , which led to the reduction of the Ra.

Equation 4.6 expresses the average *Nu* as a function of the *Ra* and the volume fraction for the natural convection of alumina nanofluids using curve fit on the data in Figure 4.18.

$$\overline{Nu} = 0.6091 Ra^{0.235} \varphi^{0.00584} \quad \leq 0.001$$
$$\overline{Nu} = 0.482 Ra^{0.2356} \varphi^{-0.026} \quad > 0.001 \quad R^2 = 94\%$$

Equation 4.6

4.6 Temperature distribution

The temperature distribution in the cavity provides useful information for the validation of numerical results. Monitoring the temperature along the cavity normalised the temperature (Equation 4. 7), and the distance across the test cell (Equation 4. 8) was defined.

$$\theta = \frac{T - T_{C_{ave}}}{T_{H_{ave}} - T_{C\,ave}}$$

Equation 4. 7

$$\delta = S / L$$

Equation 4. 8

Figure 4.19 demonstrates the temperature distribution in the test cell as a function of the normalised temperature and distance in the test cell at two concentrations of Al_2O_3-water nanofluid (d = 20–nm) (0.1 and 0.6% volume fraction).

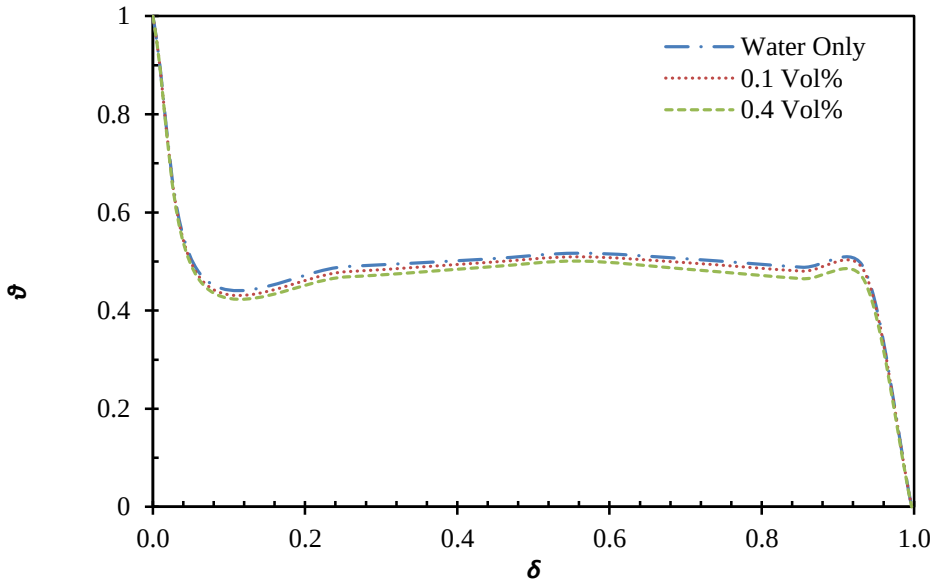

Figure 4.19: The effect of the alumina concentration on the temperature distribution across the test cell

The graph illustrates that on increasing the concentration, the temperature of the nanofluid decreases slightly. Therefore, the degradation temperature gradient results in a higher heat transfer rate, as well as a higher effective thermal conductivity. The results have the same trend as the result reported by Nnanna [131], but at a low volume fraction. However, owing to the much diluted concentrations, the temperature differences between the base fluid and the nanofluid were small.

For comparison purposes, the heat transfer rate, temperatures on the hot and the cold walls, *Ra* and average *Nu* are listed in Table 4.2 for 0.1% volume fraction of Al_2O_3-water nanofluid and in Table 4.3 for water only. By keeping the same temperature set on the walls, Table 4.2 and Table 4.3 demonstrate that the 0.1% volume fraction alumina nanofluid did not significantly change the heat transfer rate (approximately 3%). However, an average of approximately 14% enhancement in the *Nu* was observed. Changing the thermophysical properties of the nanofluid by adding nanoparticles could be the reason for this improvement.

Table 4.2: The experimental measurement of 0.1% volume fraction of Al_2O_3-water nanofluid

Test	*Q(W)*	$T_{c\text{-}wall}$(°C)	$T_{h\text{-}wall}$(°C)	$T_{c\text{-}ave}$	$T_{h\text{-}ave}$	ΔT_{ave}	T_{centre}	*Ra*	$\overline{Nu}$
1	*143.1*	T_{1c}=22.61 T_{2c}=22.25 T_{3c}=18.44	T_{1h}=52.67 T_{2h}=49.98 T_{3h}=47.16	*21.1*	*49.93*	*35.5*	*36.38*	9.36×10^{8}	*73.99*
2	*117.29*	T_{1c}=22.79 T_{2c}=22.19 T_{3c}=18.95	T_{1h}=48.55 T_{2h}=46.25 T_{3h}=43.69	*21.31*	*46.16*	*33.73*	*34.45*	7.52×10^{8}	*70.85*
3	*87.7*	T_{1c}=24.43 T_{2c}=23.86 T_{3c}=21.45	T_{1h}=44.76 T_{2h}=42.97 T_{3h}=40.97	*23.24*	*42.9*	*33.07*	*33.54*	5.67×10^{8}	*67.3*
4	*71.74*	T_{1c}=16.45 T_{2c}=15.74 T_{3c}=13.53	T_{1h}=35.69 T_{2h}=34.02 T_{3h}=32.19	*15.24*	*34*	*24.62*	*25.25*	3.67×10^{8}	*59.12*

Table 4.3 The experimental measurement of water in the test cell

Test	*Q(W)*	$T_{c\text{-}wall}$(°C)	$T_{h\text{-}wall}$(°C)	$T_{c\text{-}ave}$	$T_{h\text{-}ave}$	ΔT_{ave}	T_{centre}	*Ra*	$\overline{Nu}$
1	138.6	T_{1c}=22.81 T_{2c}=22.53 T_{3c}=17.68	T_{1h}=52.30 T_{2h}=50.34 T_{3h}=49.91	21	50.85	35.92	35.91	1.05×10^{9}	65.16
2	113.6	T_{1c}=22.73 T_{2c}=21.87 T_{3c}=18.62	T_{1h}=48.43 T_{2h}=46.57 T_{3h}=46.28	21.07	47.09	34.08	34.28	8.33×10^{8}	62.85
3	85.2	T_{1c}=24.16 T_{2c}=22.75 T_{3c}=21.05	T_{1h}=44.67 T_{2h}=43.28 T_{3h}=42.93	22.65	43.62	33.14	33.30	6.37×10^{8}	59.14
4	68.6	T_{1c}=16.07 T_{2c}=14.8 T_{3c}=13.13	T_{1h}=35.56 T_{2h}=34.42 T_{3h}=34.02	14.66	34.66	24.66	24.99	4×10^{8}	50.87

4.7 Uncertainty analysis

An uncertainty analysis was performed to show the reliability of the experimental data. The methods of Kline and McClintock [139] and Moffatt [140] were used to calculate the uncertainty of the measured data. Measurement of temperature and flow meter were the main source of errors. Equation 4.9 to Equation 4.11 were used to calculate the uncertainty of the heat transfer coefficient.

$$\delta Q = \left(\left(\frac{\partial Q}{\partial \dot{m}} \delta \dot{m} \right)^2 + \left(\frac{\partial Q}{\partial c_{p_{bf}}} \delta c_{p_{bf}} \right)^2 + \left(\frac{\partial Q}{\partial T_h} \delta T_H \right)^2 + \left(\frac{\partial Q}{\partial T_c} \delta T_C \right)^2 \right)^{\frac{1}{2}} \quad \text{Equation 4.9}$$

$$\delta h = \left(\left(\frac{\partial h}{\partial Q} \delta Q \right)^2 + \left(\frac{\partial h}{\partial A} \delta A \right)^2 + \left(\frac{\partial h}{\partial T_h} \delta T_h \right)^2 + \left(\frac{\partial h}{\partial T_c} \delta T_c \right)^2 \right)^{\frac{1}{2}} \quad \text{Equation 4.10}$$

$$\delta Nu = \left(\left(\frac{\partial Nu}{\partial h} \delta h \right)^2 + \left(\frac{\partial Nu}{\partial L_c} \delta L_c \right)^2 + \left(\frac{\partial Nu}{\partial k_{eff}} \delta k_{eff} \right)^2 \right)^{\frac{1}{2}} \quad \text{Equation 4.11}$$

All uncertainties were calculated within 95% confidence. Therefore, the standard deviation of the thermocouple and flow meter measurement was multiplied by two to reach 95% confidence zone. Table 4 4 contains instruments with their range, precision, bias and accuracy. The full uncertainty analysis is given in the appendix.

Table 4 4: Accuracy and range of instruments that were used

Instrument	Range	Accuracy
Thermocouple	<150 °C	0.02 °C[a]
Flow meter	0.0666 to 0.3333 L/s	±0.01% full scale + 2% of measured value
Weight scale	0 to 220 g	0.0001 g
Thermal bath	-30 to 200 °C	0.005 °C
Vernier	0 to 20 cm	0.02 mm

a: Calibrated with PT_100 with an accuracy of 0.005 °C, which is an internal thermocouple

The maximum uncertainty for the nanofluid heat transfer coefficient, *Nu*, and *Ra* were found to be 5.3, 4.62 and 4.45% respectively.

4.8 Conclusion

In summary, Al_2O_3-water nanofluid was characterised using TEM, SEM, zetasizer, zeta potential, the sonication effect on size distribution, UV-visible spectrophotometer and viscometer. TEM and SEM images are suitable to show the morphology of nanofluids. Due to the drying out of the sample before observing it, the reported size distribution might not match the size of the nanoparticles in the liquid suspension. However, a zetasizer has the capability of measuring a nanoparticle's size in liquid form. Therefore, the size distribution of the nanoparticles is more trustworthy. The effect of sonication energy density on the single-step prepared Al_2O_3-water nanofluid (d = 20–30 nm) was investigated using a Malvern zetasizer. The results showed that dispersed nanofluids have less sensitivity to the sonication energy density in comparison to two-step prepared nanofluids. One kJ/ml energy density reduced the average size of the two-tep preparation method of ZnO-water nanofluid (d = 20 nm) by 366%, even though the average particle size of dispersed Al_2O_3-water

nanofluid (single-step preparation method) only dropped by 20% when using the same energy density. Therefore, the energy density (α) of 1 kJ/ml is good enough to break down the loose aggregation of the nanoparticles. An average size distribution of Al_2O_3-water nanofluid was reported to be 269 nm at 25 °C, which is much bigger than that claimed by the manufacturer. The stability of the nanofluid was confirmed with a zeta potential measurement that was -32.6 mV at 25 °C for 0.05% volume fraction. The temperature and volume fraction effects on zeta potential, as well as the mean average size measurement, was discussed in detail. It was found that nanofluid has better stability at a lower temperature due to the increase in the base fluid's viscosity.

The experimental measurements of nanofluid viscosity at 0.6 % volume fraction was 7.5% higher than the viscosity of the base fluid at 25 °C. The theoretical models underpredicted the values. Furthermore, the viscosity of nanofluid decreased when the temperature was increased.

An experimental study on the natural convection cavity flow with Al_2O_3-water nanofluids has been conducted for a high *Ra* range of 3.49×10^8 to 1.05×10^9. The nanofluids (single-step preparation method) were investigated for a volume fraction range of 0 to 0.6%. Searching for the optimum value of the heat transfer coefficient at the much diluted concentration of nanofluids revealed that adding alumina nanoparticles could enhance the natural convection heat transfer coefficient by 15%, at $\varphi = 0.1$ vol.%. A further increase in the concentration of an Al_2O_3 nanoparticle has the reverse effect on the heat transfer coefficient. Therefore, the concentration of nanoparticles has an optimum value that maximises the natural heat transfer coefficient in nanofluids. This is contrary to the results of many numerical investigations of natural convection in nanofluids. Consequently, further investigations of different nanoparticles are needed to fully understand the counteracting effects of thermal conductivity and viscosity by adding nanoparticles.

5 Summary, conclusion and recommendation

The wide-spectrum application of natural convection in industries like solar collectors, electronic cooling, EMES, nuclear reactor and heating, ventilation and air conditioning (HVAC) points out its importance. However, the heat transfer coefficient of natural convection is less in comparison to other heat transfer types. Applying a new, advanced colloidal suspension (nanofluid) could enhance the natural convection heat transfer coefficient. Moreover, the contradictory results of the numerical simulations of nanofluids' natural convection, as well as the inconsistency in experimental investigations, encourage researchers to conduct more experimental studies of natural convection in nanofluids. Therefore, an experimental study on natural convection cavity flow with Al_2O_3-water nanofluids (d = 20–30 nm) has been conducted for a high *Ra* range of 3.49×10^8 to 1.05×10^9.

The constructed experimental setup has an aspect ratio of 1 and consists of two constant opposite vertical walls. The rest of the walls are insulated. A water-filled cavity confirmed the validity of the experimental setup against available data. The nanofluid (single-step preparation method) was investigated for a volume fraction range of 0 to 0.6%. The manufacturer claimed that the size of the nanoparticles were 20–30 nm. The TEM image indicated a range of particle sizes, while the zetasizer showed that the average particle size was 269 nm.

The nanofluid's stability was confirmed by using UV-visible spectroscopy and a zeta potential measurement. The absolute value of the zeta potential was greater than 30 mV. Therefore, it can be concluded that, for nanofluid investigation, TEM (for particles size), UV-visible spectroscopy (for stability) and a zetasizer (for average particles in nanofluids) must

be used to accurately characterise the nanofluid. The inconsistency of various viscosity models for nanofluids led researchers to experimentally measure the viscosities. The experimental measurements of nanofluid viscosity at 0.6% volume fraction was 7.5% higher than the viscosity of the base fluid at 25° C, and theoretical models underpredicted the values. Furthermore, the effect of a temperature range between 15 and 50 °C on nanofluid viscosity was investigated. The results showed that the viscosity of the nanofluid decreased with increasing temperature.

Various alumina-water nanofluid concentrations (0, 0.05, 0.1, 0.2, 0.4 and 0.6% volume fraction) were formulated to investigate the effect of nanofluid concentration on its heat transfer coefficient. Searching for the optimum heat transfer coefficient at a much diluted concentration of nanofluids reveals that adding alumina nanoparticles could enhance the natural convection heat transfer coefficient by 15%, at φ = 0.1 vol.%. A further increase in the concentration of Al_2O_3 nanoparticles has the reverse effect on the heat transfer coefficient. Therefore, the concentration of nanoparticles has an optimum value that maximises the natural heat transfer coefficient for nanofluids. The study's results were in contrast to the results of many numerical investigations of natural convection in nanofluids.

The temperature distribution of the nanofluid in the test cell illustrates that suspending the nanoparticles in a base fluid decreases the temperature in the test cell. Moreover, the temperature distribution gives a benchmark to validate the numerical simulation of the nanofluid's natural convection.

The following future research focuses are recommended:

- The effect of nanoparticle size and shape on the natural convection heat transfer coefficient

- Manipulating a magnetic field by using magnetic nanoparticles to enhance the natural convection heat transfer coefficient
- Investigating natural convection in nanofluids at the inverse density regime (around 4 °C for water as a base fluid)
- The experimental investigation of natural convection in nanofluids in a porous media using the test range
- The design of an experimental setup that can facilitate a wider *Ra* range

References

[1] G. Chen, 2005, Nanoscale energy transport and conversion, in *Nanoscale energy transport and conversion*, Oxford University Press, New York, NY, pp. 4–5.

[2] R.S. Vajjha, D.K. Das, 2009, Experimental determination of thermal conductivity of three nanofluids and development of new correlations, *International Journal of Heat and Mass Transfer,* 52: 4675–4682.doi:10.1016/j.ijheatmasstransfer.2009.06.027.

[3] J.C. Maxwell, 1881, *A treatise on electricity and magnetism*, 2nd ed., Clarendon press, Wortley.

[4] S.U.S. Choi, 1995, Enhancing thermal conductivity of fluids with nanoparticles, in *ASME International Mechanical Engineering Congress & Exposition*, San Francisco, CA, (pp. 99–105.

[5] S.K. Das, S.U. Choi, W. Yu, T. Pradeep, 2008, *Nanofluids science and technology*, 1st ed., Wiley, Hoboken, New Jersey, NJ, p. 407.

[6] K.E. Drexler, 2005, Productive nanosystems: the physics of molecular fabrication, *Physics Education,* 40: 339–346. doi:10.1088/0031-9120/40/4/003.

[7] J. Buongiorno, 2006, Convective transport in nanofluids, *Journal of Heat Transfer,* 128: 240–250. doi:10.1115/1.2150834.

[8] H.Ş. Aybar, M. Sharifpur, M.R. Azizian, M. Mehrabi, J.P. Meyer, 2015, A review of the thermal conductivity models for nanofluids, *Heat Transfer Engineering,* 36: 1085–1110. doi:10.1080/01457632.2015.987586.

[9] J.P. Meyer, S.A. Adio, M. Sharifpur, P.N. Nwosu, 2015, The viscosity of nanofluids: a review of the theoretical, empirical and numerical models, *Heat Transfer Engineering,* 7632. doi:10.1080/01457632.2015.1057447.

[10] C.T. Nguyen, F. Desgranges, N. Galanis, G. Roy, T. Maré, S. Boucher, Viscosity data for Al2O3-water nanofluid-hysteresis: is heat transfer enhancement using nanofluids reliable? *International Journal of Thermal Sciences,* 47: 103–111. doi:10.1016/j.ijthermalsci.2007.01.033.

[11] A. Baïri, E. Zarco-Pernia, J.M. García De María, 2014, A review on natural convection in enclosures for engineering applications. The particular case of the parallelogrammic diode cavity, *Applied Thermal Engineering,* 63: 304–322. doi:10.1016/j.applthermaleng.2013.10.065.

[12] J.A. Eastman, S.U.S. Choi, S. Li, W. Yu, L.J. Thompson, 2001, Anomalously increased effective thermal conductivities of ethylene glycol-based nanofluids containing copper nanoparticles, *Applied Physics Letters,* 78: 718–720. doi:10.1063/1.1341218.

[13] H. Akoh, Y. Tsukasaki, S. Yatsuya, A. Tasaki, 1978, Magnetic properties of ferromagnetic ultrafine particles prepared by vacuum evaporation on running oil substrate, *Journal of Crystal Growth,* 45: 495–500. doi:10.1016/0022-0248(78)90482-7.

[14] M. Chopkar, P.K. Das, I. Manna, 2006, Synthesis and characterization of nanofluid for advanced heat transfer applications, *Scripta Materialia*. doi:10.1016/j.scriptamat.2006.05.030.

[15] H. Bönnemann, S.S. Botha, B. Bladergroen, V.M. Linkov, 2005, Monodisperse copper- and silver-nanocolloids suitable for heat-conductive fluids, *Applied Organometallic Chemistry*, 19: 768–773. doi:10.1002/aoc.889.

[16] M. Brust, M. Walker, D. Bethell, D.J. Schiffrin, R. Whyman, 1994, Synthesis of thiol-derivatised gold nanoparticles, *Chemical Communications,* 1994: 801–802. doi:10.1039/c39940000801.

[17] M. Chandrasekar, S. Suresh, A. Chandra Bose, 2010, Experimental investigations and theoretical determination of thermal conductivity and viscosity of Al_2O_3/water nanofluid, *Experimental Thermal and Fluid Science,* 34: 210–216. doi:10.1016/j.expthermflusci.2009.10.022.

[18] R. Saleh, N. Putra, S.P. Prakoso, W.N. Septiadi, 2013, Experimental investigation of thermal conductivity and heat pipe thermal performance of ZnO nanofluids, *International Journal of Thermal Sciences,* 63: 125–132. doi:10.1016/j.ijthermalsci.2012.07.011.

[19] W. Yu, H. Xie, 2012, A review on nanofluids: preparation, stability mechanisms, and applications, *Journal of Nanomaterials*, 2012: 1–17. doi:10.1155/2012/435873.

[20] X.J. Wang, X. Li, S. Yang, 2009, Influence of pH and SDBS on the stability and thermal conductivity of nanofluids, *Energy and Fuels,* 23: 2684–2689. doi:10.1021/ef800865a.

[21] D. Zhu, X. Li, N. Wang, X. Wang, J. Gao, H. Li, 2009, Dispersion behavior and thermal conductivity characteristics of Al_2O_3–H_2O nanofluids, *Current Applied Physics,* 9: 131–139. doi:10.1016/j.cap.2007.12.008.

[22] J. Lee, Y.J. Yoon, J.K. Eaton, K.E. Goodson, S.J. Bai, Analysis of oxide (Al_2O_3, CuO, and ZnO) and CNT nanoparticles disaggregation effect on the thermal conductivity and the viscosity of nanofluids, *International Journal of Precision Engineering and Manufacturing,* 15: 703–710. doi:10.1007/s12541-014-0390-1.

[23] P. Warrier, A. Teja, 2011, Effect of particle size on the thermal conductivity of nanofluids containing metallic nanoparticles, *Nanoscale Research Letters,* 6: 247. doi:10.1186/1556-276X-6-247.

[24] C.H. Chon, K.D. Kihm, S.P. Lee, S.U.S. Choi, 2005, Empirical correlation finding the role of temperature and particle size for nanofluid (Al_2O_3) thermal conductivity enhancement, *Applied Physics Letters,* 87: 1–3. doi:10.1063/1.2093936.

[25] K. Goudarzi, F. Nejati, E. Shojaeizadeh, S.K. Asadi Yousef-abad, 2015, Experimental study on the effect of pH variation of nanofluids on the thermal efficiency of a solar collector with helical tube, *Experimental Thermal and Fluid Science,* 60: 20–27. doi:10.1016/j.expthermflusci.2014.07.015.

[26] H. Konakanchi, R.S. Vajjha, G. Chukwu, D.K. Das, 2014, Measurements of pH of Three nanofluids and development of new correlations, *Heat Transfer Engineering*, 2014: 81–90. doi:10.1080/01457632.2014.906286

[27] Qsonica, 2015, Sonicator ultrasonic processor, Part no. Q700, 2015: 1–29. http://www.sonicator.com/literature/manuals/q700manual_rev_6-12.pdf (accessed 16 May 2016).

[28] S.J. Chung, J.P. Leonard, I. Nettleship, J.K. Lee, Y. Soong, D.V. Martello, 2009, Characterisation of ZnO nanoparticle suspension in water: the effectiveness of ultrasonic dispersion, *Powder Technology,* 194: 75–80. doi:10.1016/j.powtec.2009.03.025.

[29] K.S. Suganthi, K.S. Rajan, 2014, A formulation strategy for preparation of ZnO-propylene glycol-water nanofluids with improved transport properties, *International Journal of Heat and Mass Transfer,* 71: 653–663. doi:10.1016/j.ijheatmasstransfer.2013.12.044.

[30] K. Kwak, C. Kim, 2005, Viscosity and thermal conductivity of copper oxide nanofluid dispersed in ethylene glycol, *Korea Australia Rheology Journal*, 17: 35–40.

[31] T-K. Hong, H-S. Yang, C.J. Choi, 2005, Study of the enhanced thermal conductivity of Fe nanofluids, *Journal of Applied Physics,* 97: 064311. doi:10.1063/1.1861145.

[32] J.H. Lee, K.S. Hwang, S.P. Jang, B.H. Lee, J.H. Kim, S.U.S. Choi, 2008, Effective viscosities and thermal conductivities of aqueous nanofluids containing low volume concentrations of Al_2O_3 nanoparticles, *International Journal of Heat and Mass Transfer*, 51: 2651–2656. doi:10.1016/j.ijheatmasstransfer.2007.10.026.

[33] M.J. Pastoriza-Gallego, C. Casanova, R. Páramo, B. Barbés, J.L. Legido, M.M. Piñeiro, 2009, A study on stability and thermophysical properties (density and viscosity) of Al_2O_3 in water nanofluid, *Journal of Applied Physics,* 106: 1–8. doi:10.1063/1.3187732.

[34] R. Rajagopalan, P.C. Hiemenz, 1986, *Principles of colloid and surface chemistry*, 1st ed., CRC Press, New York, NY.

[35] L. Jiang, L. Gao, J. Sun, 2003, Production of aqueous colloidal dispersions of carbon nanotubes, *Journal of Colloid and Interface Science*, 260: 89–94. doi:10.1016/S0021-9797(02)00176-5.

[36] T. Yousefi, F. Veysi, E. Shojaeizadeh, S. Zinadini, 2012, An experimental investigation on the effect of Al_2O_3-H_2O nanofluid on the efficiency of flat-plate solar collectors, *Renewable Energy*, 39: 293–298. doi:10.1016/j.renene.2011.08.056.

[37] E.A. Dennis, 1973, Kinetic dependence of phospholipase A2 activity on the detergent Triton X 100, *Journal of Lipid Research,* 14: 152–159.

[38] R.J. Hunter, 2001, *Foundations of colloid science*, 2nd ed., Oxford University Press, Oxford, p. 435.

[39] M. Sakamoto, Y. Kanda, M. Miyahara, K. Higashitani, 2002, Origin of long-range attractive force between surfaces hydrophobized by surfactant adsorption, *Langmuir*, 18: 5713–5719. doi:10.1021/la025701j.

[40] E.V. Timofeeva, M.R. Moravek, D. Singh, 2011, Improving the heat transfer efficiency of synthetic oil with silica nanoparticles, *Journal of Colloid and Interface Science,* 364: 71–79. doi:10.1016/j.jcis.2011.08.004.

[41] S.M.S. Murshed, K.C. Leong, C. Yang, 2005, Enhanced thermal conductivity of TiO_2-water based nanofluids, *International Journal of Thermal Sciences,* 44: 367–373. doi:10.1016/j.ijthermalsci.2004.12.005.

[42] K.S. Suganthi, K.S. Rajan, 2012, Temperature induced changes in ZnO-water nanofluid: zeta potential, size distribution and viscosity profiles, *International Journal of Heat and Mass Transfer,* 55: 7969–7980. doi:10.1016/j.ijheatmasstransfer.2012.08.032.

[43] A. Ghadimi, I.H. Metselaar, 2013, The influence of surfactant and ultrasonic processing on improvement of stability, thermal conductivity and viscosity of titania nanofluid, *Experimental Thermal and Fluid Science*, 51: 1–9. doi:10.1016/j.expthermflusci.2013.06.001.

[44] K. Rohini Priya, K.S. Suganthi, K.S. Rajan, 2012, Transport properties of ultra-low concentration CuO-water nanofluids containing non-spherical nanoparticles, *International Journal of Heat and Mass Transfer*, 55: 4734–4743. doi:10.1016/j.ijheatmasstransfer.2012.04.035.

[45] P. Garg, J.L. Alvarado, C. Marsh, T.A. Carlson, D.A. Kessler, K. Annamalai, 2009, An experimental study on the effect of ultrasonication on viscosity and heat transfer performance of multi-wall carbon nanotube-based aqueous nanofluids, *International Journal of Heat and Mass Transfer,* 52: 5090–5101. doi:10.1016/j.ijheatmasstransfer.2009.04.029.

[46] H. Zhu, C. Zhang, Y. Tang, J. Wang, B. Ren, Y. Yin, 2007, Preparation and thermal conductivity of suspensions of graphite nanoparticles, *Carbon,* 45: 226–228.

[47] Malvern, n.d., Zeta potential: an introduction in 30 minutes. http://www.malvern.com/en/support/resource-center/technical-notes/TN101104ZetaPotentialIntroduction.aspx (accessed 16 May 2016).

[48] D. Lee, J-W. Kim, B.G. Kim, 2006, A new parameter to control heat transport in nanofluids: surface charge state of the particle in suspension, *Journal of Physical Chemistry,* B. 110: 4323–4328. doi:10.1021/jp057225m.

[49] J.M. Berg, A. Romoser, N. Banerjee, R. Zebda, C.M. Sayes, 2009, Toxicological evaluations, *Nanotoxicology*, 3: 276–283. doi:10.3109/17435390903276941.

[50] S. Witharana, I. Palabiyik, Z. Musina, Y. Ding, 2013, Stability of glycol nanofluids – the theory and experiment, *Powder Technology,* 239: 72–77. doi:10.1016/j.powtec.2013.01.039.

[51] L. Colla, L. Marinelli, L. Fedele, S. Bobbo, O. Manca, 2015, Characterisation and simulation of the heat transfer behaviour of water-based ZnO nanofluids, *Journal of Nanoscience and Nanotechnology*, 15: 3599–3609. doi:10.1166/jnn.2015.9864.

[52] H. Chang, M.H. Tsai, 2008, Synthesis and characterisation of ZnO nanoparticles having prism shape by a novel gas condensation process, *Reviews on Advanced Materials Science,* 18: 736–745.

[53] S.J. Chung, J.P. Leonard, I. Nettleship, J.K. Lee, Y. Soong, D.V. Martello, 2009, Characterisation of ZnO nanoparticle suspension in water: effectiveness of ultrasonic dispersion, *Powder Technology,* 194: 75–80. doi:10.1016/j.powtec.2009.03.025.

[54] M. Sharifpur, S.A. Adio, J.P. Meyer, 2015, Experimental investigation and model development for effective viscosity of Al2O3-glycerol nanofluids by using dimensional analysis and GMDH-NN methods, *International Communications in Heat and Mass Transfer,* 68: 208–219. doi:10.1016/j.icheatmasstransfer.2015.09.002.

[55] P. Garg, J.L. Alvarado, C. Marsh, T.A. Carlson, D.A. Kessler, K. Annamalai, 2009, An experimental study on the effect of ultrasonication on viscosity and heat transfer performance of multi-wall carbon nanotube-based aqueous nanofluids, *International Journal of Heat and Mass Transfer,* 52: 5090–5101. doi:10.1016/j.ijheatmasstransfer.2009.04.029.

[56] E.B. Haghighi, M. Saleemi, N. Nikkam, Z. Anwar, I. Lumbreras, M. Behi, 2013, Cooling performance of nanofluids in a small diameter tube, *Experimental Thermal and Fluid Science,* 49: 114–122. doi:10.1016/j.expthermflusci.2013.04.009.

[57] J. Lee, Y.J. Yoon, J.K. Eaton, K.E. Goodson, S.J. Bai, 2014, Analysis of oxide (Al_2O_3, CuO, and ZnO) and CNT nanoparticles disaggregation effect on the thermal conductivity and the viscosity of nanofluids, *International Journal of Precision Engineering and Manufacturing,* 15: 703–710. doi:10.1007/s12541-014-0390-1.

[58] D. Zhu, S. Wu, N. Wang, 2010, Thermal physics and critical heat flux characteristics of Al_2O_3-H_2O nanofluids, *Heat Transfer Engineering,* 31: 1213–1219. doi:10.1080/01457631003733019.

[59] F.S. Javadi, R. Saidur, M. 2013, Kamalisarvestani, investigating performance improvement of solar collectors by using nanofluids, *Renewable and Sustainable Energy Reviews*, 28: 232–245. doi:10.1016/j.rser.2013.06.053.

[60] I.M. Mahbubul, I.M. Shahrul, S.S. Khaleduzzaman, R. Saidur, M.A. Amalina, A. Turgut, 2015, Experimental investigation on effect of ultrasonication duration on colloidal dispersion and thermophysical properties of alumina – water nanofluid, *International Journal of Heat and Mass Transfer*, 88: 73–81. doi:10.1016/j.ijheatmasstransfer.2015.04.048.

[61] W. Yu, H. Xie, L. Chen, Y. Li, Investigation of thermal conductivity and viscosity of ethylene glycol based ZnO nanofluid, *Thermochimica Acta*, 491: 92–96. doi:10.1016/j.tca.2009.03.007.

[62] N. Putra, W. Roetzel, S.K. Das, 2003, Natural convection of nano-fluids, *Heat and Mass Transfer/Waerme- Und Stoffuebertragung*, 39: 775–784. doi:10.1007/s00231-002-0382-z.

[63] L. Chen, H. Xie, Y. Li, W. Yu, 2008, Nanofluids containing carbon nanotubes treated by mechanochemical reaction, *Thermochimica Acta*, 477: 21–24. doi:10.1016/j.tca.2008.08.001.

[64] D. Cabaleiro, M.J. Pastoriza-Gallego, M.M. Piñeiro, L. Lugo, 2013, Characterisation and measurements of thermal conductivity, density and rheological properties of zinc oxide nanoparticles dispersed in (ethane-1,2-diol+water) mixture, *Journal of Chemical Thermodynamics*, 58: 405–415. doi:10.1016/j.jct.2012.10.014.

[65] S. Mo, Y. Chen, L. Jia, X. Luo, 2012, Investigation on crystallisation of TiO_2-water nanofluids and deionized water, *Applied Energy*, 93: 65–70. doi:10.1016/j.apenergy.2011.07.014.

[66] Malvern, 2014, Zeta potential characterisation of concentrated titanium dioxide slurries with the ZEN1010 U sing high concentration cell, 2014: 2–5. http://www.malvern.com/en/support/resource-center/application-notes/AN101104TitaniumDioxideSlurries.aspx (accessed 16 May 2016).

[67] C.J. Ho, M.W. Chen, Z.W. Li, 2008, Numerical simulation of natural convection of nanofluid in a square enclosure: effects due to uncertainties of viscosity and thermal conductivity, *International Journal of Heat and Mass Transfer*, 51: 4506–4516. doi:10.1016/j.ijheatmasstransfer.2007.12.019.

[68] S.M.S. Murshed, K.C. Leong, C. Yang, 2008, Investigations of thermal conductivity and viscosity of nanofluids, *International Journal of Thermal Sciences*, 47: 560–568. doi:10.1016/j.ijthermalsci.2007.05.004.

[69] C.J. Ho, W.K. Liu, Y.S. Chang, C.C. Lin, 2010, Natural convection heat transfer of alumina-water nanofluid in vertical square enclosures: an experimental study, *International Journal of Thermal Sciences*, 49: 1345–1353. doi:10.1016/j.ijthermalsci.2010.02.013.

[70] G. Colangelo, E. Favale, A. De Risi, D. Laforgia, Results of experimental investigations on the heat conductivity of nanofluids based on diathermic oil for high temperature applications, *Applied Energy*, 97: 828–833. doi:10.1016/j.apenergy.2011.11.026.

[71] S.K. Das, N. Putra, P. Thiesen, W. Roetzel, 2003, Temperature dependence of thermal conductivity enhancement for nanofluids, *Journal of Heat Transfer*, 125: 567. doi:10.1115/1.1571080.

[72] Z. Said, M.H. Sajid, M.A. Alim, R. Saidur, N.A. Rahim, 2013, Experimental investigation of the thermophysical properties of AL_2O_3-nanofluid and its effect on a flat plate solar collector, *International Communications in Heat and Mass Transfer*, 48: 99–107. doi:10.1016/j.icheatmasstransfer.2013.09.005.

[73] R.M. Mostafizur, M.H.U. Bhuiyan, R. Saidur, A.R. Abdul Aziz, 2014, Thermal conductivity variation for methanol based nanofluids, *International Journal of Heat and Mass Transfer*, 76: 350–356. doi:10.1016/j.ijheatmasstransfer.2014.04.040.

[74] M.J. Pastoriza-Gallego, L. Lugo, D. Cabaleiro, J.L. Legido, M.M. Piñeiro, 2014, Thermophysical profile of ethylene glycol-based ZnO-nanofluids, *Journal of Chemical Thermodynamics*, 73: 23–30. doi:10.1016/j.jct.2013.07.002.

[75] H. Xie, W. Yu, Y. Li, L. Chen, 2011, Discussion on the thermal conductivity enhancement of nanofluids, *Nanoscale Research Letters*. 6: 124. doi:10.1186/1556-276X-6-124.

[76] L. Syam Sundar, E. Venkata Ramana, M.K. Singh, A.C.M. Sousa, 2014, Thermal conductivity and viscosity of stabilized ethylene glycol and water mixture Al_2O_3 nanofluids for heat transfer applications: an experimental study, *International Communications in Heat and Mass Transfer* 56: 86–95. doi:10.1016/j.icheatmasstransfer.2014.06.009.

[77] H.Ş. Aybar, M. Sharifpur, M.R. Azizian, M. Mehrabi, J.P. Meyer, 2015, A review of thermal conductivity models for nanofluids, *Heat Transfer Engineering*, 36: 1085–1110. doi:10.1080/01457632.2015.987586.

[78] J.C. Maxwell, 1873, *Electricity and magnetism*, Clarendon Press, Oxford.

[79] R.M. Mostafizur, M.H.U. Bhuiyan, R. Saidur, A.R.A. Aziz, 2014, Thermal conductivity variation for methanol based nanofluids, *International Journal of Heat and Mass Transfer*, 76: 350–356. doi:10.1016/j.ijheatmasstransfer.2014.04.040.

[80] C. Kleinstreuer, Y. Feng, 2011, Experimental and theoretical studies of nanofluid thermal conductivity enhancement: a review, *Nanoscale Research Letters*, 6: 439. doi:10.1186/1556-276X-6-439.

[81] M. Sharifpur, T. Ntumba, J.P. Meyer, 2012, Parametric analysis of effective thermal conductivity models for nanofluids, *ASME 2012 International Mechanical Engineering Congress and Exposition*, 2012: 1–11.

[82] P.K. Namburu, D.P. Kulkarni, A. Dandekar, D.K. Das, 2007, Experimental investigation of viscosity and specific heat of silicon dioxide nanofluids, *IET Micro and Nano Letters*, 2: 67–71. doi:10.1049/mnl.

[83] P.K. Namburu, D.P. Kulkarni, D. Misra, D.K. Das, 2007, Viscosity of copper oxide nanoparticles dispersed in ethylene glycol and water mixture, *Experimental Thermal and Fluid Science*, 32: 397–402. doi:10.1016/j.expthermflusci.2007.05.001.

[84] Z. Jia-Fei, L. Zhong-Yang, N. Ming-Jiang, C. Ke-Fa, 2009, Dependence of nanofluid viscosity on particle size and pH value, *Chinese Physics Letters*, 26 :066202. doi:10.1088/0256-307X/26/6/066202.

[85] A. Einstein, 1656, *Investigations on the theory of the Brownian movement*, Courier Corporation.

[86] H.C. Brinkman, 1952, The viscosity of concentrated suspensions and solutions, *Journal of Chemical Physics*, 20: 571. doi:10.1063/1.1700493.

[87] N.P. Cheremisinoff, 1986, *Encyclopedia of fluid mechanics. 3: Gas-liquid flows*, Elsevier, Amsterdam.

[88] B.C. Pak, Y.I. Cho, 1998, Hydrodynamic and heat transfer study of dispersed fluids with submicron metallic oxide particles, *Experimental Heat Transfer*, 11: 151–170. doi:10.1080/08916159808946559.

[89] R.S. Vajjha, D.K. Das, B.M. Mahagaonkar, 2009, Density measurement of different nanofluids and their comparison with theory, *Petroleum Science and Technology*, 27: 612–624. doi:10.1080/10916460701857714.

[90] J. Buongiorno, 2006, Convective transport in nanofluids, *Journal of Heat Transfer*, 128: 240. doi:10.1115/1.2150834.

[91] S-Q. Zhou, R. Ni, 2008, Measurement of the specific heat capacity of water-based Al_2O_3 nanofluid, *Applied Physics Letters*, 92: 093123. doi:10.1063/1.2890431.

[92] R.S. Vajjha, D.K. Das, 2009, Specific heat measurement of three nanofluids and development of new correlations, *Journal of Heat Transfer*, 131: 071601. doi:10.1115/1.3090813.

[93] A.G.A. Nnanna, 2007, Experimental model of temperature-driven nanofluid, *Journal of Heat Transfer*, 129: 697. doi:10.1115/1.2717239.

[94] A.K. Nayak, R.K. Singh, P.P. Kulkarni, 2010, Measurement of volumetric thermal expansion coefficient of various nanofluids, *Technical Physics Letters*, 36: 696–698. doi:10.1134/S1063785010080055.

[95] C.T. Nguyen, G. Roy, N. Galanis, S. Suiro, S. Malo, 2006, Heat transfer enhancement by using Al_2O_3-water nanofluid in a liquid cooling system for microprocessors 2 experimental setup, *4th WSEAS, Elounda*, Greece, 2006: 103–108.

[96] M. Lomascolo, G. Colangelo, M. Milanese, A. de Risi, 2015, Review of heat transfer in nanofluids: conductive, convective and radiative experimental results, *Renewable and Sustainable Energy Reviews*, 43: 1182–1198. doi:10.1016/j.rser.2014.11.086.

[97] H. Chen, W. Yang, Y. He, Y. Ding, L. Zhang, C. Tan, 2008, Heat transfer and flow behaviour of aqueous suspensions of titanate nanotubes (nanofluids), *Powder Technology*, 183: 63–72. doi:10.1016/j.powtec.2007.11.014.

[98] Y. Xuan, Q. Li, Investigation on convective heat transfer and flow features of nanofluids, *Journal of Heat Transfer*, 125: 151. doi:10.1115/1.1532008.

[99] T. Tanaka, J.K. Eaton, 2008, Classification of turbulence modification by dispersed spheres using a novel dimensionless number, *Physical Review Letters*, 101: 1–4. doi:10.1103/PhysRevLett.101.114502.

[100] E.B. Haghighi, M. Saleemi, N. Nikkam, R. Khodabandeh, M.S. Toprak, M. Muhammed, 2014, Accurate basis of comparison for convective heat transfer in nanofluids, *International Communications in Heat and Mass Transfer*, 52: 1–7. doi:10.1016/j.icheatmasstransfer.2014.01.002.

[101] Z. Wu, L. Wang, B. Sundén, 2013, Pressure drop and convective heat transfer of water and nanofluids in a double-pipe helical heat exchanger, *Applied Thermal Engineering*, 60: 266–274. doi:10.1016/j.applthermaleng.2013.06.051.

[102] Z. Haddad, H.F. Oztop, E. Abu-Nada, A. Mataoui, 2012, A review on natural convective heat transfer of nanofluids, *Renewable and Sustainable Energy Reviews*, 16: 5363–5378. doi:10.1016/j.rser.2012.04.003.

[103] K. Khanafer, K. Vafai, M. Lightstone, 2003, Buoyancy-driven heat transfer enhancement in a two-dimensional enclosure utilising nanofluids, *International Journal of Heat and Mass Transfer*, 46: 3639–3653. doi:10.1016/S0017-9310(03)00156-X.

[104] E.J. Wasp, J.P. Kenny, R.L. Gandhi, 1977, Solid-liquid flow: slurry pipeline transportation [pumps, valves, mechanical equipment, economics], *Ser. Bulk Materials Handling*, 1.

[105] E. Büyük Öğüt, 2009, Natural convection of water-based nanofluids in an inclined enclosure with a heat source, *International Journal of Thermal Sciences*, 48: 2063–2073. doi:10.1016/j.ijthermalsci.2009.03.014.

[106] E. Abu-Nada, 2009, Effects of variable viscosity and thermal conductivity of Al_2O_3-water nanofluid on heat transfer enhancement in natural convection, *International Journal of Heat and Fluid Flow*, 30: 679–690. doi:10.1016/j.ijheatfluidflow.2009.02.003.

[107] C.T. Nguyen, F. Desgranges, G. Roy, N. Galanis, T. Maré, S. Boucher, 2007, Temperature and particle-size dependent viscosity data for water-based nanofluids – hysteresis phenomenon, *International Journal of Heat and Fluid Flow*, 28: 1492–1506. doi:10.1016/j.ijheatfluidflow.2007.02.004.

[108] K.C. Lin, A. Violi, 2010, Natural convection heat transfer of nanofluids in a vertical cavity: effects of non-uniform particle diameter and temperature on thermal conductivity, *International Journal of Heat and Fluid Flow*, 31: 236–245. doi:10.1016/j.ijheatfluidflow.2009.11.003.

[109] Z. Haddad, E. Abu-Nada, H.F. Oztop, A. Mataoui, 2012, Natural convection in nanofluids: are the thermophoresis and Brownian motion effects significant in nanofluid heat transfer enhancement? *International Journal of Thermal Sciences*, 57: 152–162. doi:10.1016/j.ijthermalsci.2012.01.016.

[110] F.S. Oueslati, R. Bennacer, 2011, Heterogeneous nanofluids: natural convection heat transfer enhancement, *Nanoscale Research Letters*, 6: 222. doi:10.1186/1556-276X-6-222.

[111] Y. He, C. Qi, Y. Hu, B. Qin, F. Li, Y. Ding, 2011, Lattice Boltzmann simulation of alumina-water nanofluid in a square cavity, *Nanoscale Research Letters*, 6: 184. doi:10.1186/1556-276X-6-184.

[112] G.A. Sheikhzadeh, M. Dastmalchi, H. Khorasanizadeh, 2013, Effects of nanoparticles transport mechanisms on Al_2O_3-water nanofluid natural convection in a square enclosure, *International Journal of Thermal Sciences*, 66: 51–62. doi:10.1016/j.ijthermalsci.2012.12.001.

[113] X. Meng, Y. Li, Numerical study of natural convection in a horizontal cylinder filled with water-based alumina nanofluid, *Nanoscale Research Letters*, 10: 2–11. doi:10.1186/s11671-015-0847-x.

[114] V. Bianco, O. Manca, S. Nardini, K. Vafai, 2015, *Heat transfer enhancement with nanofluids*, Taylor & Francis, New York, NY.

[115] K. Khanafer, K. Vafai, M. Lightstone, 2003, Buoyancy-driven heat transfer enhancement in a two-dimensional enclosure utilising nanofluids, *International Journal of Heat and Mass Transfer*, 46: 3639–3653. doi:10.1016/S0017-9310(03)00156-X.

[116] A. Amiri, K. Vafai, 1994, Analysis of dispersion effects and non-thermal equilibrium, non-Darcian, variable porosity incompressible flow through porous media, *International Journal of Heat and Mass Transfer*, 37: 939–954. doi:10.1016/0017-9310(94)90219-4.

[117] P. Charunyakorn, S. Sengupta, S.K. Roy, 1991, Forced convection heat transfer in microencapsulated phase change material slurries: flow in circular ducts, *International Journal of Heat and Mass Transfer*, 34: 819–833. doi:10.1016/0017-9310(91)90128-2.

[118] S.E.B. Maïga, C.T. Nguyen, N. Galanis, G. Roy, 2004, Heat transfer behaviours of nanofluids in a uniformly heated tube, *Superlattices and Microstructures*, 35: 543–557. doi:10.1016/j.spmi.2003.09.012.

[119] A.C. Eiyad Abu-Nada, Ziyad Masoudc, Hakan F. Oztopd, 2010, Effect of nanofluid variable properties on mixed convection in a square cavity, *International Journal of Thermal Sciences*, 49: 479–491. doi:10.1016/j.ijthermalsci.2011.09.003.

[120] H.C. Chan, 2005, Empirical correlation finding the role of temperature and particle size for nanofluid, Al_2O_3 thermal conductivity enhancement, *Applied Physics Letters*, 87:153107.

[121] J. Xu, B. Yu, M. Zou, P. Xu, 2006, A new model for heat conduction of nanofluids based on fractal distributions of nanoparticles, Journal of Physics D: Applied Physics, 39: 4486–4490. doi:10.1088/0022-3727/41/13/139801.

[122] S.P. Jang, J.H. Lee, K.S. Hwang, S.U.S. Choi, 2007, Particle concentration and tube size dependence of viscosities of Al_2O_3-water nanofluids flowing through micro- and minitubes, *Applied Physics Letters*, 91: 2–4. doi:10.1063/1.2824393.

[123] M. Corcione, M. Cianfrini, A. Quintino, 2013, Two-phase mixture modeling of natural convection of nanofluids with temperature-dependent properties, *International Journal of Thermal Sciences*, 71: 182–195. doi:10.1016/j.ijthermalsci.2013.04.005.

[124] M. Corcione, 2011, Empirical correlating equations for predicting the effective thermal conductivity and dynamic viscosity of nanofluids, *Energy Conversion and Management*, 52: 789–793. doi:10.1016/j.enconman.2010.06.072.

[125] H. Aminfar, M.R. Haghgoo, 2013, Brownian motion and thermophoresis effects on natural convection of alumina-water nanofluid, *Proceedings of the Institution of Mechanical Engineers, Part C: Journal of Mechanical Engineering Science*, 227: 100–110.

[126] M. Alipanah, A.A. Ranjbar, A. Zahmatkesh, 2014, Numerical study of natural convection in vertical enclosures utilizing nanofluid, *Advances in Mechanical Engineering*, 6: 392610.

[127] N. Putra, W. Roetzel, S.K. Das, 2003, Natural convection of nano-fluids, *Heat and Mass Transfer*, 39: 775–784. doi:10.1007/s00231-002-0382-z.

[128] D. Wen, Y. Ding, 2005, Formulation of nanofluids for natural convective heat transfer applications, *International Journal of Heat and Fluid Flow*, 26: 855–864. doi:10.1016/j.ijheatfluidflow.2005.10.005.

[129] W.H. Leong, K.G.T. Hollands, A.P. Brunger, 1998, Experimental Nusselt numbers for a cubical-cavity benchmark problem in natural convection, *International Journal of Heat and Mass Transfer*, 42: 1979–1989. doi:10.1016/S0017-9310(98)00299-3.

[130] S. Cioni, S. Ciliberto, J. Sommeria, 1996, Experimental study of high-Rayleigh-number convection in mercury and water, *Dynamics of Atmospheres and Oceans*, 24: 117–127. doi:10.1016/0377-0265(95)00453-X.

[131] A.G. Nnanna, 2006, Experimental model of temperature-driven nanofluid, *Journal of Heat Transfer*, 129: 697–704. doi:10.1115/1.2717239.

[132] C.H. Li, G.P. Peterson, 2010, Experimental studies of natural convection heat transfer of Al_2O_3/DI water nanoparticle suspensions (nanofluids), *Advances in Mechanical Engineering*, 2010. doi:10.1155/2010/742739.

[133] Y. Hu, Y. He, C. Qi, B. Jiang, H. Inaki Schlaberg, 2014, Experimental and numerical study of natural convection in a square enclosure filled with nanofluid, *International Journal of Heat and Mass Transfer*. 78: 380–392. doi:10.1016/j.ijheatmasstransfer.2014.07.001.

[134] C.J. Ho, D-S. Chen, W-M. Yan, O. Mahian, 2014, Buoyancy-driven flow of nanofluids in a cavity considering the Ludwig–Soret effect and sedimentation: numerical study and experimental validation, *International Journal of Heat and Mass Transfer*, 77: 684–694. doi:10.1016/j.ijheatmasstransfer.2014.05.059.

[135] Burkert, 2015, Type 8081 – Ultrasonic flowmeter without display. http://www.burkert.com/en/type/8081 (accessed 16 May 2016).

[136] B. Berkovsky, V. Polevikov, 1977, Numerical study of problems on high-intensive free convection, *Proceedings of International Turbulent Buoyant Convection Seminar*, 1977: 443–455.

[137] M. Mahdavi, H. Ghodsinezhad, M. Sharifpur, J.P. Meyer, 2015, Boundary condition investigation for cavity flow natural convection, *11th International Conference on Heat Transfer, Fluid Mechanics and Thermodynamics*, Kruger National Park, South Africa, 2015: 813–818.

[138] J.T. Edward, 1970, Molecular volumes and the Stokes-Einstein equation, *Journal of Chemical Education*, 47: 261. doi:10.1021/ed047p261.

[139] S.J. Kline, F.A. McClintock, 1953, Describing uncertainties in single-sample experiments, *Mechanical Engineering*, 75: 3–8.

[140] R.J. Moffat, 1988, Describing the uncertainties in experimental results, *Experimental Thermal and Fluid Science*, 1: 3–17. doi:10.1016/0894-1777(88)90043-X.

[141] C. Babbage, 1871, Error analysis and significant figures, *Analysis*, 1871: 1–6.

[142] J.A. Olivier, 2009, Single-phase heat transfer and pressure drop of water cooled at a constant wall temperature inside horizontal circular smooth and enhanced tubes with different inlet configuration in the transitional flow regime, Phd thesis, University of Pretoria.

[143] R.J. Moffat, 1988, Describing the uncertainties in experimental results, *Experimental Thermal and Fluid Science*, 1: 3–17. doi:10.1016/0894-1777(88)90043-x.

[144] D.G. Kröger, 2004, Appendix A: properties of biological fluids, *Air-Cooled Heat Exchangers and Cooling Towers*, PennWell Corporation, Tulsa, OK, 2004: 448–451. doi:10.1016/B978-0-08-087780-8.00143-1.

Appendix A: Thermocouples calibration

A.1 Introduction

This chapter discusses the calibration method of thermocouples and gives the calibration factors for each thermocouple.

A.2 Thermocouples calibration

Thermocouples were calibrated using a thermostat bath (PR20R-30 Polyscience) with an accuracy of ±0.005 °C. The temperature ranges from 5 to 65 °C with an interval of 10 °C were chosen and 600 temperature measurements with a frequency of 2 at the desired temperature set were acquired. This process was repeated three times and the average measured temperature (the average of reading temperatures by thermocouples) was plotted against the reference temperatures (using PT-100, the internal thermocouple of the thermostat bath) for all thermocouples, as shown in Figure A. 4. To obtain the calibration factors, a linear curve was fitted as shown in Equation A. 1.

$$T_{cal} = mT_{uncal} + c \qquad \text{Equation A. 1}$$

To minimise the error, the average m and average c, the result of the three measurements, were used as the calibration factor for each thermocouple. Figure A. 4 shows a linear relationship between the uncalibrated temperature and the reference temperature. Thermocouples have different factors due to using different channels of the data logger, as well as different characteristics of the thermocouple's junction during the soldering process.

CH_0

y = 1.0040x - 0.4106
R² = 1.0000

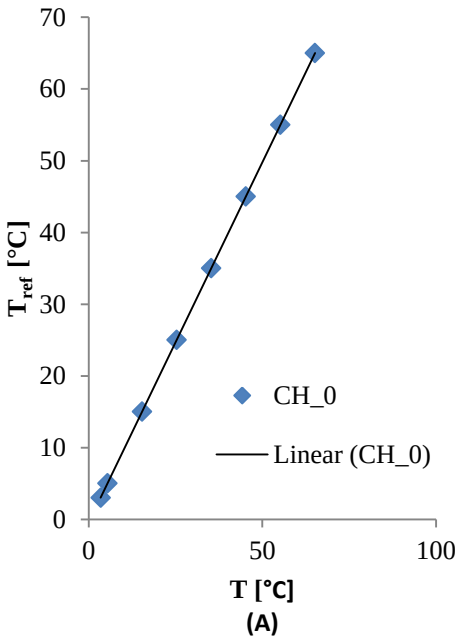

(A)

CH_1

y = 1.0053x - 0.3232
R² = 1

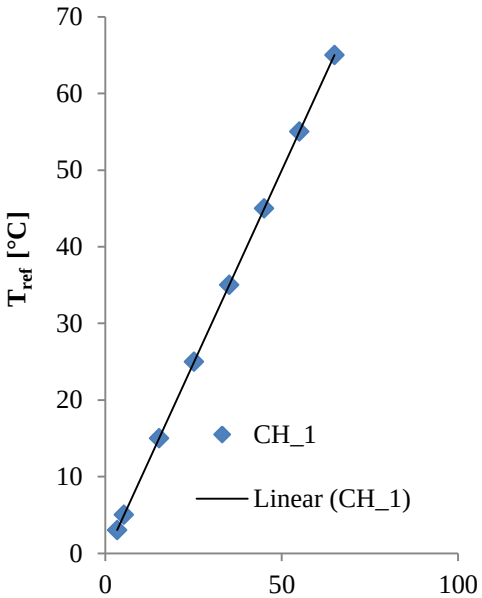

(B)

CH_2

y = 1.005x - 0.4686
R² = 1

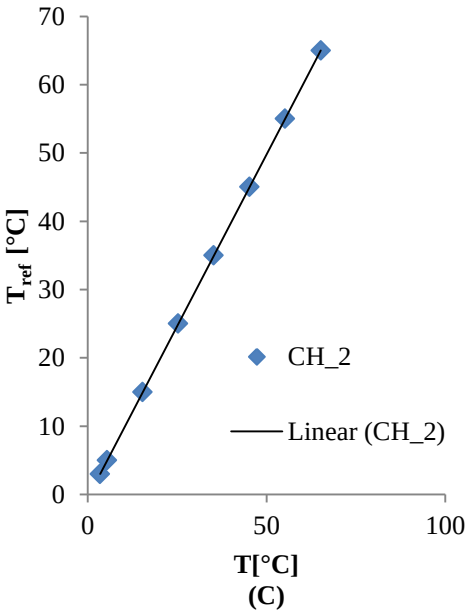

(C)

CH_3

y = 1.0038x - 0.1919
R² = 1

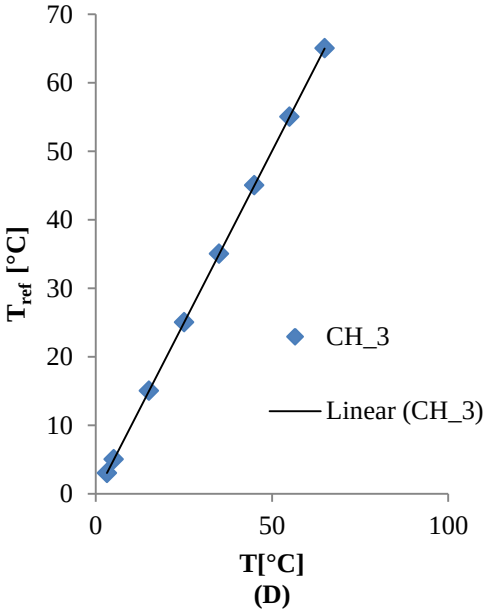

(D)

CH_4

y = 1.0049x - 0.2551
R² = 1

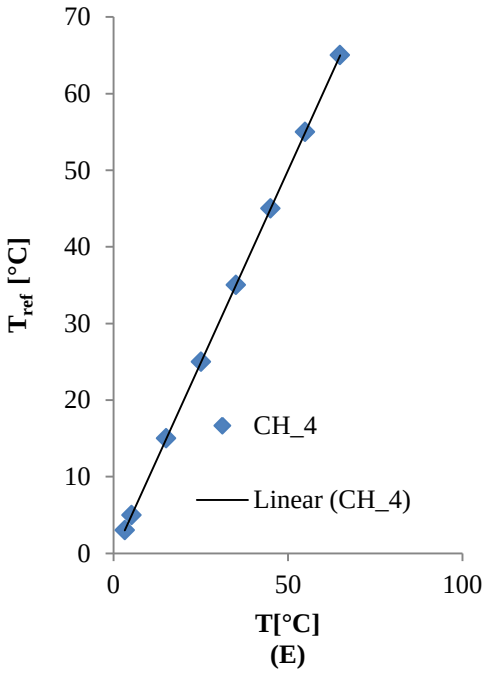

(E)

CH_5

y = 1.0041x - 0.3736
R² = 1

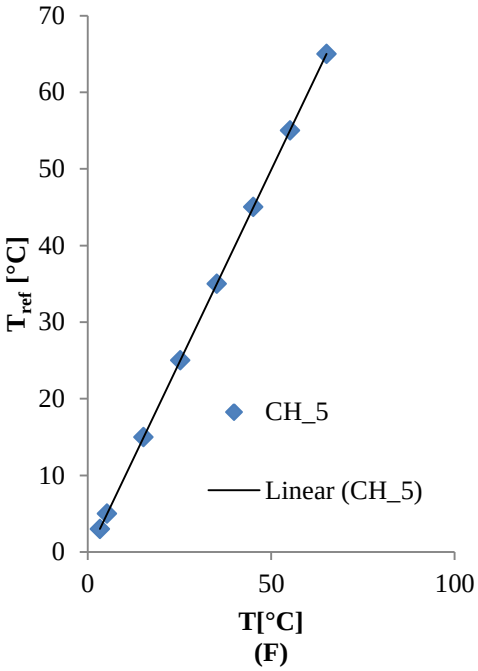

(F)

CH_6

y = 1.0046x - 0.1794
R² = 1

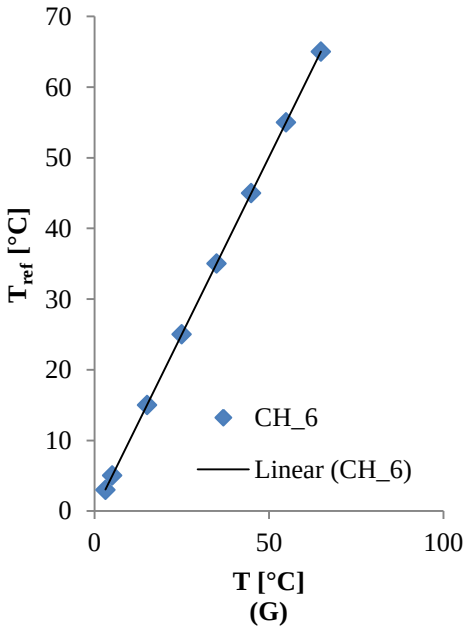

(G)

CH_7

y = 1.0048x - 0.3881
R² = 1

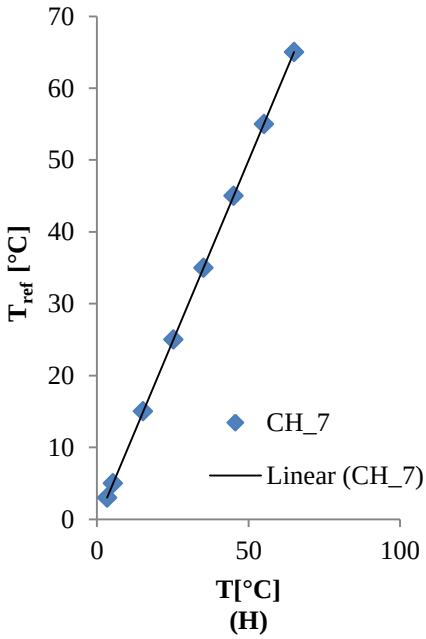

(H)

CH_8

y = 1.0061x - 0.7662
R² = 1

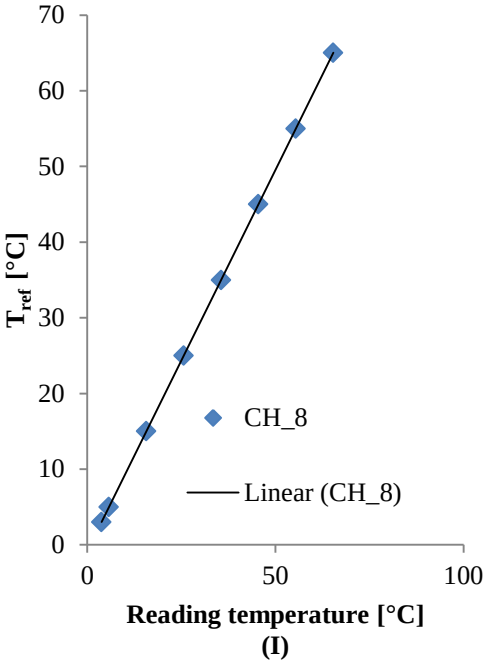

(I)

CH_9

y = 1.0032x - 0.8234
R² = 1

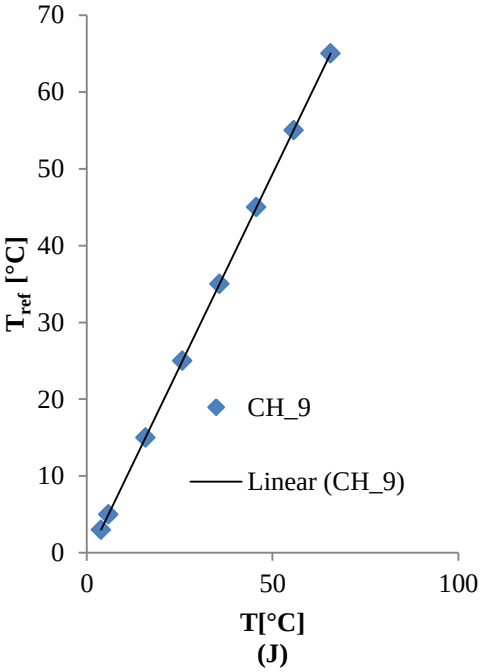

(J)

CH_10

y = 1.0037x - 0.2009
R² = 1

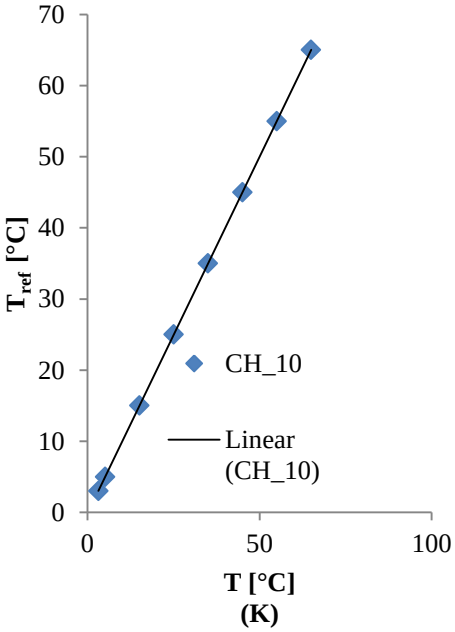

(K)

CH_11

y = 1.0053x - 0.6934
R² = 1

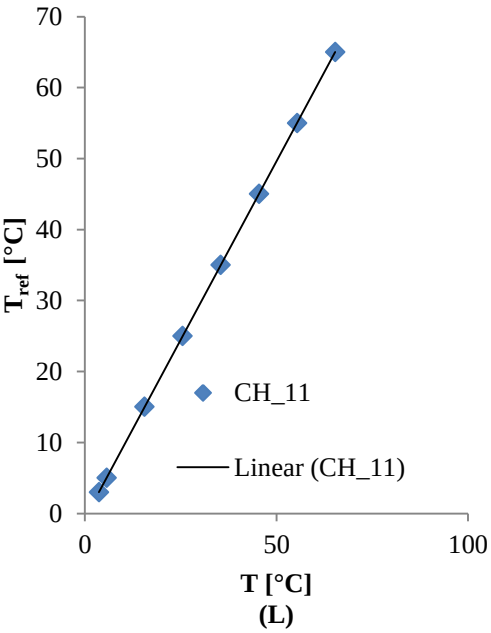

(L)

CH_12

y = 1.0056x - 0.8037
R² = 1

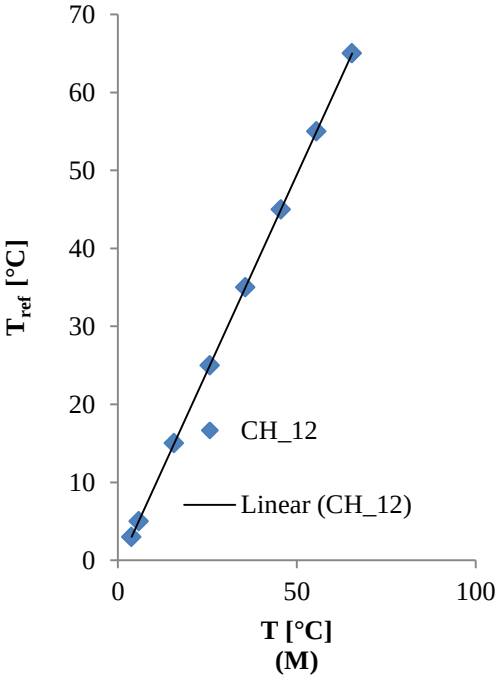

CH_13

y = 1.005x - 0.7972
R² = 1

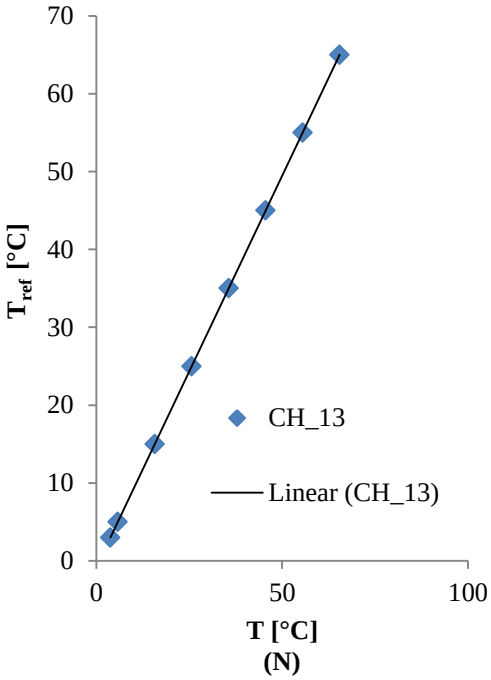

CH_14

y = 1.0045x - 0.7174
R² = 1

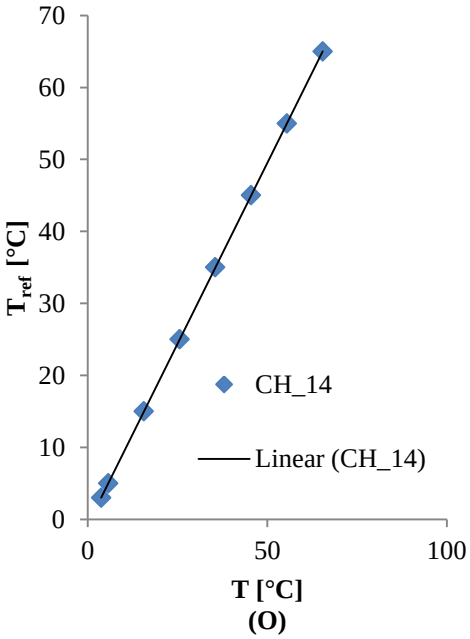

CH_15

y = 1.0047x - 0.7454
R² = 1

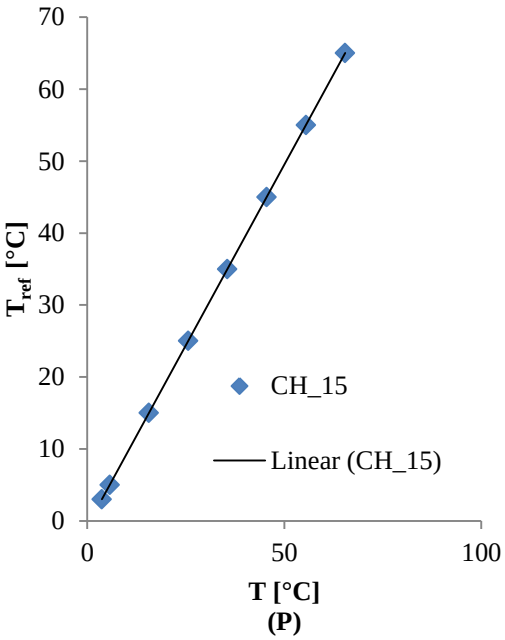

CH_15

y = 1.0047x - 0.7454
R² = 1

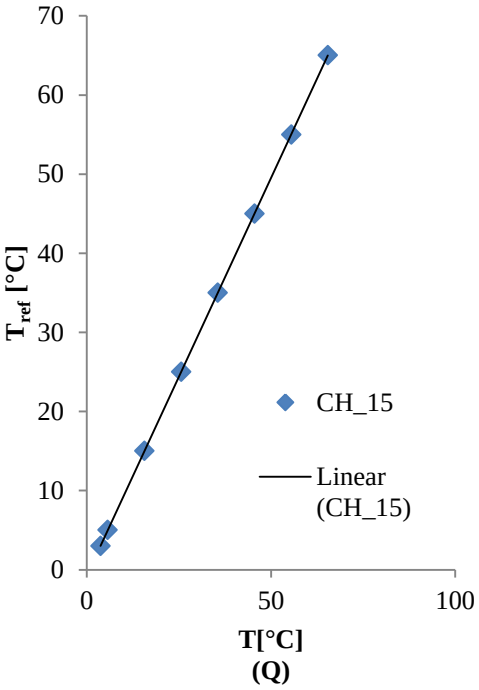

CH_16

y = 1.005x - 0.755
R² = 1

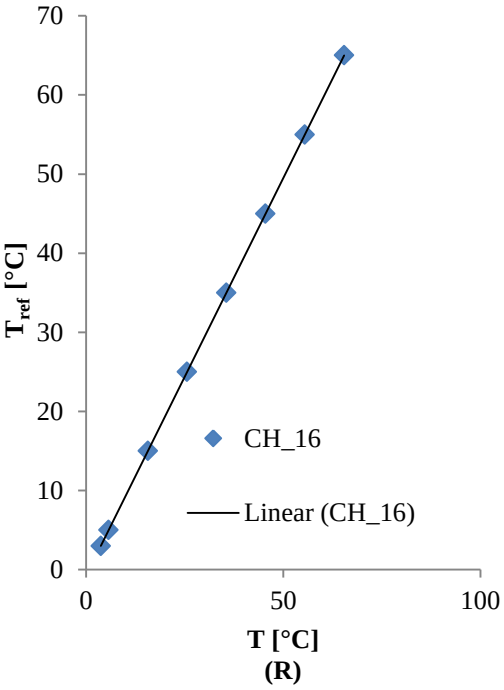

CH_17

y = 1.0062x - 0.6085
R² = 1

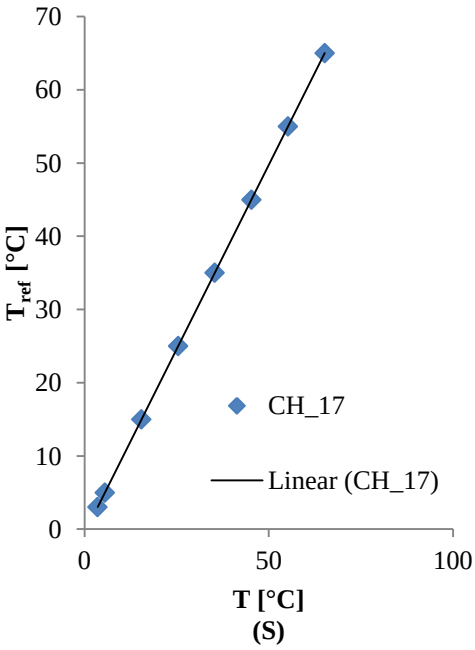

CH_18

y = 1.0054x - 0.5498
R² = 1

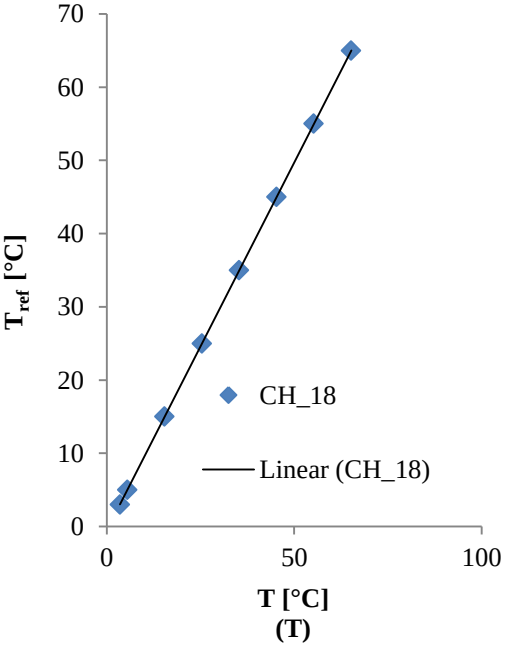

CH_19

y = 1.0043x - 0.5134
R² = 1

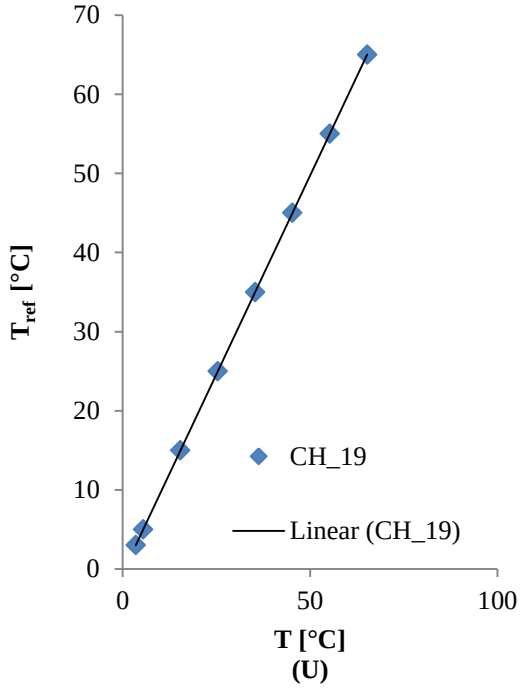

CH_20

y = 1.0057x - 0.8238
R² = 1

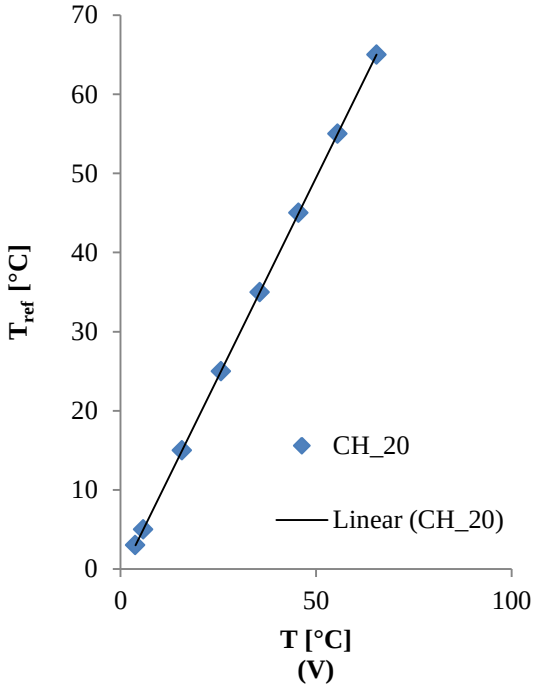

CH_21

y = 1.0048x - 0.8987
R² = 1

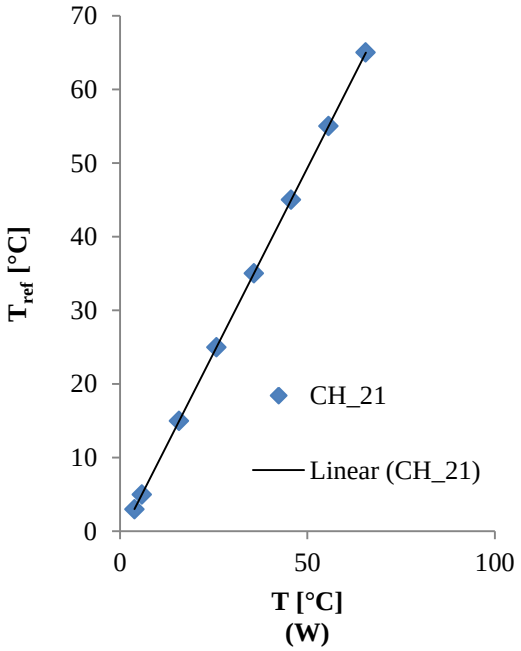

CH_22

y = 1.0046x - 0.6177
R² = 1

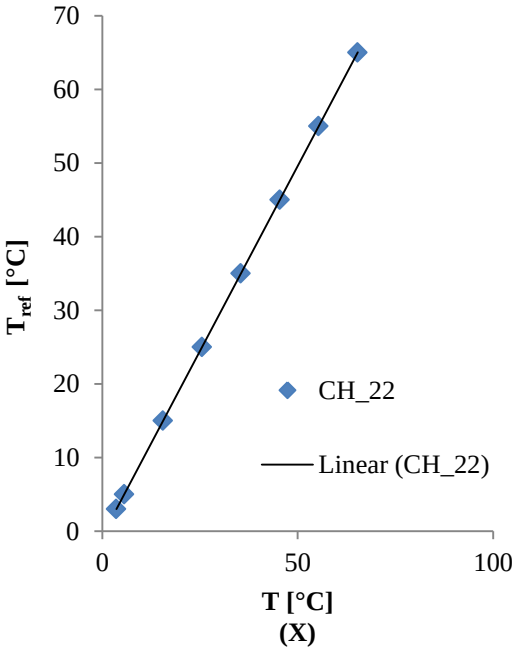

CH_23

y = 1.0048x - 0.8616
R² = 1

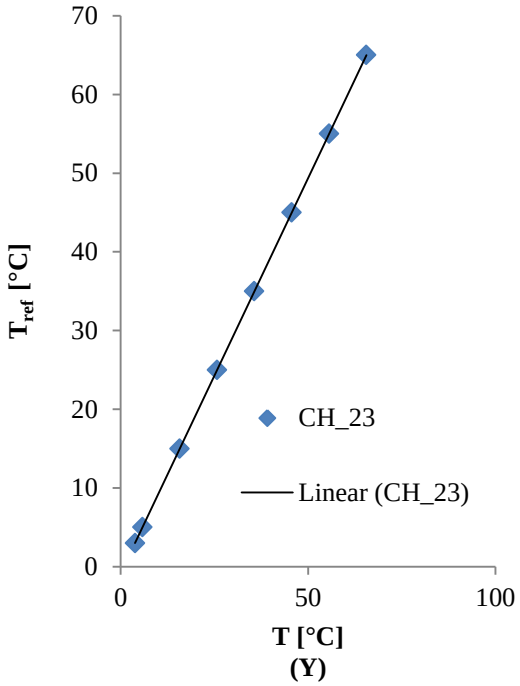

CH_24

y = 1.0038x - 0.1038
R² = 1

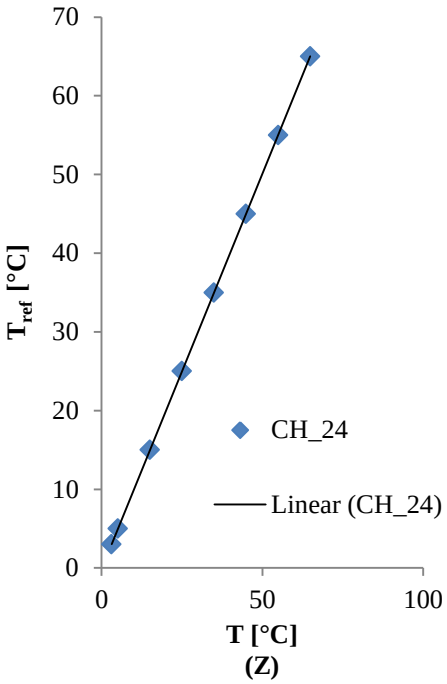

CH_25

y = 1.0046x - 0.2688
R² = 1

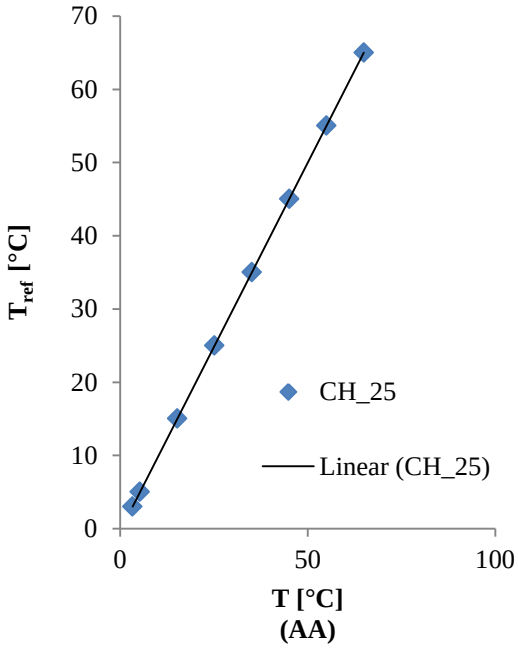

CH_27

y = 1.0041x - 0.261
R² = 1

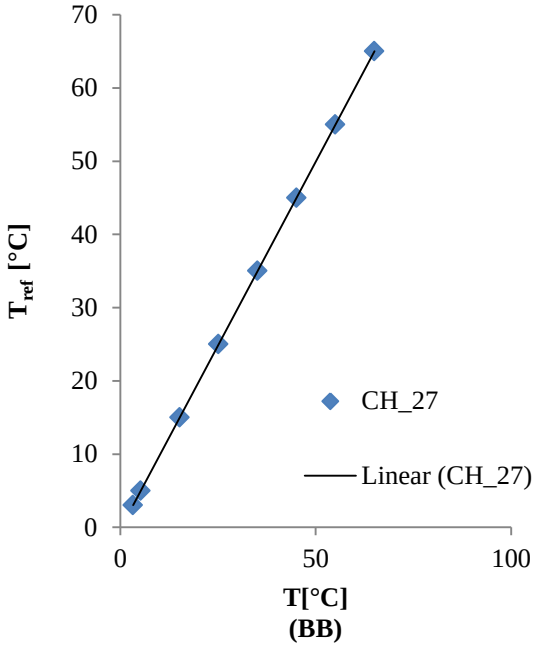

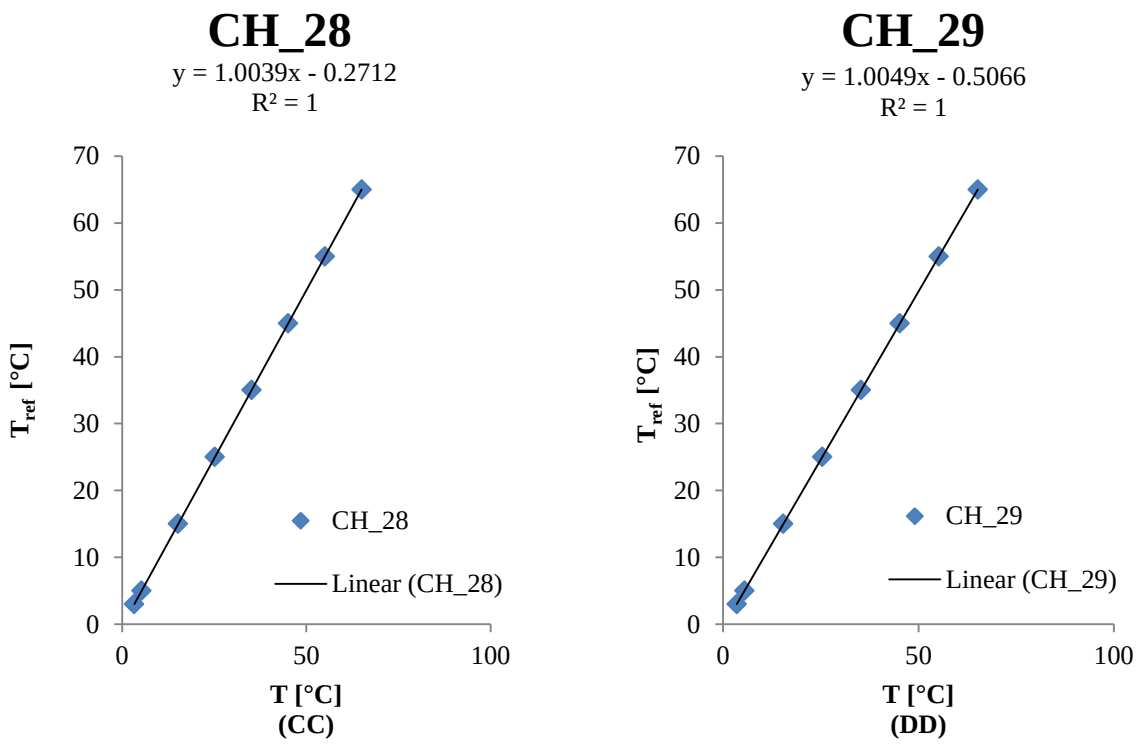

Figure A. 4: The average temperatures as measured by thermocouples inside the thermostat bath versus the reference temperatures

In this study, the thermocouples were not soldered to the surfaces. The thermocouples were held inside the cavity at the centerline using a string. The thermocouples, which measured the wall surface temperature, were also dipped 2 mm inside the walls and the first thermal conductivity glow was used. After this, a thin layer of silicon paste was applied. Therefore, the characteristics of the thermocouples were the same as the calibrated thermocouples in the thermostat bath. Figure A. 5 shows the position of the thermocouples in the experimental setup.

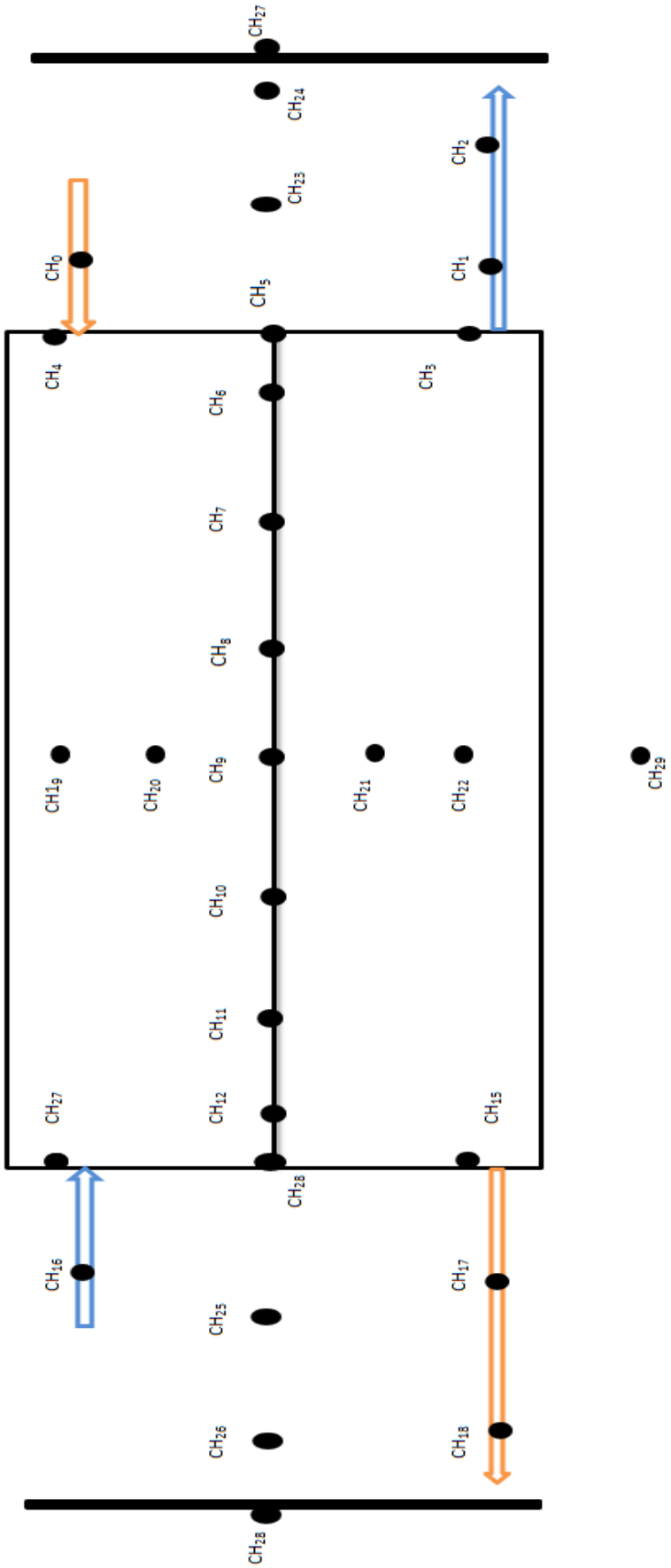

Figure A. 5: The thermocouples station in the experimental setup (rotated 90 degree CCW)

Table A. 2: The average calibration factors of thermocouples

Thermocouples	m	c	Thermocouples	m	c
CH_0	1.004	-0.4311	**CH_16**	1.0052	-0.759
CH_1	1.005	-0.3546	**CH_17**	1.0064	-0.67
CH_2	1.0051	-0.4956	**CH_18**	1.0044	-0.52
CH_3	1.004	-0.2181	**CH_19**	1.0047	-0.538
CH_4	1.0047	-0.2693	**CH_20**	1.0059	-0.841
CH_5	1.0045	-0.3953	**CH_21**	1.0052	-0.902
CH_6	1.0047	-0.1878	**CH_22**	1.0049	-0.638
CH_7	1.0049	-0.4161	**CH_23**	1.0051	-0.873
CH_8	1.0058	-0.7817	**CH_24**	1.0041	-0.129
CH_9	1.0039	-0.8175	**CH_25**	1.005	-0.298
CH_10	1.0039	-0.205	**CH_26**	1.0045	-0.139
CH_11	1.0053	-0.708	**CH_27**	1.0043	-0.293
CH_12	1.0056	-0.815	**CH_28**	1.0041	-0.287
CH_13	1.0052	-0.808	**CH_29**	1.0052	-0.547
CH_14	1.0046	-0.697			
CH_15	1.0051	-0.773			

To ensure successful calibration, four temperature points, 8.5, 27.6, 36.8 and 51.9 °C were chosen. The temperature difference between the calibrated and uncalibrated temperature is shown in Figure A. 6.

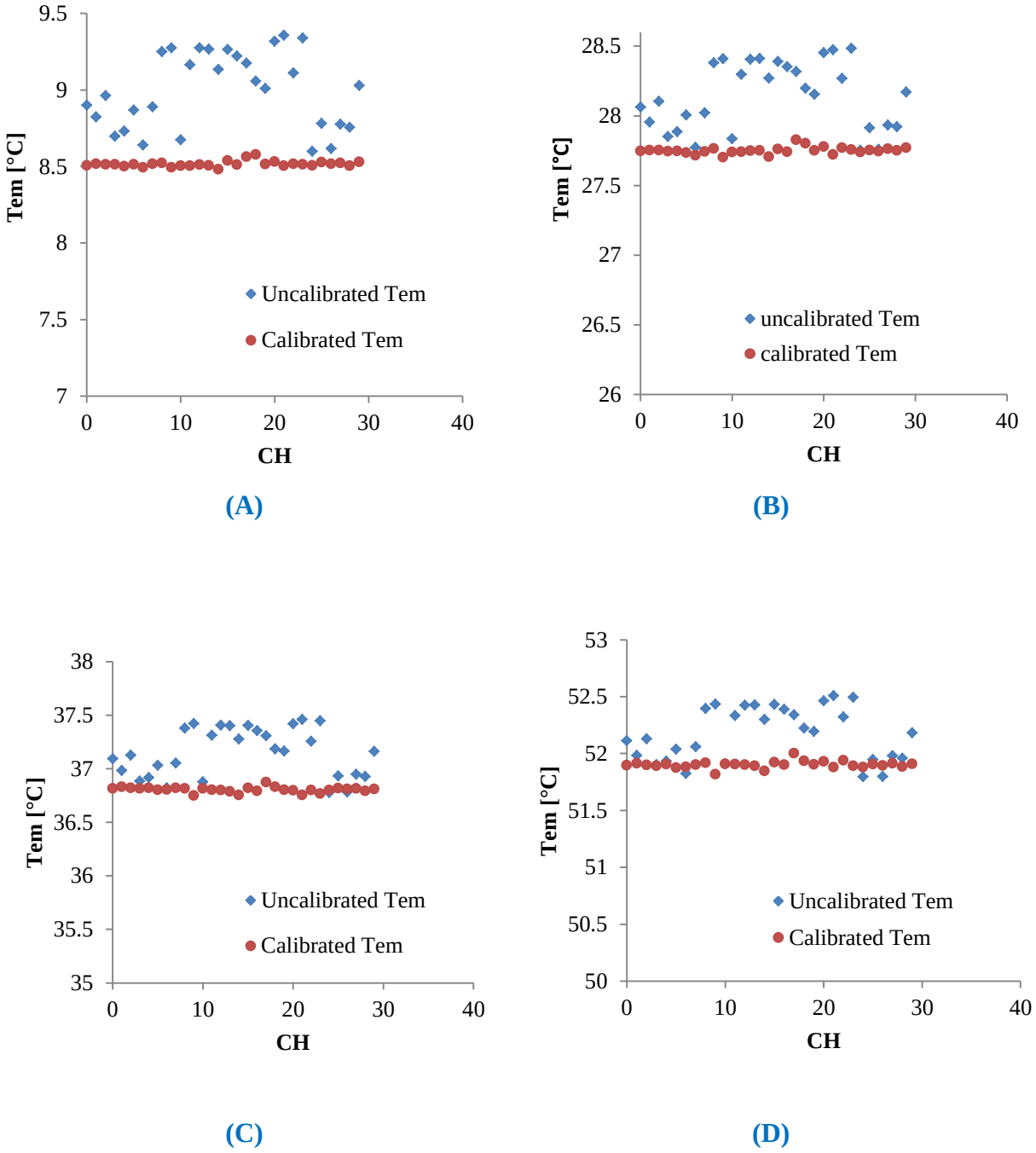

Figure A. 6: Calibrated and uncalibrated temperature of thermocouples channels at (A) 8.5 °C, (B) 27.6 °C, (C) 36.8 °C and (D) 51.9 °C

The figure illustrates the successful calibration of the thermocouples, in which thermocouples were calibrated to ±0.02 °C accuracy.

A.3 Conclusion

This appendix explained the calibration of thermocouples. The calibration of thermocouples using a thermostat bath with an accuracy of ±0.005 °C was done, as the thermocouples were not soldered after the calibration. The average standard deviation of thermocouples in the range from 5 to 65 °C was 0.0041 °C, and the accuracy of the calibrated thermocouples was approximately 0.02 °C.

Appendix B: Uncertainty analysis

B.1 Introduction

The experimental study involves many measurements. Therefore, the possible value of error for measurement values, which deviate from the unknown true value, should be described. This study aimed to investigate nanofluids' heat transfer coefficient in natural convection. In this chapter, the uncertainty of the experimental measurement, which was used to estimate the error of the calculated desired parameters such as natural convection heat transfer coefficient, Nu and Ra, was studied in detail.

B.2 Theory of uncertainty analysis

The uncertainty analysis has two components, which are known as a systematic error (bias, B) and random error (precision, P) [140]. The bias error is an error that is usually specified by the manufacturer of an instrument and it repeats whenever a measurement is made. Random errors are the result of a random fluctuation in several repeated measurements of a physical quantity due to, for example, the uncontrollable initial conditions and an inaccurately defined quantity to be measured [141]. If we have some experimental measurement, we usually combined them using a formula. Therefore, to estimate the propagated errors, I need to know how to combine the errors. The magnitude of the bias and precision errors will correspond to a probability of 95% that the actual error will not be more than the estimated figure [142].

The uncertainty of a single measurement is calculated using Equation B.1.

$$\delta x_i = \sqrt{(B_i)^2 + (P_i)^2} \qquad \text{Equation B. 1}$$

x_i is a single physical measured quantity, which is as big as twice the standard deviation[142]. For R, which is a function of many measured variables as shown in Equation B. 2, if the uncertainty of a x_i is known, the uncertainty of R is calculated using Equation B. 3 [142].

$$R = R(x_1, x_2, x_3, x_4, ..., x_n) \qquad \text{Equation B. 2}$$

$$\delta R = \frac{\partial R}{\partial x_i}\delta x_i$$ Equation B. 3

The partial differential uncertainty coefficient is called the sensitivity coefficient of the calculated parameter with respect to the specific measured variables. It shows the error contribution of the variable in the total uncertainty of the interested parameter. For a parameter with many independent variables, uncertainty of R is defined in Equation B.4[143].

$$\delta R = \sqrt{(\frac{\partial R}{\partial x_1}\delta x_1)^2 + (\frac{\partial R}{\partial x_2}\delta x_2)^2 + \ldots + (\frac{\partial R}{\partial x_n}\delta x_n)^2}$$ Equation B. 4

Thermocouples, flow meters, the volume of fluid and the mass of nanoparticles is the main source of error in this study. Each of the instruments has the manufacturer's specification for accuracy, which was taken as the bias. The precision of the instruments is obtained by capturing 1 000 samples and then calculating the average standard deviation, which is multiplied by two to fall into the 95% confidence region.

Table B. 3 shows instruments with their range and the errors that were used in this study.

To calculate the uncertainty of the natural convection heat transfer coefficient, two extremes, the highest *Ra* and the lowest *Ra* that is the result of various wall temperature differences, were calculated.

Table B. 3 Independent reading error in apparatus

Instruments	Symbols	Range	Uncertainty
Flow meter	$\delta\dot{m}$	0.0666 to 0.3333 *L/s*	±2.01%
Weight scale	δm_p	0 to 220 g	±0.0001 g
Thermocouples	δT	-200 to 150 °C	±0.02 °C
Volume	δV	0 to 1000 ml	±0.05 ml
Viscosity	$\delta\mu$	0.3 to 10000 mPa.s	±3.16%
Length	δl	0 to 20 cm	±0.02 mm

The following equations were used to calculate the uncertainty of parameters:

$$\delta T_{in} = \delta T_0$$ **Equation B. 5**

$$\delta T_{out} = \sqrt{(\delta T_1)^2 + (\delta T_2)^2 + (\delta T_3)^2}$$ **Equation B. 6**

T is the absolute temperature at the following correlations.

$$k_w = k_{bf} = -6.14255\times10^{-1} + 6.9962\times10^{-3}T - 1.01075\times10^{-5}T^2 + 4.74737\times10^{-12}T^4 \ [W/mK]$$ [144] **Equation B. 7**

$$\delta k_{bf} = \sqrt{\left(\frac{\partial k_{bf}}{\partial T}\delta T\right)^2}$$ **Equation B. 8**

$$\rho_{bf} = (1.49343\times10^{-3} - 3.7164\times10^{-6}T + 7.09782\times10^{-9}T^2 - 1.90321\times10^{-20}T^6)^{-1}, kg/m^3$$ [144] **Equation B. 9**

$$\delta\rho_{bf} = \sqrt{\left(\frac{\partial\rho_{bf}}{\partial T}\delta T\right)^2}$$ **Equation B. 10**

$$c_{p_{bf}} = 8.15599\times10^{3} - 2.80627\times10T + 5.11283\times10^{-2}T^{2} - 2.17582\times10^{-13}T^{6}\ J/kg.K \quad [144]$$

Equation B. 11

$$\delta c_{p_{bf}} = \sqrt{(\frac{\partial c_{p_{bf}}}{\partial T}\delta T)^{2}}$$

Equation B. 12

$$C_{p_{nf}} = \frac{(1-\varphi)(\rho c_{p})_{bf} + (\rho c_{p})_{np}}{\rho_{nf}}$$

Equation B. 13

$$\varphi = \frac{v_{p}}{v_{p}+v_{f}} = \frac{\frac{m_{p}}{\rho_{p}}}{\frac{m_{p}}{\rho_{p}}+v_{f}}$$

Equation B. 14

$$\delta\varphi = \sqrt{(\frac{\partial\varphi}{\partial m_{p}}\delta m_{p})^{2} + (\frac{\partial\varphi}{\partial v_{f}}\delta v_{f})^{2}}$$

Equation B. 15

$$\rho_{nf} = \varphi\rho_{p} + (1-\varphi)\rho_{bf}$$

Equation B. 16

$$\delta\rho_{nf} = \sqrt{(\frac{\partial\rho_{nf}}{\partial\varphi}\delta\varphi)^{2} + (\frac{\partial\rho_{nf}}{\partial\rho_{bf}}\delta\rho_{bf})^{2}}$$

Equation B. 17

$$\delta c_{p_{nf}} = \sqrt{(\frac{\partial c_{p_{nf}}}{\partial\varphi}\delta\varphi)^{2} + (\frac{\partial c_{p_{nf}}}{\partial\rho_{bf}}\delta\rho_{bf})^{2} + (\frac{\partial c_{p_{nf}}}{\partial c_{p_{bf}}}\delta c_{p_{bf}})^{2}}$$

Equation B. 18

$$\dot{\bar{q}} = \dot{m}c_{p}(T_{in} - T_{out})$$

Equation B. 19

$$\delta\dot{\bar{q}} = \sqrt{(\frac{\partial\dot{\bar{q}}}{\partial\dot{m}}\delta\dot{m})^{2} + (\frac{\partial\dot{\bar{q}}}{\partial c_{p}}\delta c_{p})^{2} + (\frac{\partial\dot{\bar{q}}}{\partial T_{in}}\delta T_{in})^{2} + (\frac{\partial\dot{\bar{q}}}{\partial T_{out}}\delta T_{out})^{2}}$$

Equation B. 20

$$\dot{\bar{q}} = h_{nf}A\Delta T$$

Equation B. 21

$$\Delta T = \bar{T}_{H} - \bar{T}_{C}$$

Equation B. 22

$$\bar{T}_H = \frac{T_3 + T_4 + T_5}{3}$$

$$\bar{T}_C = \frac{T_{15} + T_{27} + T_{28}}{3}$$

$$\delta T_H = \sqrt{3(\frac{\partial T_H}{\partial T}\delta T)^2}$$ **Equation B. 23**

$$\delta T_C = \sqrt{3(\frac{\partial T_C}{\partial T}\delta T)^2}$$ **Equation B. 24**

$$\bar{h}_{nf} = \frac{\dot{\bar{q}}}{A(\bar{T}_H - \bar{T}_C)}$$ **Equation B. 25**

$$A = W \times H$$ **Equation B. 26**

$$\delta A = \sqrt{(\frac{\partial A}{\partial W}\delta W)^2 + (\frac{\partial A}{\partial H}\delta H)^2}$$ **Equation B. 27**

$$\delta W = \delta H = \delta L$$ **Equation B. 28**

$$\delta \bar{h}_{nf} = \sqrt{(\frac{\partial \bar{h}_{nf}}{\partial \dot{\bar{q}}}\delta \dot{\bar{q}})^2 + (\frac{\partial \bar{h}_{nf}}{\partial A}\delta A)^2 + (\frac{\partial \bar{h}_{nf}}{\partial \bar{T}_H}\delta \bar{T}_H)^2 + (\frac{\partial \bar{h}_{nf}}{\partial \bar{T}_C}\delta \bar{T}_C)^2}$$ **Equation B. 29**

$$\bar{N}u_{nf} = \frac{\bar{h}_{nf} l}{k_{nf}}$$ **Equation B. 30**

$$\delta \bar{N}u_{nf} = \sqrt{(\frac{\partial \bar{N}u_{nf}}{\partial h_{nf}}\delta h_{nf})^2 + (\frac{\partial \bar{N}u_{nf}}{\partial l}\delta l)^2 + (\frac{\partial \bar{N}u_{nf}}{\partial k_{nf}}\delta k_{nf})^2}$$ **Equation B. 31**

$$k_{nf} = k_{bf}\frac{k_p + 2k_{bf} - 2\varphi(k_{bf} - k_p)}{k_p + 2k_{bf} + \varphi(k_{bf} - k_p)}$$ **Equation B. 32**

$$\delta k_{nf} = \sqrt{\left(\frac{\partial k_{nf}}{\partial k_{bf}}\delta k_{bf}\right)^2 + \left(\frac{\partial k_{nf}}{\partial \varphi}\delta\varphi\right)^2}$$ **Equation B. 33**

$$Ra_{nf} = \frac{g\beta_{nf}(\bar{T}_H - \bar{T}_C)\rho_{nf}{}^2 c_{p_{nf}} l_c{}^3}{\mu_{nf}\ k_{nf}}$$ **Equation B. 34**

$$\beta_{bf} = (0.000000841\times T^3 - 0.000155704\times T^2 + 0.015892349\times T - 0.055807193)\times 10^{-3}$$ [1/K] [144] **Equation B. 35**

$$\delta\beta_{bf} = \sqrt{\left(\frac{\partial\beta_{bf}}{\partial T}\delta T\right)^2}$$ **Equation B. 36**

$$\beta_{nf} = \frac{\beta_p\rho_p + (1-\varphi)\beta_{bf}\rho_{bf}}{\rho_{nf}}$$ **Equation B. 37**

$$\delta\beta_{nf} = \sqrt{\left(\frac{\partial\beta_{nf}}{\partial\varphi}\delta\varphi\right)^2 + \left(\frac{\partial\beta_{nf}}{\partial\beta_{bf}}\delta\beta_{bf}\right)^2 + \left(\frac{\partial\beta_{nf}}{\partial\rho_{bf}}\delta\rho_{bf}\right)^2 + \left(\frac{\partial\beta_{nf}}{\partial\rho_{nf}}\delta\rho_{nf}\right)^2}$$ **Equation B. 38**

$$\delta Ra_{nf} = \sqrt{\begin{aligned}&\left(\frac{\partial Ra_{nf}}{\partial\beta_{nf}}\delta\beta_{nf}\right)^2 + \left(\frac{\partial R_{nf}}{\partial\bar{T}_H}\delta\bar{T}_H\right)^2 + \left(\frac{\partial R_{nf}}{\partial\bar{T}_C}\delta\bar{T}_C\right)^2 + \\ &\left(\frac{\partial Ra_{nf}}{\partial\rho_{nf}}\delta\rho_{nf}\right)^2 + \left(\frac{\partial Ra_{nf}}{\partial l_c}\delta l_c\right)^2 + \left(\frac{\partial Ra_{nf}}{\partial c_{p_{nf}}}\delta c_{p_{nf}}\right)^2 \\ &+\left(\frac{\partial Ra_{nf}}{\partial\mu_{nf}}\delta\mu_{nf}\right)^2 + \left(\frac{\partial Ra_{nf}}{\partial k_{nf}}\delta k_{nf}\right)^2\end{aligned}}$$ **Equation B. 39**

Table B. 4 summarises the uncertainty of parameters that are of interest in this experiment.

Table B. 4: Maximum uncertainties of the experiment due to propagated errors

Error	Description	Value
$\delta T_{in}/T_{in}$	Inlet temperature (H.E)	0.037%
$\delta T_{out}/T_{out}$	Outlet temperature (H.E)	0.021%
$\delta\dot{m}/\dot{m}$	Mass flow rate	1.6%
$\delta k_{bf}/k_{bf}$	Thermal conductivity of the base fluid	0.8%
$\delta k_{nf}/k_{nf}$	Thermal conductivity of the nanofluid	1.8%
$\delta\rho_{bf}/\rho_{bf}$	Density of the base fluid	0.013%
$\delta\rho_{nf}/\rho_{nf}$	Density of the nanofluid	0.021%
$\delta c_{p_{bf}}/c_{p_{bf}}$	Specific heat of the base fluid	0.033%
$\delta c_{p_{nf}}/c_{p_{nf}}$	Specific heat of nanofluid	0.051%
$\delta\bar{\dot{q}}/\bar{\dot{q}}$	Average heat transfer	3.15%
$\delta\bar{h}_{nf}/\bar{h}_{nf}$	Average heat transfer coefficient	5.31%
$\delta\bar{N}u_{nf}/\bar{N}u_{nf}$	Nusselt number	4.62%
$\delta Ra_{nf}/Ra_{nf}$	Rayleigh number	4.45%

B.3 Conclusion

Error analysis of the desired parameters showed that the reported value of the parameters is in the range of the experimental work, which is less than 5%. In this study, the maximum reported errors for the natural convection heat transfer coefficient, *Nu*, *Ra* and average heat transfer rate were 5.31 4.62, 4.45% and 3.15, respectively.